January 2014

KINETICS OF POLYMER CYCLIZATION REACTION AND NOVEL COVALENT DNA CROSS-LINKING ASSAYS

Reza Afra
Purdue University

Graduate School Form 30
Updated 1/15/2015

PURDUE UNIVERSITY
GRADUATE SCHOOL
Thesis/Dissertation Acceptance

This is to certify that the thesis/dissertation prepared

By Reza Afra

Entitled

KINETICS OF POLYMER CYCLIZATION REACTION
AND NOVEL COVALENT DNA CROSS-LINKING ASSAYS

For the degree of Doctor of Philosophy

Is approved by the final examining committee:

Brian A. Todd
Chair

Kenneth P. Ritchie

Paul F. Muzikar

Nikolai R. Skrynnikov

To the best of my knowledge and as understood by the student in the Thesis/Dissertation Agreement, Publication Delay, and Certification Disclaimer (Graduate School Form 32), this thesis/dissertation adheres to the provisions of Purdue University's "Policy of Integrity in Research" and the use of copyright material.

Approved by Major Professor(s): Brian A. Todd

Approved by: Mark Haugan 11/12/2014

Head of the Departmental Graduate Program Date

KINETICS OF POLYMER CYCLIZATION REACTION AND NOVEL COVALENT DNA CROSS-LINKING ASSAYS

A Dissertation

Submitted to the Faculty

of

Purdue University

by

Reza Afra

In Partial Fulfillment of the

Requirements for the Degree

of

Doctor of Philosophy

August 2015

Purdue University

West Lafayette, Indiana

TABLE OF CONTENTS

LIST OF TABLES

LIST OF FIGURES

Figure Page

Figure Page

ABBREVIATIONS

SSS	Szabo, Schulten and Schulten
WF	Wilemski-Fixman
RG	Renormalization Group
ND	Non draining
FD	Free draining
EV	Excluded Volume
WLC	Worm-like Chain
dsDNA	double-stranded DNA
ssDNA	single-stranded DNA
nt	nucleotides
bp	base pairs
kb	kilo base pairs
ODN	Oligo deoxyribonucleotide or DNA oligonucleotide
RT	Room Temperature
DI	Deionized
CEU	Cohesive End Units
PB	Phosphate Buffer
PEG	Poly(ethylene glycol)
PEO	Poly(ethylene oxide)
PS	Poly(styrene)
PDMS	Poly(dimethylsiloxane)
EDTA	ethylenediaminetetraacetic acid
NHS	N-Hydroxysuccinimide
dNTP	deoxyribonucleotide triphosphate
dGTP	deoxyguanosine triphosphate

dCTP	deoxycytidine triphosphate
dATP	deoxyadenosine triphosphate
dTTP	deoxythymidine triphosphate
SPAAC	Strain-Promoted Alkyne-Azide Cycloaddition
BCN	bicyclo[6.1.0]nonyne
DMSO	dimethyl sulfoxide
DABSYL	dimethylaminoazobenzenesulfonic acid
DBO	2,3-diazabicyclo[2.2.2]oct-2-ene

ABSTRACT

Afra, Reza PhD, Purdue University, August 2015. Kinetics of polymer cyclization reaction and novel covalent DNA cross-linking assays. Major Professor: Brian A. Todd.

In this dissertation I first do an extensive review of polymer cyclization kinetics. Different theories of polymer cyclization kinetics, their assumptions and their predictions are presented along with the predictions of computer simulations. In addition, the experimental results for synthetic and biological polymers are summarized.

Secondly, from our Brownian dynamics simulations of the worm-like chain we discovered that the polymer cyclization kinetics cannot be adequately described by transition-state-like theories that reduce the high dimensional kinetics to a one dimensional diffusion along a reaction coordinate. It is common in Brownian dynamics simulations of WLC to discretize time step. In our simulations, however, we recovered the continuum limit for time by extrapolating the time steps to zero and found that finite time steps lead to erroneous results for cyclization kinetics. This is the only work to date that shows the inadequacy of 1D diffusion-reaction models in capturing the kinetics of polymer cyclization.

Lastly, we developed novel assays for covalently crosslinking DNA. To this end, we screened different crosslinking methods and found that Iodine-mediated disulfide bonding and copper-free azide-alkyne cycloaddition are the most viable paths to ligase-free DNA crosslinking. We developed methodologies for labeling and purification of dsDNA with those reactive moieties and carried out experiments to test the yield of these chemistries at low DNA concentrations. Our results establish a method for crosslinking long linear dsDNA through their ends.

1. Polymer Cyclization Kinetics

Polymer cyclization has been the subject of extensive study since it is a way to probe the internal dynamics of isolated polymer chains [1]. Furthermore, polymer cyclization is an elementary step in many biological [2,3] as well as polymer synthesis processes [4]. The chief aim of this review is to present a review of various theoretical and experimental advancements over the past few decades in the area of polymer cyclization. While the dependence of cyclization kinetics on various properties of polymer-solvent systems is discussed, our major focus is on the dependence of the kinetics on the length of polymer, reaction radius, the solvent and the type of the polymer.

1.1 Introduction

The kinetics of contact formation between the ends of a single polymer chain is a topic of broad interests for it occurs in processes involving biological [2, 3] and synthetic polymers [1]. In cellular processes the contact formation is an elementary step toward the formation of ordered structures of nucleic acids [3] and proteins [2]. Linear synthetic polymers are also capable of undergoing cyclization which leads to the formation of cyclic byproducts that terminate the polymerization reaction [5]. Much effort over the past few decades has been devoted to the theoretical [6–9] and experimental [1] investigation of polymer cyclization. The main aim of this review is presenting both theoretical advancements and experimental finding for the polymer cyclization kinetics of a single chains in dilute solution. In particular we present the scaling of cyclization kinetics with the chain length. We review the major existing theories of polymer cyclization, their assumptions and their predictions about different polymer-solvent systems. Furthermore, we review the predictions of

computer simulations and finally we review the experiments on the cyclization kinetics of synthetic polymers, nucleic acids, and polypeptide chains.

1.2 Theories of Polymer Cyclization

1.2.1 Wilemski-Fixman Theory

Wilemski and Fixman (WF) introduced a general framework for calculating kinetics in reaction-diffusion processes [10] and applied it to the specific problem of calculating the reaction rate between terminal reactive groups of a Rouse chain [7,11].

The starting point in WF theory is a diffusion equation coupled with a sink term that accounts for the reactivity of the terminal reactive groups.

$$\frac{\partial p}{\partial t} - \mathcal{D}p = -uS(\mathbf{r})p. \tag{1.1}$$

This equation determines the time evolution of $p(\mathbf{r}, t|\mathbf{r}_0)$, the conditional probability density of finding the chain at the conformational state $\mathbf{r}$, given that the system has initially been at $\mathbf{r}_0$. $S(\mathbf{r})$ is the sink function and specifies the spatial dependence of the reactive region. For instance, a delta function sink means reactions occur only at the origin. u is the probability density of reaction given that the sinks overlap. u quantifies the sink strength; for $u = 0$ no reaction occurs and for $u \to \infty$ the reactants react instantaneously upon reaching the sink. Finally, $\mathcal{D}$ is the diffusion operator whose exact form is specified by the polymer model. The solution to Eq. 1.1 in terms of the Green's function of the sink-free differential equation is

$$p(\mathbf{r}, t|\mathbf{r}_0) = G(\mathbf{r}, t|\mathbf{r}_0) - u \int dt' \int d\mathbf{r}_0 G(\mathbf{r}, t - t'|\mathbf{r}_0) S(\mathbf{r}) p(\mathbf{r}, t|\mathbf{r}_0) \tag{1.2}$$

The quantity of greatest interest is the survival probability $\phi(t)$, defined as the probability that a chain is unreacted at t and is equal to the fraction of unreacted chains. Defining $\psi(\mathbf{r}, t)$ as the probability density that a chain has the conformation $\mathbf{r}$ and is still unreacted, $\phi(t)$ is obtained from integrating $\psi(\mathbf{r}, t)$ over all the possible chain conformations.

$$\phi(t) = \int \psi(\mathbf{r}, t) d\mathbf{r}. \tag{1.3}$$

$\psi(\mathbf{r},t)$ is in turn obtained from integrating $p(\mathbf{r},t|\mathbf{r}_0)$ over the initial conformations. WF theory assume that the system is initially in equilibrium, $\psi(\mathbf{r}_0,0) = p_{eq}(\mathbf{r}_0)$, which leads to the following equation for the survival probability

$$\phi(t) = \int d\mathbf{r} \int d\mathbf{r}_0 p(\mathbf{r},t|\mathbf{r}_0) p_{eq}(\mathbf{r}_0). \tag{1.4}$$

An exact expression for $\phi(t)$ is then obtained form Eqs 1.2, 1.3 and 1.4.

$$\phi(t) = 1 - u \int_0^t dt \int d\mathbf{r}' S(\mathbf{r}') \psi(\mathbf{r}',t). \tag{1.5}$$

The integrand of the time integral is the joint probability of finding two reactive groups near each other. Denoting this probability by $v(t)$, the differential equation corresponding to Eq. 1.4 is $\frac{d\phi(t)}{dt} = -uv(t)$. The physical interpretation of this equation is that the time evolution of the survival probability is proportional to the probability of finding active reactive groups near each other.

The common way to obtain closed form expression for integral equations of the form Eq. 1.5 is the start from an educated guess for ψ. WF proposed the following *ansatz* referred to as the "closure approximation"

$$\begin{cases} \psi(\mathbf{r},t) = p_{eq}(\mathbf{r}) f(t), \\ v(t) = v_{eq} f(t). \end{cases} \tag{1.6}$$

Which assumes that the spatial form of the probability distribution can be approximated by the equilibrium distribution. The time dependence is obtained by multiplying both sides of the first equation with $S(\mathbf{r})$ and integrating over the conformational space. The second equation ensures that the closure approximation does not affect the sink occupancy $v(t)$. This is necessary since the temporal change of $\phi(t)$ directly depends on the sink occupancy.

It is then straightforward to obtain a solution for $\phi(t)$ and the mean lifetime defined as $\tau = \int_0^\infty \phi(t)dt$ using Laplace transformation. We will not present the details of derivation here and skip to the final results,

$$\tau = \frac{1}{kv_{eq}} + \int_0^\infty dt \left(\frac{C(t)}{v_{eq}^2} - 1 \right). \tag{1.7}$$

Where $C(t)$ is the sink-sink correlation function. For a spherically symmetric sink this quantity is expressed as

$$C(t) = \int d\mathbf{r} \int d\mathbf{r}_0 S(r) G(\mathbf{r}, t|\mathbf{r}_0) S(r_0) P_{eq}(r_0). \tag{1.8}$$

It is assumed that an steady-state is established at long time; the Green's function approaches the equilibrium distribution and from Eq. 1.8 the sink-sink correlation function becomes $C(\infty) = v_{eq}^2$. The first term in Eq. 1.7 is the reaction-limited term and dominates when $u \to 0$. In this limit the mean lifetime is proportional to the probability of finding proximate sinks. The second term is the diffusion-limited term and dominates when $u \to \infty$.

1.2.2 Predictions Of Wilemski-Fixman Theory For Rouse Chain

WF theory predicts that the cyclization time of long free-draining Rouse chain is linearly dependent on the maximum relaxation time of the Rouse chain and nearly independent on the size of the capture radius, that is $\tau \propto \tau_m \propto N^2$, where N is the number of beads in Rouse chain. Interestingly, this is in sharp contrast with the results for harmonic spring model (Rouse chain with $N = 2$) where the cyclization time scales with the inverse of the capture radius [8,11]. This dependence on the capture radius is intuitive because one would expect from transition state theory for the kinetics to be dependent on the probability of the transition state, which in turn depends on the size of the reaction radius. The peculiar independence of the cyclization kinetics of the free-draining Rouse chain on the reaction radius was explained by Doi who pointed out that this peculiarity arises form from the behavior of the chain end monomers [8]. He showed that the dependence of the cyclization time on the ratio of size of the capture radius to the root mean square end-to-end distance a/R is dependent on the time correlation of end-to-end vector. Yang and Cao pointed out that the second term in Eq. 1.7 includes two contributions, at short times the dynamics is dominated by the short time fluctuation of end-to-end distance and at longer times the dynamic is dominated by global relaxation of the chain [12]. The former is dependent upon

the reaction radius and has the simple form known for Smoluchowski reaction rate $\tau \propto R^3/a \propto b^3N^{3/2}/a$, while the latter scales as b^2N^2. The relative magnitude of these two terms determines the nature of the dependence of cyclization kinetics on the capture radius and it can be seen that a transition occurs roughly around $N \sim (a/b)^2$. Obviously, for a harmonic spring model ($N = 1, a < b$) no transition occurs and the kinetics is dependent on the capture radius. On the other hand, for very long chains the global relaxation dominates the sink-sink correlation function and kinetics becomes independent of the capture radius. For the Non-draining Rouse chain WF found $\tau \sim N^{3/2}$ with a weak dependence on the sink size [11]. In this case both the short term contribution and the maximum relaxation time scales as $N^{3/2}$ and consequently the cyclization time scales with $N^{3/2}$ as well.

Table 1.1.
Scaling exponent of a Rouse chain by WF theory along with RG and SSS theories discussed in the following sections. Presence or absence of excluded volume interactions and hydrodynamic interactions alters the cyclization kinetics.

	without excluded volume		with excluded volume	
	free draining	non-draining	free draining	non-draining
WF	2	1.5	–	–
RG	2	1.5	2.2	1.875
SSS	1.5	–	1.8	–

1.2.3 Predictions Of Wilemski-Fixman Theory For Other Polymer Dynamics Models

Other properties of polymeric liquids have also been investigated within the framework of WF theory. Chakrabarti [13] generalized WF theory to Rouse chain in viscoelastic fluid and found that up to a certain chain length cyclization is faster in

viscoelastic fluid than in Newtonian fluid and after that threshold the order is reversed. Interestingly, in viscoelastic fluids no scaling was observed.

Another effect deemed important particularly in polypeptide contact formation is internal friction [14]. It has been shown [15] that internal friction slows down the cyclization with dependence on the chain length weaker than internal-friction-free Rouse and Zimm chains. The scaling predicted to be $\tau \sim N^{1.1-1.3}$ for the Rouse chain and $\tau \sim N^{0.5-0.8}$ for the Zimm chain with weaker length dependence at higher internal friction.

1.2.4 Validity Of Wilemski-Fixman's Closure Approximation

The validity of closure approximation has been studied extensively [12, 16–20] and it is argued that its correctness depends on the relation between the diffusion term and the reaction term in Eq. 1.1 or, the relation between two time scales, the diffusional relaxation time and the reaction time. Polymers exhibit a spectrum of relaxation times and their spontaneous fluctuations relax to equilibrium after the maximum relaxation time, τ_m. Therefore, the relevant diffusional time scale for polymer reactions is the longest relaxation time. The closure approximation is plausible when the intrinsic reaction rate is small or the diffusional relaxation is fast [21], $k\tau_m \to 0$, because in these cases chain remains always near equilibrium. A perturbation analysis by Weiss confirms this point [19]. For slowly relaxing systems or larger reaction rates there is no reason to assume that a chain will remain near equilibrium; In fact, one would intuitively expect significant departure from equilibrium in these cases. Nevertheless, WF approximation yields surprisingly satisfactory predictions for these cases. Sunagawa and Doi examined the validity of WF theory for the harmonic spring polymer model (reactants attached by a harmonic spring) and an infinitely reactive spherically symmetric sink [18]. They found that WF theory slightly overestimates the reaction time but its accuracy improves as the sink size approaches zero. Battezati et al. further expanded the analysis for harmonic spring model by examining the effect of

different sinks on the reaction rate [22] . They showed that the rate for three choices of sink, delta function, step function and Gaussian function can be expressed as a series of a/R powers

$$\tau = \tau_m(a_{-1}(a/R)^{-1} + a_0 + a_1(a/R) + O((a/R)^2). \tag{1.9}$$

Where a_ks are constants of the same order of magnitude for different sinks and a/R is the capture radius normalized to the polymer length. These results suggest that for a harmonic spring polymer the qualitative features of the mean reaction dynamics are independent of the exact form of the sink. The qualitative agreement between the looping kinetics for delta sink, for which WF is exact, and forms of sink suggests that for reactants in a harmonic potential WF theory is safely applicable as long as $a/R \ll 1$.

Brownian dynamic simulations for a Rouse chain and infinitely reactive delta sink suggest that WF theory's accuracy improves as $a/R \to 0$. Srinivas et. al. performed Brownian dynamics simulation for the Rouse chain and a sink with the form $(a/r)^{-6}$ and found that survival probability predicted by WF theory is only satisfactory when the $a/R \ll 1$. The results of these simulations as well as variational approximations suggest that survival probability predicted by WF approximation is an upper bound on the survival probability and thereby, WF overestimates the reaction time [23].

1.2.5 Validity Of Markovian Approximation In Wilemski-Fixman Theory

It should be noted that the satisfactory agreement between the mean cyclization time predicted by WF theory and simulations does not mean the assumptions are always valid. To see this imagine a polymer with delta-sink, the closure approximation approximates the probability distribution of reactive conformation with the equilibrium conformation. This implies that all degrees of freedom of the chain have relaxed to equilibrium before the sinks overlap; the chain forgets all its fluctuations instantaneously. This is the Markovian assumption implicit in WF theory. The validity this

assumption has been recently discussed and it was shown that Markovian assumption leads to overestimation of both survival probability and mean lifetime [24–26].

1.2.6 Renormalization Group Theory

Friedman and O'Shaughnessy [27–36] developed a scheme based on Renormalization Group theory (RGT) to obtain cyclization rates. This approach has the advantage that the closure approximation of WF theory is not needed. Akin to a paramagnet near the Curie temperature that shows long range correlations in spin fluctuation, a long polymer exhibits long range correlation in chain fluctuations [37,38]. The correlation length of the monomer density fluctuations at this long chain limit is of the order of R. The physics of critical systems is dominated by these long range correlations and is independent of the microscopic fluctuations. It is known that at the critical point(e.g. $N \to \infty$) these systems show universal behavior and physical observables are governed by scaling laws an example being the well-known $R \sim N^{\nu}$ scaling relation. These scaling laws are universal, that is, the macroscopic observables (e.g. coil size, osmotic pressure, cyclization rate) are independent of the microscopic properties (e.g. chemical composure of monomers, reactivity of end monomers, sink size) of the system.

In critical systems short range fluctuation can be eliminated through a coarse graining method first introduced by Kadanov [39] for Ising model where the elementary length of the system (lattice spacing) is gradually enlarged. de Gennes [40] first noted the analogy between the magnetic systems and polymers and introduced a method similar to Kadanov's known as decimation procedure. In this procedure polymer is described in terms of blocks of monomers and the block size is gradually enlarged. Upon gradual coarse graining the interaction parameters of the system are drawn to *fixed points*. At these fixed points scaling laws emerge and the system will be invariant under further coarse graining. Oono [41] advanced this general scheme to renormalize the divergent perturbation series of various physical quantities of poly-

mers and obtain scaling laws for these quantities. Friedman and O'Shaughnessy adapted Oono's scheme to obtain the universal scaling laws for cyclization rate in different polymer models.

Here we review the basic procedure of renormalization. Let G be a certain quantity whose value from "bare" (non renormalized) calculation is G_B. Under renormalization all quantities are scaled in the form $\Gamma = Z_\Gamma \Gamma_0$ where Z_Γ is the scaling coefficients for the quantity Γ so in general we have $G_B = Z_G^{-1} G(\{Z_\Gamma \Gamma_0\})$. $\{Z_\Gamma \Gamma_0\}$ represents the set of all variables G depends on. Since the bare quantities are independent of the level of coarse graining we can write [42, 43]

$$L\frac{\partial G_B}{\partial L} = 0. \tag{1.10}$$

Using the chain rule we will have equations of the form $(\frac{\partial \ln Z_\Gamma}{\partial \ln L})_{\Gamma' \neq \Gamma}$ which determine the change of various physical parameters upon coarse graining. Fixed points of physical quantities are zeros of these equations. These fixed points represent universal values of the renormalized parameters the are independent microscopic details.

1.2.7 Predictions Of Renormalization Group Theory For Rouse Chain

Here we introduce the application of this scheme to the cyclization kinetics in Rouse chain. For a chain whose dynamic is governed by Eq. 1.1 and a delta sink the rate is

$$k = u_0 < \delta(\mathbf{r}) > + u_0^2 \int_0^\infty dt[< \delta((\mathbf{r}(0))\delta((\mathbf{r}(t)) > - < \delta((\mathbf{r}) >^2] + O(u_0^3). \tag{1.11}$$

This equation to the second order in u_0 is the same as Eq. 1.7. One can rewrite this equation as a series expansion in the powers of a coupling constant defined as $w_0 = u_0 \xi_0 L^{\epsilon/2}$ where L is a phenomenological length that sets the level of coarse graining, ζ_0 is the microscopic friction coefficient and $\epsilon = 4 - d$. For a Rouse chain this bare perturbation series is

$$-kN_0^2 = A\frac{w_0}{\xi_0}(\frac{N_0}{L})^{\epsilon/2} + \frac{w_0^2}{\xi_0}(\frac{N_0}{L})^{\epsilon}(B/\epsilon + const.). \tag{1.12}$$

This bare perturbation series is singular at $d = 4$ and also divergent for long chain (Large N_0) at other dimensions.

The coupling constant then is renormalized $w = Z_w w_0$ where Z_w is the scaling coefficient. Assuming that Z_w^{-1} is Taylor expandable, $Z_w = 1 + w^2 + \cdots$, one obtains to the first order $w_0 = w + A_1 w^2 + \cdots$. Substituting this in Eq. 1.12 and solving for the value of A_1 which removes the singularity from perturbation series one obtains $w_0 = w - \frac{1}{64\pi\epsilon} w^2 + \cdots$. The cyclization rate $k \equiv k(L, w, N, \zeta)$ is independent of the level of description of the system, that is $L\frac{\partial k}{\partial L} = 0$. Using the chain rule one obtains for the Rouse chain,

$$L\frac{\partial w}{\partial L} + \beta(w)\frac{\partial w}{\partial L} = 0. \tag{1.13}$$

Where $\beta(w) = L(\frac{\partial w}{\partial L})_{\tilde{w_0}, N_0, \zeta_0}$ and $\tilde{w_0} = w_0 L^{-\epsilon/2}$. One may wonder why there is no dependence on N or ζ. In the presence of hydrodynamic and excluded volume interactions there are terms associated with these two variables into the RG equation. However in the absence of these interactions $Z_N = Z_\zeta = 1$ and the terms associated with them drop out.

Using the expression for w in terms of w_0 one finds $\beta(w) = (w/128\pi)(w - w^*)$ which has two zeros: $w^* = 0, -64\pi\epsilon$. The negative w^* is the stable fixed point meaning the upon renormalization transformation the value of the coupling constant is drawn to this point regardless of its microscopic value, w_0. Figure 1.1 illustrates the flow of the coupling constant as a result renormalization transformation. From L $(\frac{\partial w}{\partial L})_{\tilde{w_0}, N_0, \zeta_0} = w/128\pi(w - w^*)$ it is apparent that the change in w is positive with increasing L when $\beta(w) > 0$ negative when $\beta(w) < 0$. Therefore, all points with and negative microscopic coupling constant arrive finally at the stable fixed point upon renormalization transformation.

The scaling relation for the cyclization rate is obtained by evaluating Eq. 1.12 at the stable fixed point and taking the limit at $N \to \infty$

$$k = 16\epsilon/\pi\zeta N^2. \tag{1.14}$$

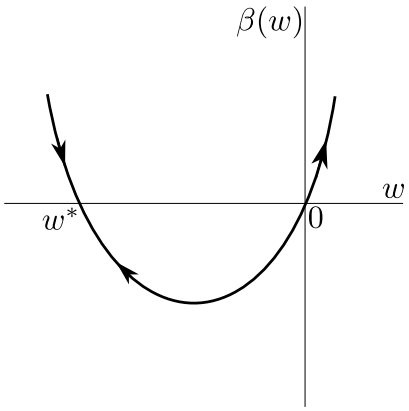

Figure 1.1. Phase portrait of the flow equation for the sink strength w. Upon renormalization *all* points with negative microscopic values of w are drawn to the stable fixed point $w^* = -64\pi\epsilon$.

To the first order in ϵ. The maximum relaxation time of the Rouse chain in 3D is $\tau_m = \frac{N^2\zeta}{3\pi^2 T}$ and a universal relation is obtained $k\tau_m = 0.52$, in good agreement with the prediction of WF that $k\tau_m = 0.46$. This scaling relation suggests that, as expected, the rate is independent of the bare sink strength u_0. For finite chains an interpolative formula is obtained

$$k = \frac{X}{1+X} 16\epsilon/\pi\zeta N^2. \tag{1.15}$$

Where $X = (N/L)^{\frac{\epsilon}{2}} \frac{w}{w-w^*}$. This equation interpolates between two extremes: high molecular weight chains with highly reactive sink $X \gg 1$ where $k \sim N^2$ and low molecular weight chains with weekly reactive sink ($X \ll 1$) where $k \sim N^{d/2}$.

1.2.8 Predictions Of Renormalization Group Theory For Other Polymer Dynamics Models

For the Rouse chain with volume interactions RG predicts $k = 8\epsilon/\pi\zeta N^{2.2}$ again at $N \to \infty$. In both of these free draining (no hydrodynamic interactions) models $k \propto 1/\tau_m \propto N^{-z\nu}$, where z is the dynamical exponent given by $\tau_m \propto R^z$. Apparently, the rate depends on a single time scale, the longest relaxation time of the chain,

suggesting a diffusion-controlled (DC) behavior [32, 34]. In short, FD models exhibit DC kinetics at $N \to \infty$. Also note that in accordance with Doi's and WF's prediction at this limit the rate becomes independent of the sink size.

For the non-draining models (Zimm in theta solvent and Zimm in good solvent) hydrodynamic effects are accounted for by a dimensionless coupling constant $\xi_0 \equiv (\zeta_0/\eta_0)L^{\epsilon/2}$ in addition to the sink coupling constant and excluded volume constants, w_0 and e_0. For Zimm chain in theta solvent volume interactions are absent and at the fixed points for e and ξ one finds $\beta(w) = w^2/128\pi$ indicating the absence of a non vanishing fixed point. RG predicts [32, 34]

$$k = -(\frac{12}{\pi^2 \eta N^{d/2} \epsilon})\frac{1}{X}. \tag{1.16}$$

Where $X = \frac{128\pi}{w} - \ln(N/L)$. This equation predicts $k = C\frac{N^{\nu d}}{ln(N/L)}$ in the $N \to \infty$ and C is a universal constant. For the large enough values of N the logarithmic correction becomes independent of N and in 3D one obtains $k \sim N^{-3/2}$ in agreement with WF's prediction.

For Zimm chain at the fixed points for e and ξ ($e^* = \pi^2\epsilon/2$ and $\xi^* = 2\pi^2\epsilon$) two zeros exist for $\beta(w) = -w(w^* - w)/128\pi$: $w^* = 16\pi\epsilon, 0$. In this case the non vanishing point is positive and a similar analysis with the analysis shown in Figure 1.1 shows that this point is unstable. The rate is this case is given by [32, 34]

$$k = (\frac{2}{\pi^3 \eta})(\frac{L}{N})^{\nu d} L^{-\frac{d}{2}} \frac{1}{X - 1}. \tag{1.17}$$

Where $X = (\frac{N}{L})^{\frac{\epsilon\nu}{4}}(\frac{w - w^*}{w})$. Simple analysis shows for $N \to \infty$ one obtains $k \sim p_{eq}$ (≈ 0) $k \sim N^{\nu(d+g)}$. $g = \epsilon/4 + O(\epsilon^2)$ is the correlation hole exponent which arises due to excluded volume interactions. The direct proportionality of the rate with the equilibrium probability suggests that the cyclization kinetics in good solvents obeys the law of mass action.

Additionally, Yeung and Friedman [35,44] determined the cyclization rate of Rouse and Zimm polymers initially in a ring conformation and found that the cyclization rate of a chain initially at equilibrium or in ring condition are related at times faster

than the maximum relaxation time; $k_{eq} \propto t^{1-\sigma}$ and $k_{eq} \propto t^{-\sigma}$, where $\sigma = 5/4$ for ultra long Rouse chains and $\sigma = -1$ for ultra long Zimm chain.

1.2.9 Regimes Of Polymer Cyclization Kinetics Predicted By Renormalization Group Theory

The RG theory results suggests that the nature of the cyclization kinetics in infinitely long polymer chains is independent of the detail of the reactive group and is determined by the polymer-solvent model. Strictly speaking, the class of reaction is determined by the exponent $\theta = d + g/z$. For $\theta < 1$ the kinetics is diffusion controlled while for $\theta > 1$ it obeys the law of mass action. The marginal case of $\theta = 1$ occurs in Zimm chain in Θ solvent in which the diffusion-limited and law of mass action kinetics predict same scaling relations. This classification is a generalization of de Gennes classification of reaction-diffusions to compact and non-compact [45]. For a Rouse chain ($g = 0$, $z = 4$ and $\theta = d/z$) the number of points in the conformational space visited after time t is proportional to t while the number of points in the volume explored after t is $\sim t^{d/z}$. When $d/z < 1$ then the number of visited points exceeds the number of points in the explored space and hence the volume is searched *compactly*. In this case the sink overlap is frequent and reaction kinetic shifts towards the diffusion-controlled regime. In contrast, when $d/z > 1$ ($d > 4$) the available conformational space is searched sparsely, sink overlap is infrequent and the reaction kinetics obeys the law of mass action [34].

1.2.10 Single Reaction Coordinate Theory

Wilemski and Fixman included the reactivity in the reaction-diffusion equation by adding a source term to the high dimensional diffusion equation and calculated. In their approach the reaction time is a sum of a reaction-limited term and the diffusion-limited term or the mean first passage time, τ. In WF theory diffusion-limited term is related to sink-sink correlation function. This is not the only way to obtain the mean

first passage time. Indeed, the traditional method of finding the first passage time which bypasses the solution of the time dependent reaction-diffusion and obtains the mean first passage time from an inhomogeneous differential equitation [46–48]. For a one-dimensional Smoluchowski equation the solution to this equation is obtained in the form of a quadrature [9, 49]. Smoluchowski equation describes a *Markovian* drift-diffusion process and hence its transition probability satisfies the Chapman-Kolmogorov equation [50].

$$p(x,t|x_0,t_0) = \int_{-\infty}^{\infty} p(x,t|x',t')p(x',t'|x_0,t_0)dx'. \tag{1.18}$$

The survival probability, the probability that the diffuser has not yet reached the absorbing boundary at time t reads [51]

$$\phi(y,t) = \int_a^L p(x,t|y,0)dy. \tag{1.19}$$

The probability that the particle is absorbed in a short interval after t, termed as the first passage time probability density is

$$f(y,t) = -\frac{\partial\phi(y,t)}{\partial t}. \tag{1.20}$$

The time dependence of the $f(y,t)$ probability contains the information on the kinetics of the process. It is straightforward to establish from this equation by differentiation that the survival probability satisfies the following Smoluchowski equation for the adjoint diffusion operator.

$$\frac{\partial\phi(x,t)}{\partial t} = \mathcal{D}^\dagger\phi(x,t). \tag{1.21}$$

Using the equation for the lifetime and 1.21 one obtains an equation for the τ

$$\mathcal{D}^\dagger\tau(x) = -1. \tag{1.22}$$

Although Eq. 1.22 is valid in all dimension it can be solved analytically only for effectively one dimensional systems. In particular for a one-dimensional draft-diffusion process, diffusion in an one potential of the mean force, a solution in the form of a quadrature is readily obtainable

$$\tau(y) = \int_a^{y'} \frac{p_{eq}(y'')}{D(y'')} \int_y^L \frac{dy'}{p_{eq}(y')}. \tag{1.23}$$

Where $p_{eq}(y) = e^{-U(y)}$ is the equilibrium probability of the location of the diffuser. Szabo, Schulten and Schulten [9] generalized the above method to diffusion-reaction with a partially absorbing boundary condition, or radiation boundary condition $j(a,t) = up(a,t)$ and a reflecting boundary condition $j(L,t) = 0$. The quantity commonly measured in experiments is the mean reaction time. SSS obtained this quantity by averaging $\tau(y)$ over the *equilibrium* probability density. The resulting equilibrium averaged reaction time reads [9, 49, 52]

$$\tau = \int_{\alpha}^{L} \frac{1}{D(x)p_{eq}(x)}\, dx \left(\int_{x}^{L} p_{eq}(y)\, dy \right)^{2} + (up_{eq}(a))^{-1}. \tag{1.24}$$

Note that resemblance between Eqs. 1.24 and 1.7. Indeed, For systems with spherical symmetry and governed by Smoluchowski equation and a localized fully absorbing boundary the former reduces to the latter.

1.2.11 Predictions Of Single Reaction Coordinate Theory For Rouse Chain

SSS calculated the diffusion-controlled cyclization time ($u \to \infty$ in Eq. 1.24) for a Gaussian chain by using a single diffusion constant. For a small sink SSS model predicts $\tau \sim \frac{N^{3/2}}{Da}$ [6, 9, 49] [9, 49]. This prediction disagrees with several computer simulations and WF and RG's prediction that $\tau \propto N^2$ and independent of reaction radius. However, Toan et. al. [6] found that when a scale-dependent diffusion coefficient, instead of a constant is used the prediction of SSS theory matches those of other theories.

1.2.12 Predictions Of Single Reaction Coordinate Theory For Other Polymer Dynamics Models

The SSS model and its high barrier equivalent, Kramers rate theory [53], are regarded commonly regarded as the appropriate model for the cyclization of wormlike chain (WLC) polymers [54–57]. WLC is the standard model for the semiflexible polymer [58], polymers that show stiffness on the length scales beyond their monomer

length. The stiffness of these polymers is commonly parametrized with a persistence length, l_p, which is the length over which the directional correlation of the chain draws to $1/e$ [59]. The relaxation of these polymers is much faster than flexible chains and the local equilibrium assumption is valid for these chains [60]. In these polymers the bending energy imposes a high barrier for the cyclization. It is known [61,62] that at the high barrier limit the MFPT is equal to the inverse of the Kramers' escape rate. Kramers scape rate then yields a simple analytical formula for τ [54,60]

$$\tau \sim \frac{1}{DP'_{eq}(\alpha)} \sim \frac{1}{\alpha D G_{eq}(0)}. \tag{1.25}$$

Where $P_{eq}(r) = 4\pi r^2 G_{eq}(r)$. Note that DP'_{eq} is the steady state probability flux on the surface of the sink.

Finally, similar to WF approach, SSS's approach is based on the assumption the process is Markovian [63] and approximate reactive conformations with equilibrium reactive conformations. Recently, some authors have calculated the first passage time without Markovian assumption [24, 25, 25, 26]. It is desirable to study the effect of non-Markovian dynamics on polymer cyclization kinetics.

1.2.13 Validity Of Single Reaction Coordinate Theory For Rouse Chain

SSS model has been widely employed to interpret computer simulations and experiments. In some cases and regimes the model yields satisfactory results while in others it fails both qualitatively and quantitatively. The failure of the SSS model is commonly attributed to the local equilibrium assumption. To reduce the high dimensional dynamics of a polymer to one-dimensional Smoluchowski equation Szabo et. al. approximated the high dimensional probability density of the polymer by the equilibrium probability of internal coordinates given a certain end-to-end distance multiplied by the time-dependent probability of end-to-end distance. $p(\mathbf{r}, t) = p_{eq}(\mathbf{r}_i|r)p(r, t)$ where $\mathbf{r}_i$ is the set of all the internal coordinates (all coordinates except the coordinates of the end monomers) [63]. This assumption reduces the high dimensional diffusion equation of the chain to a one dimensional Smoluchowski equation. This

approximation is commonly referred to as the local equilibrium approximation and is thought to be valid when $\tau_m < \tau$. This validity of the this assumption is therefore depends on the polymer-solvent model, the polymer length and sink size.

A critical assumption in the passage time approach is that the survival probability behaves as single exponential $\phi(t) \sim e^{-kt}$ (i.e. is Poissonian) implying that the process has a simple first order kinetics [9, 64]. The validity of this assumption depends on the relative spacing between the eigenvalue of the Smoluchowski operator and their coefficients in the eigenvalue expansion. The eigenfunction expansion of the survival probability and mean first passage time are $\phi(t) = \sum_{i=0}^{\infty} C_i e^{-\beta\lambda_i t}$ $\tau = \sum_{i=0}^{\infty} \frac{C_i}{\beta\lambda_i}$ respectively , where λ_i are eigenvalues of the Smoluchowski operator. It is known that the spectrum of Smoluchowski equation is non-negative and in ascending order [47]. The kinetics is Poissonian when the first eigenvalue is much smaller than other eigenvalues so that the main contribution comes from the first term [64].

Recently Amitai et al. [64,65] calculated MFPT in the full conformational space of the polymer (i.e. without dimensional reduction) and found that cyclization kinetics for free and confined Rouse chain is almost Poissonian and the kinetics is dominated by single time scale, the inverse of the largest eigenvalue of the diffusion equation; $\tau \approx \frac{1}{\lambda_0}$. Amitai et al found that for $a/b \leq 1/\sqrt{N}$ the expansion of the first eigenvalue leads to the following equation for the cyclization time of a Rouse chain in 3 dimensions.

$$\tau = (\frac{N}{2D\kappa})^{3/2} \frac{\sqrt{2}}{D4\pi a} + A_3 \frac{b^2}{D} N^2 + O(1). \tag{1.26}$$

Where κ is the spring constant in the Rouse model, b the equilibrium average spring length and A_3 is a constant. This equation suggest that two different scaling relations observed for the Rouse chain originate from the expansion of the first eigenvalue. The crossover between the two scaling regimes, commonly observed in computer simulations [6,66], is determined solely by N and a. At large N the second term is dominant and $\tau \sim N^2$ in accordance with prediction based on WF approximation [7, 8] and RG [32, 34]. At smaller length the scaling is given by $\tau \sim \frac{N^{3/2}}{a}$. Note that there is no discordance with predictions Doi and RG because those predictions are valid for long chains.

1.3 Simulations

1.3.1 Simulation Methodology

Due to the inherent complexity of polymer dynamics, an analytical treatment of cyclization kinetics that takes all physical characteristics of the system into account has been elusive; the problem becomes intractable as one goes beyond infinitely long Rouse Chain with localized and perfectly absorbing sinks.

Computational techniques allow one to build more complicated and more realistic models of polymer dynamics. The time scale of polymer cyclization kinetics typically lies beyond the time scales where all-atom Molecular Dynamics is applicable and hence except polymer chain with a few monomers one has recourse to course-grained models.

It is customary to model the linear polymers as either bead-spring or bead-rod systems where each bead represents a group of chemical monomers and springs (or rods) model the physical interactions and constraints [67–71].

The simplest system for polymer dynamics is the Rouse chain; a series of N beads connected through $N-1$ harmonic springs. Each bead represent a large number of chemical monomers that interacts only with its nearest neighbors through Hookean springs. The model also ignores any interactions. Although the Rouse model ignores many features of real polymer, similar to other ideal systems in physics (e.g. ideal gas, ideal Hydrogen atom) it is the starting point upon which more sophisticated models can be built. Moreover, numerically calculated cyclization kinetics of the Rouse chain provides a benchmark to test validity of various cyclization kinetic theories [63].

The dynamics of polymer chains is commonly modeled using Brownian Dynamics [72]. Kinetic Monte Carlo methods can also be used to examine scaling [57, 66] methods. Here we give a very brief introduction to the rudiments of BD simulations. A polymer in solution collides incessantly with the solvent molecules. The total effect of the collisions is modeled by a random force and a friction force on the beads.

Additionally, each bead experiences a systematic force from its nearest neighbors. The equation of motion of each bead of mass m is governed [73] by the *Langevin Equation*,

$$m\dot{\mathbf{v}}_j = -\lambda \mathbf{v}_j + \mathbf{f} + \mathbf{g}(t). \tag{1.27}$$

Here $\mathbf{v}_j$ and $\dot{\mathbf{r}}_j$ are respectively the velocity and the acceleration of the j^{th} bead. The first term is the friction force. The second term is the systematic force which for a Rouse chain is calculated from the potential of the chain [73].

$$\mathbf{f} = -\frac{k}{2}\sum_{j=2}^{N} \nabla(\mathbf{r}_j - \mathbf{r}_{j-1})^2. \tag{1.28}$$

Where $k = \frac{3k_BT}{b^2}$ is the spring constant. The last term is a random force satisfying,

$$\langle \mathbf{g}_j(t)\rangle = 0, \quad \langle g_{j\alpha}(t) g_{k\beta}(t')\rangle = 2\lambda k_B T \delta_{jk}\delta_{\alpha\beta}\delta(t-t'). \tag{1.29}$$

Where α and β specify the vector components.

A bead collides many times during its observation time and because of the Central Limit Theorem the random force is Gaussian.Furthermore, because the collisions have no directional preference the mean force is zero. The second equation reflects the fact that forces at two different times are completely uncorrelated.

Inertia can be ignored at time scales much greater than the momentum relaxation time m/λ and Eq. 1.27 reduces to the equation for Brownian motion

$$\lambda \mathbf{v} = \mathbf{f} + \mathbf{g}(t). \tag{1.30}$$

There are various schemes for integrating Eq. 1.30 and propagating the conformations of Rouse chain in time [72]. A widely used algorithm is the Ermak-McCammon algorithm [63, 74].

$$r_j(t_{k+1}) = r_j(t_k) + f^s \delta t + \sqrt{(}2D\delta t) W_j. \tag{1.31}$$

Were W_j is the Weiner process defined as $\dot{W}(t) = \sqrt{2\lambda k_B T}\, g(t)$ [47].

In order to calculate the cyclization time the chain conformations are propagated in time until the end beads reach a certain distance of each other. Typically, the cyclization time is calculated by averaging over several simulations each starting from a initial conformation randomly sampled from equilibrium distribution.

1.3.2 Simulation Of Cyclization Kinetics For Rouse Chain

The scaling of the cyclization time with of the chain length and capture radius can be written in the general form $\tau \propto (a/b)^{\upsilon} N^{\gamma}$. Three distinct scaling regimes can be identified for the Rouse chain: For long chains (hundreds of beads) simulations suggest that $\upsilon \to 0$ and $\gamma = 2$ [6, 36, 75, 76]. This scaling is in agreement with the predictions of Wilemski-Fixman, Doi [7, 8] and de Gennes [45] [34] that for large N the cyclization time becomes independent of the capture radius and scales with the maximum relaxation time. Below $N \approx 100$ with $a/b > 1$ the dependence on the capture radius becomes stronger ($\upsilon \uparrow$) while the dependence on N remains unchanged. This regime is consistent with the predictions of the Toan's augmented SSS model [6] and WF [7]. For $a/b < 1$ the dependence on chain length becomes weaker($\gamma = 1.65-2$) and finally the SSS scaling regime ($\upsilon = -1, \gamma = 1.5$) emerges when $a\sqrt{N}/b \ll 1$ [6, 57, 63] and its predictions become exact for $N = 1$ and 2 [63]. As is apparent form Figure 1.2 that as the length of chain grows the dependence of the cyclization rate on a/b becomes weaker and approaches the asymptotic value of zero for ultra large chains. The jump in the values of υ occurs around $N \sim (a/b)^2$, in agreement with the prediction by Yang and Cao [12] and indicates a transition from $a-$dependent regime (kinetics dominated by high frequency fluctuation) to $a-$independent regime (kinetics dominated by slowest mode).

A persistent question in polymer cyclization kinetics is if the kinetics can be described by a single time scale. In other words, does the survival probability decay exponentially? Several authors answered yes to this question for Rouse chain [36, 64, 77]. Yeung and Friedman [36], for example, found that the survival probability of chains with up to $N = 800$ decay almost exponentially for $t > \tau_m$. Amitai [64] found that with $N = 16, 32$ and $a/b = 0.1$ the survival probability [36] is well-approximated by a single exponential but more exponential terms are needed for larger chains ($N = 64$) with larger capture radius($a/b = 0.4$). The general conclusion that can

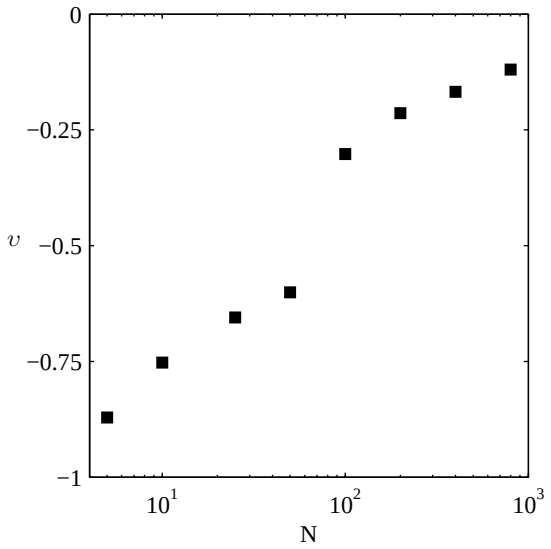

Figure 1.2. Scaling exponent, υ, of the cyclization time of Rouse chain as a function of the chain length, N [36]. The approach of υ to zero for long chains is in agreement with capture-radius-independent cyclization predicted by renormalization group theory and Wilemski-Fixman theory.

be made is that the smaller the chain length and the capture radius the better the survival probability can be fit by a single exponential.

1.3.3 Simulation Of Cyclization Kinetics For Chains With Excluded Volume And Hydrodynamic Interactions

The cyclization kinetics of more complex polymer models has also been simulated by several groups. For the Rouse chain with excluded volume simulations report $y = 2.1 - 2.4$ [6, 76–79], in satisfactory agreement with the values the prediction of RG theory $\gamma = 2.2$. Toan et. al.'s simulation [6] suggest that in poor solvent $\gamma = 1$ which indicates that the chains cyclizes much faster poor solvent than in good solvent.

For a chain with hydrodynamic interactions in theta solvent Ortiz-Repiso et. al. [76] reports $\gamma = 1.69$ for $a/b = 0.5$ and $\gamma = 1.81$ for $a/b = 1$. For a chain with both

hydrodynamic and excluded volume interactions they report $\gamma = 2$ for $a/b = 0.5$ and $\gamma = 2.23$ for $a/b = 1$ both being higher than the values predicted by RG, $\gamma = 1.764$.

1.3.4 Simulation Of Cyclization Kinetics For Worm-like Chain Polymers

Polymers exhibit backbone rigidity on various length scales depending on their molecular structure. The rigidity is commonly characterized by the persistence length l_p, formally defined as the characteristic length over which the directional correlation of the chain decays by a factor of $1/e$ [73],

$$\langle \mathbf{t}(s) \cdot \mathbf{t}(0) \rangle_{eq} = \langle cos(\theta) \rangle_{eq} = e^{-s/l_p}. \tag{1.32}$$

Where $\mathbf{t}(s)$ is the unit vector tangent to the chain contour, θ is the angel between two points on chain contour separated by s.

The statics and dynamics of chain with contour length much longer than l_p resembles that of flexible chains [80]. In the opposite extreme, chains with length much smaller than l_p are described as elastic rods [80,81]. The statics and dynamics of polymers at these regimes are analytically tractable and has been studied extensively [82]. However, the length of many polymers lie between these two extremes. These polymers are commonly referred to as semiflexible polymers and the standard model for them is the wormlike chain model [83]. In WLC model a polymer is described as an inextensible differentiable curve with harmonic bending energy [73].

In contrast to flexible polymers where cyclization time is an increasing function of chain length, WLC exhibits two distinct regimes separated by a minimum [54, 56, 60, 84, 85]. This minimum, located between 2-4 l_p emerges due to the interplay between the entropy and bending energy of the chain. For very long chains the two ends have to search through many highly probable states before they find each other. On the other hand, in very short chains a loop is highly improbable because the bending energy needed for cyclization is much greater than the thermal energy. Therefore, it takes short chains a long time to obtain this energy from the solution and cyclize. In contrast to long chains, the cyclization time of the short chains has a very strong

dependence on length and increases exponentially as the chain length approaches zero. At some point in between these two regimes the cyclization energy has a minimum for which the cyclization time is minimum (Figure 1.3).

The analytical treatment of WLC kinetics through WF theory has proven to be formidable and only tractable with unrealistic approximations such as approximating the equilibrium probability distribution of the WLC to be Gaussian [86]. SSS theory, on the other hand, is widely viewed as being capable of adequately capturing the WLC cyclization kinetics. Because the bending energy cost reduces the probable phase space of the semiflexible polymers, their relaxation time to equilibrium is short and satisfies the local equilibrium condition($\tau_m < \tau$) necessary for the validity of SSS theory. In addition, since the probability density around the capture radius is small SSS model can be simplified to Kramers rate theory. Kramers rate theory predicts a very simple relation for the cyclization time of a WLC,

$$\tau \propto \frac{1}{DP'(\alpha)}. \tag{1.33}$$

Where the prime sign denotes differentiation with respect to end-to-end distance r. SSS theory and Kramers rate theory can be collectively called single reaction coordinate theories because they reduce the kinetics to diffusion along an effective reaction coordinate.

The qualitative and quantitative agreement of WLC kinetics with the predictions of single reaction coordinate theories have been studied and the results suggest that the theory makes correct qualitative predictions over a limited range of parameter space of l/l_p and $\alpha = a/l_p$.

The results of several simulations [54, 56, 60, 84, 85] for WLC are compared in Figure 1.3. The graph indicated that SSS theory correctly predicts some of the qualitative features of the WLC cyclization kinetics; it predicts the existence of two distinct regimes and a minimum. Furthermore, it predicts the location of the minimum between 2-4 l/l_p. However, there are quantitative disagreement between SSS theory and simulations. In particular, SSS theory predicts a stronger dependence on

chain length when compared to Afra and Todd's simulation based on the a chain-length dependent diffusion constant. The explicit $\alpha-$dependence of the cyclization

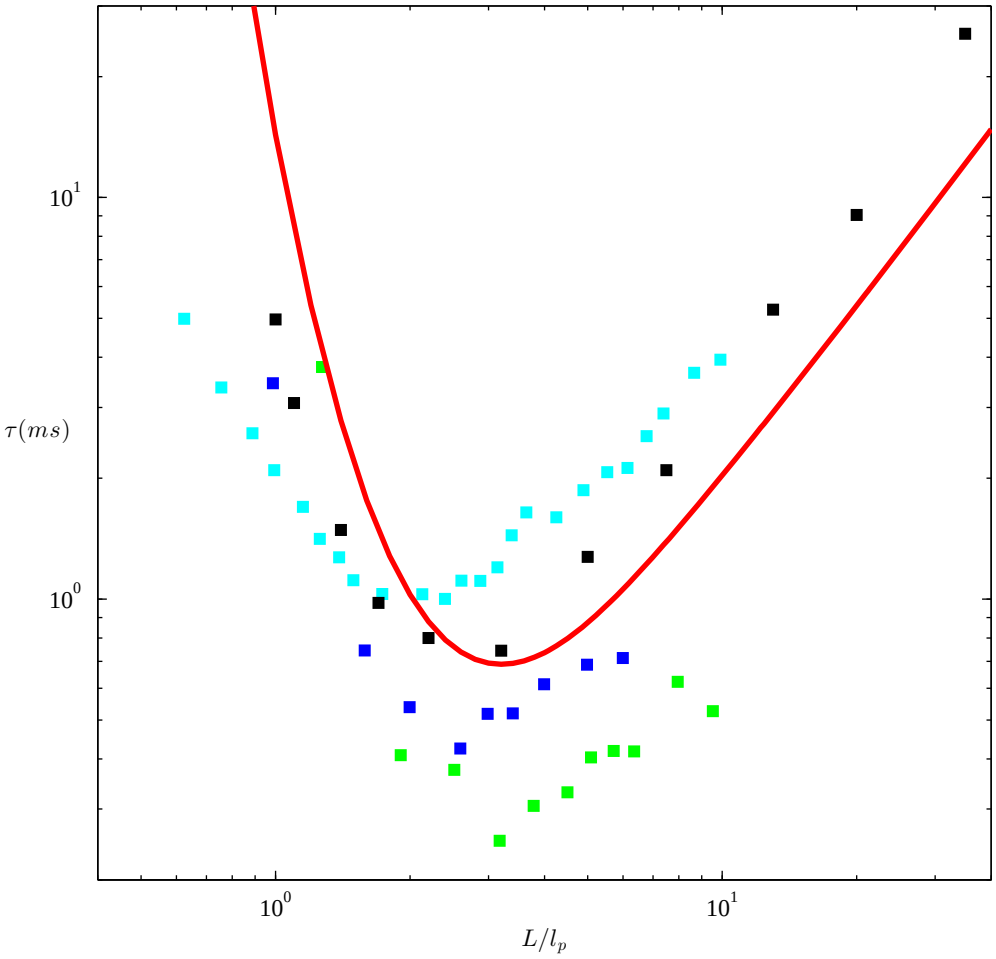

Figure 1.3. Cyclization time from several Brownian Dynamics simulations of the wormlike chain are compared with the single reaction coordinate theory(red solid line) by Szabo et. al. [9]. Data are adapted from Afra and Todd([60], black), Hyoen and Thirumalai([56], green), Chen et. al.([57], cyan) and Baleff et. al.([85], blue)

.

time in the limit $\alpha \to 0$ can be obtained by introducing the equilibrium Green's func-

tion $G_{eq}(r)$ defined by $P_{eq}(r) = 4\pi r^2 G_{eq}(r)$ in the limit $\alpha \to 0$ and Eq. 1.33 takes the form [54, 60]

$$\tau = \frac{1}{8\pi D \alpha G_{eq}(0)}. \tag{1.34}$$

$G_{eq}(r)$ is the radial probability distribution of end-to-end distance and $G_{eq}(0)$ is the loop formation probability [54, 87, 88]. $\tau \propto \alpha^{-1}$ scaling is the signature of 1D diffusion models and can used as a test for the applicability of these models for cyclization kinetics. Mixed results are reported regarding the agreement of the simulated cyclization time with 1D diffusion models based on the dependence of the cyclization time on α. While some authors [54, 57] find agreement with 1D diffusion models over a certain range of α Afra and Todd [60] found a range of α where cyclization time shows a weaker dependence on the capture radius.

These disagreeing results can be attributed to different methodology of simulations. The common approach to cyclization kinetics of WLC is to discretize the chain [70, 89–92] with bending energy between nearest neighbors and discretized the continuous time with discrete time steps. Afra and Todd have recently implemented an alternative approach and extrapolated the cyclization times obtained from the discretized time and discretized WLC to the continuum limit and found that time and space discretization leads to erroneous estimation of the cyclization time.

Additionally, some simulations [56, 84, 93] are based an indirect method in which the cyclization time is not calculated directly but it is obtained from the dissociation time of initially cyclized chains and the following approximation:

$$\frac{P(cyclized)}{P(dissociated)} \approx \frac{\tau}{\tau_{dis}}. \tag{1.35}$$

It is also worth noting that the effective diffusion coefficient of end-to-end vector in most simulations of the WLC is approximated by a constant that is fitted across the calculated cyclization times [54, 56, 84]. However, this coefficient has a weak dependence on the chain length and only for long chains it approaches a constant.

These differences between the simulation technique can account for their disagreements.

1.4 Experiments

The cyclization kinetics of synthetic [1, 94–112] and biological [113–124] polymers has been measured over the past few decades by various photo-physical methods. Commonly, polymer termini are labeled with photo-excitable probes that form encounter complexes upon end-end collision.The rate of encounter complex formation is determined by monitoring the characteristic absorption or emission of that encounter complex. Commonly the dependence of cyclization rate is measured as a function of the degree of polymerization, as measuring dependence on capture radius is much more difficult.

1.4.1 Cyclization Kinetics In Synthetic Polymers

The cyclization kinetics of synthetic polymers, in particular Polystyrene (PS) and Polyethylene Oxide (PEO) has been studied extensively. The effect of various parameters such as degree of polymerization [1, 95, 96, 106, 107, 110, 125], solvent quality [1, 96–98], viscosity [97, 98], temperature [99–102], probe size [95] and dangling ends [112] has been the subject of these studies. These studies show a wide range of scaling exponent of the cyclization rate $k \propto N^{-\gamma}$ with γ ranging from 1 to 1.9 [1, 95, 96, 106, 107, 110, 125].

Winnik pioneered using *pyrene excimer* formation [125] to investigate various aspects of polymer cyclization. In these experiments, derivatives of pyrene, a tetracyclic aromatic hydrocarbon, are attached to the ends of a polymer chain. Upon irradiation pyrene is excited and emits a blue-violet light. The pyrene in excited state can form a complex known as *pyrene excimer* upon encounter with a second pyrene in ground state through a diffusion-controlled process. Pyrene excimer has a broad emission spectra with peak in blue-green region and distinctly different from the pyrene monomer emission [94]. This red shift in the emission allows one to measure the kinetics of excimer formation via a combination of time-resolved and steady state

fluorescent measurements. By monitoring the decay of the excited monomer one can obtain the cyclization rate from Eq. 1.36 [94]

$$\langle k \rangle = \frac{1}{\langle \tau \rangle} - \frac{1}{\tau^{\circ}_{py}}. \tag{1.36}$$

Where $\langle \ldots \rangle$ denotes averaging over the distribution of chain length in a sample, $\langle \tau \rangle$ is the average lifetime of pyrene measured in time-resolved fluorescent measurement when the excited state of monomer decays through either naturally or excimer formation. τ°_{py} is the natural lifetime of the pyrene monomer [126].

The accuracy of $\langle k \rangle$ obtained from eq 1.36 becomes poor for the long chain where τ becomes the comparable to τ°. This limitation is circumvented by steady state fluorescent measurements; the cyclization rate of a long chain is determined from the cyclization rate of a short chain using the relation between the relative intensities of an excimer and a monomer for short chain(2), and long chain(1),

$$\frac{(I_e/I_m)_1}{(I_e/I_m)_2} = \frac{\langle k_1 \rangle}{\langle k_2 \rangle}. \tag{1.37}$$

Which is based on the fact that $I_e \propto k_{1\&2} I_m$ [94].

The cyclization rate measurement in theta solvent is a way to study the dynamics of polymer chains in the absence of excluded volume perturbations. Winnik measured the cyclization rate for pyrene modified PS (Py_2-PS) chains with number average molecular weight in the range $M_n = 2.9 - 99.7$ kDa ($N = 60 - 1920$) in theta solvent (Cyclohexane, 34.5 C) and found $\gamma = 1.62$ [94, 127]. An alternative method for measuring the cyclization kinetics is to decay of the triplet state of anthryl group via triplet-triplet electron transfer. In this method, chain termini are substituted with anthryl moieties instead of pyrene derivatives. Horie et. al. studied the cyclization of PS chains in theta solvent using this technique and found a biphasic behavior with $\gamma = 1.5$ for $N \leq 300$ and $\gamma = 1.0$ for $N > 300$, in disagreement with the results obtained from pyrene excimer measurements [96].

In a good solvent, one would intuitively expect to see a slower cyclization kinetics compared to theta solvent because the chain is swollen and the probability of the

Table 1.2.
The scaling coefficient of cyclization kinetics with the degree of polymerization for different polymers and solvent conditions.

Polymer	Solvent	γ	Reference
PS	Good	1.6	[103]
PS	Good	1.4	[107]
PS	Good	1.5 for $N > 300$	[96]
PDMS	Good	1.5	[110]
PS	Theta	1.6	[103]
PS	Theta	1.5	[96]

ends meeting is reduced. Winnik measured the cyclization rate of PS chains with $M_n = 3900 - 27000$(M_n is the number averaged molecular weight) and found that in toluene (good solvent for PS) $\gamma = 1.62$. It is important in these measurements to take into account the molecular weight of the end labels. Winnik found that correction for the effect of end labels reduces $\gamma = 1.62$ to 1.52. After taking into account the polydispersity of their samples this value drops to 1.35, much smaller than what is predicted by different theories [94] These findings highlighted the sensitivity of γ to polydispersity and emphasized the need for samples with very narrow length distribution. Ushiki et al 1983 introduced an alternative method and measured the cyclization rate of photo dimerization of anthryl moieties attached to the end of PS chain, anthryl$_2$-PS, in good solvent(benzene) with $N = 280 - 3000$ and found 1.4 ± 0.2 [107]. Winnik's data suggests that the cyclization rate is enhanced in theta solvent [1] while other authors have found contradictory results. For instance, Ghiggino et. al. studied the Py$_2$-PEO chains, $M_w = 1070, 1350, 3700$(M_w is the weight averaged molecular weight), and did not observed an increase in cyclization between good and theta solvents [98]. Yet Martinho [105] who studied the cyclization rate for Py$_2$-PS a mixture of cyclopentane and acetone and found that with changing the concentration

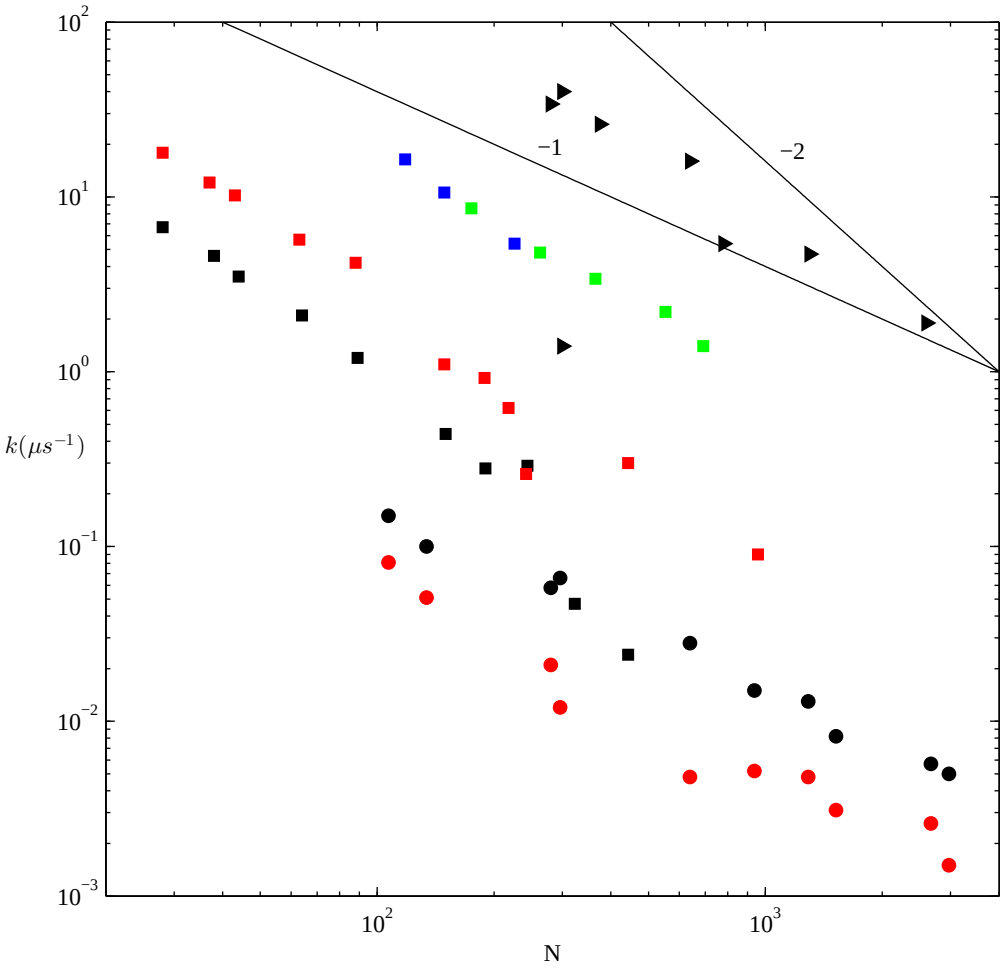

Figure 1.4. The cyclization rate for different synthetic polymers in different solvents as a function of average degree of polymerization. PS in theta solvent(red): Winnik et al. [103] (red squares), Horie et. al. [96] (red circles). PS in good solvent(black): Winnik et. al. [103] (black squares), Horie et. al. [96] (black circles), Ushiki et. al. (black triangles). And, polycarbonate [106] (blue squares) and PDMS [110] (green squares), both in good solvents.

of acetone, which causes a change in the strength of excluded volume interactions the value of γ varies, reaching a maximum near the solvent mixture with strongest excluded volume interactions.

Opposite to a good solvent, in a poor solvent a polymer chain collapses making its size much smaller than the size at theta point [37]. The comparison of cyclization of a polycarbonate chain in good (acetone) and poor (acetonitrile) solvent shows that the cyclization rate is enhanced in poor solvent [106], a finding that is supported by simulations. [6].

Another factor impacting the cyclization kinetics is the chemical composure of the monomers. While the global behavior of the chain are expected to be independent of the type of monomer, the magnitude of the cyclization rate shows dependence on monomers. For instance, a study on PDMS polymers with $M_n = 6,640 - 258,000$ kDa in good solvent suggest shows that PDMS cyclizes two times faster compared to PS in the solvent of the same solvent power and viscosity [110]. These results also show that $\gamma = 1.5$, in agreement with the prediction of WF theory for non-draining chains. This can attributed to the fact that conformational changes are more difficult for PS with bulky phenyl side groups than for PDMS.

Another important factor is dependence of the cyclization kinetics on solvent viscosity; $k_c \propto \eta^{\beta}$. As mentioned earlier, $\beta = 1$ is an indicator encounter-limited kinetics. Several studies shows that the $\beta = 1$ which indicates that the pyrene excimer formation is diffusion controlled [97, 98]. For instance, Cheung et. al. [97] studied cyclization kinetics of Py_2-PEO with polymer with $M_n = 9600$ in 12 solvents and found that in 10 out of 12 solvents $\beta = 1$.

It is expected that the cyclization rate would increase with the size of the probe relative to the size of polymer. Sinclair et. al. compared the pyrene excimer formation rate and pyrene-dimethylaniline exciplex formation rate of PS chains in a good solvent (Toluene 22°C) and observed that substitution of a pyrene with the larger dimethylaniline leads to enhanced cyclization rates [104]. Experiments on the role of probe size on the cyclization rate are scant and further work is needed to fully clarify the capture radius dependence of polymer cyclization rate.

1.4.2 Cyclization Kinetics In Nucleic Acids

Contact formation between distal segments is an elementary step in many biological processes including RNA folding, protein folding, transcriptional regulation of gene expression, chromosomal packaging and viral DNA packaging. Most biopolymers have significant backbone rigidity compared to synthetic polymers and fall into category of semiflexible polymers. Experimental studied have been conducted to measure the cyclization rate of unstructured polypeptides and ssDNA. Of special interest is the dependence of cyclization rate on the length, viscosity and sequence.

The cyclization rate of short single-stranded polynucleotides has been studied by several authors. The collision between distal nucleotides along a strand is a necessary step for the formation of hydrogen bonds between bases that leads to the formation of secondary structures [3]. The kinetics of DNA hairpin formation as the simplest nucleic acid secondary structure has been widely studied. In a pioneering work Bonnet et. al. measured the closing rate of a hairpin and found that the closing rate scales with loop length with a scaling exponent 2.6 ± 0.3 [123]. In their work they obtained that scaling based on a two state model in which the strand is considered in either closed or open state. Further studies however has shown that a two state kinetic model is inadequate to describe the hairpin loop formation due to the non-negligible time scale of stem formation [128].

The first measurement of end-to-end collision kinetics of ssDNA was performed by Wang and Nau who measured the looping rate for 2-5 nt long oligonucleotides using DBO (2,3-diazabicyclo-[2.2.2]- oct-2-ene) as fluorophore and terminal guanine base as quencher($DBO - poly(dX)_n - dG, X = dA, dC, dU or dT$) by measuring the difference between the fluorescence decay of DBO in the absence and presence of Guanine [124]. They found that the cyclization rate varies form 0.1 to $9\mu s$ (Fig. 1.5) and has strong length and sequence dependence with poly-dA exhibiting kinetics one order of magnitude slower than their polypyrimidine counterparts. This effect is attributed to the stronger base stacking interactions in polyadenylates. Due to the

short lifetime of DBO compared to oligonucleotide cyclization kinetics this method was not suitable for oligonucleotides longer than 5 nucleotides.

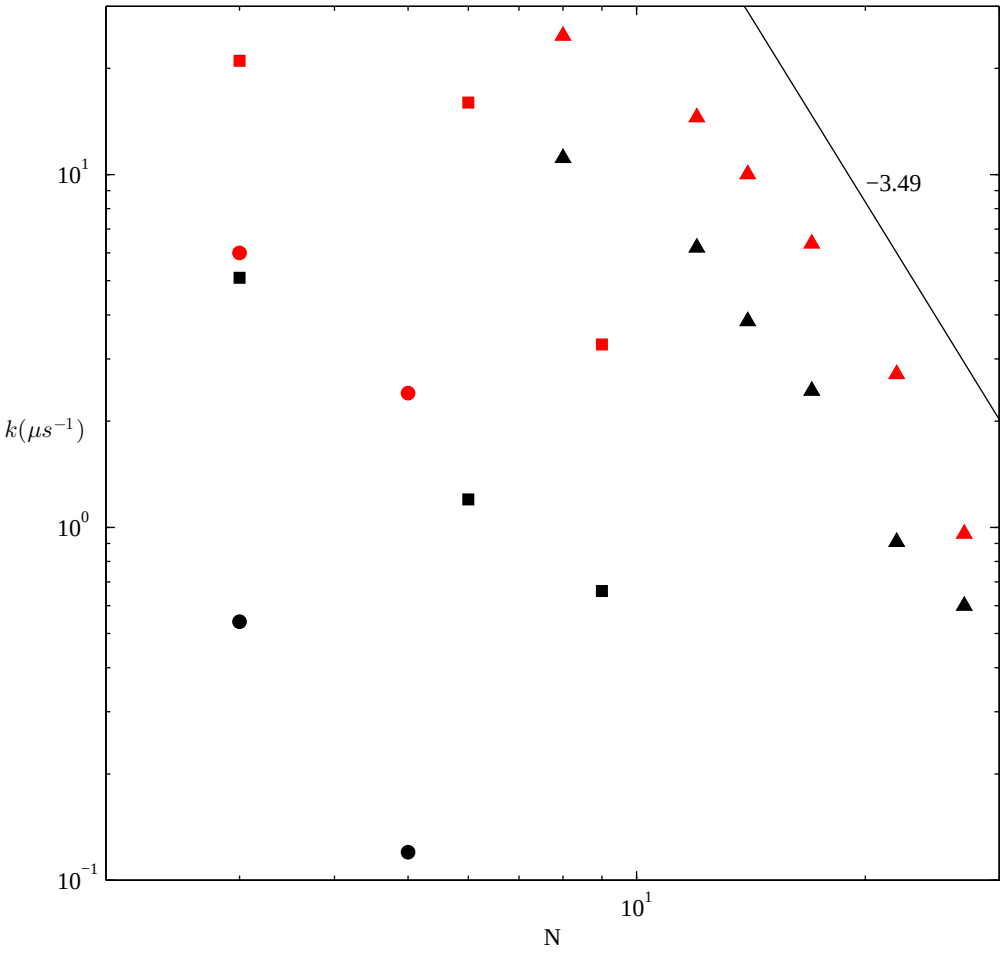

Figure 1.5. Cyclization rate of polynucleotides: red symbols represent polythymines and black symbols represent polyadenines. Data are adapted from Uzawa et. al. [121] (triangles), Kawai et. al. [120] (squares) and Wang and Nau [124] (circles).

Kawai et. al. measured the cyclization kinetics for longer oligonucleotides by monitoring the kinetics of pyrene dimer radial cation formation (Fig. 1.5) for pairs of pyrene groups attached to the ends of polynucleotides [120,129,130]. In this method one of the pyrenes tagged to the oligonucleotide is ionized to pyrene radical cation ($Py^{\cdot+}$) by two-photon ionization. Upon encounter with the ground state pyrene at

the other end the pair form a pyrene dimer radical cation ($Py_2^{\cdot+}$). Their data confirms the faster kinetics in polythymines.

Uzawa et. al. measured the cyclization rate of poly-dT in the range of 6-26 nucleotides (Fig. 1.5) using a long-lived ruthenium complex as chromophore, and DABSYL and Viologen as quencher [121]. Their data shows a biphasic behavior; week length dependence for strands shorter than 11 nucleotides and a strong, $\gamma = 3.49 \pm 0.13$, length dependence for longer strands. More recently, Uzawa et. al. has repeated their measurements with DABSYL as the quencher and found a scaling exponent of $\gamma = 3.52 \pm 0.87$ for poly-dT and $\gamma = 2.99 \pm 0.45$ for polyadenines bearing terminal thymines [122]. This length dependence is in contrast with the theoretical predictions and the measured length dependence in uncharged and unstructured polypeptides. Uzawa et al. suggest that this strong dependence is due to the non-trivial electrostatic effects which are more pronounced for relatively short oligonucleotides. They attribute the week length dependence for strands smaller than 11 nt to the effect of flexible spacer arms used to tag the DNA with luminophore-quencher pair.

It is clear form Fig. 1.5 that polythymines cyclize faster than polyadenines. This has been attributed to the stronger stacking interactions in poly(adenine) [122]. While the cyclization of polythymine is limited by entropic search through chain conformations until the ends meet, the cyclization of polyadenine requires overcoming energetic barrier of stacking interactions.

Uzawa's scaling relation contrasts that found by Qu et al who measured the cyclization rate for 2 to 16 nucleotide-long poly(thymine) protruding a dsDNA [131]. They used PET-FCS, Photo-induced Electron Transfer Fluorescence Correlation Spectroscopy and found $k \sim L^{-1.4 \pm 0.2}$, in agreement with SSS prediction for a Gaussian chain.

1.4.3 Contact Formation Kinetics In Polypeptides

Diffusion-limited contact between polypeptide segments is an elementary step in protein folding and this process sets an upper limit on protein folding [132]. Kinetics of inter-segmental contact formation has been studied extensively and the dependence of the kinetics on the number of residues [113–117], denaturant type [115, 117–119] and sequence of amino acids [116, 117] have been the subject of these investigations.

These studies show that the contact formation kinetics is dependent on the number of polypeptide bonds; the common trend in polypeptide chains with different sequences shows a biphasic behavior similar to the behavior observed in polynucleotides. For short polypeptides the cyclization kinetics is insensitive to the chain length yet it shows strong length dependence for long polypeptides. Similar to cyclization kinetics in oligonucleotides the cyclization kinetics in polypeptides is sequence dependence. Kinetic measurements on a number of polypeptides with a tryptophan-DBO (fluorophore-quencher) pair separated by six identical amino acids shows that the cyclization rate varies by as much as two orders of magnitude depending on the type of amino acid [116].

The most pronounced difference in chain-length dependence of kinetics is between the poly (glycine-serine) chains for which $\gamma = 1.36 - 1.8$ and poly(proline) where $\gamma = 4.4$. The reason for this difference is attributed to the fact that poly(proline) are significantly stiffer than their poly glycine-serine counterparts [116, 117].

While poly (glycine-serine) peptides can be characterized as flexible polymers, Buscaglia et. al. found in experiments on cysteine-(alanine-glycine-glutamine)$_j$-tryptophan, $(j = 1 - 9)$ that the chains are well described by a wormlike chain with excluded volume and a persistence length of 0.4 nm, roughly the size of an amino acid [115]. Krieger et. al. compared the cyclization rate between poly(glycine-serine) and poly(serine) polypeptide chains and found that the substitution of the flexible glycine with serine leads to slower contact formation kinetics [117].

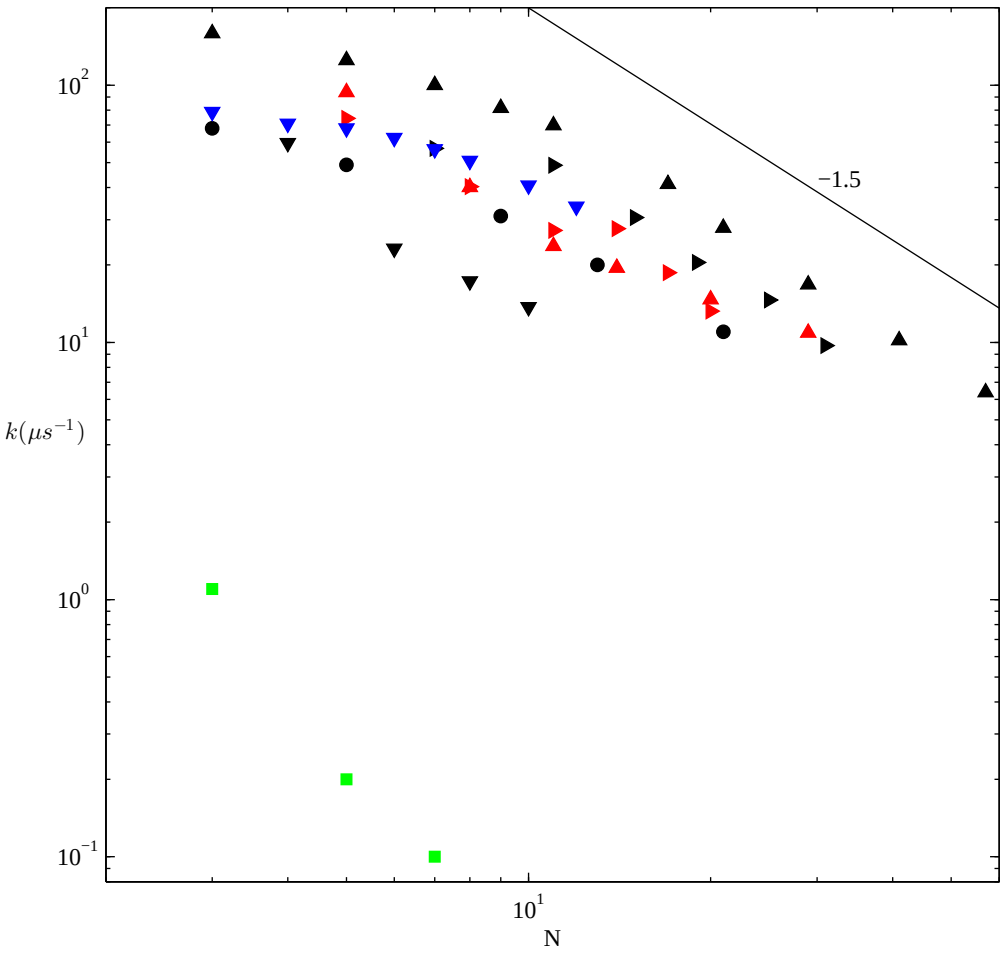

Figure 1.6. The dependence of polypeptide contact formation kinetics on the number of amino acid residue. The kinetic data for poly(glycine-serine)(black symbols,Refs. [113,116,117,133]), poly(alanine-glycine-serine) (Refs. [114, 115], red symbols), poly(serine) ([117], blue triangles) and poly(proline)([116], green squares).

Since the size of a polypeptide chain is small, it is imaginable that the long range electrostatic interactions would also alter the cyclization rate. However, the effect of charge on cyclization kinetics has been studied by changing the state of protonation of polypeptides with negatively charged (tryptophan-(aspartic acid)$_6$-DBO), positively charged (tryptophan-(lysine)$_6$-DBO) and uncharged (tryptophan-(glutamine)$_6$-DBO) backbone and minimal charge dependence was observed [116].

The presence of denaturants such as guanidine hydrochloride, ethanol and urea also affects the cyclization rate. The logarithm of cyclization rates has been shown to drop linearly with increasing the concentration of these three denaturants with rates dropping by as much as one order of magnitude in the presence of 8 M guanidine hydrochloride [117]. In a study on cysteine-(alanine-glycine-glutamine)$_j$-tryptophan it was found that the diffusion-limited rates are significantly smaller in denaturant and exhibit a steeper length dependence. Krieger et. al. found that in the presence of 8 M guanidine hydrochloride the length dependence of poly (glycine-serine) cyclization rate is slightly steeper with ($\gamma = 1.8 \pm 0.1$) compared to the cyclization in aqueous solution($\gamma = 1.7 \pm 0.1$). The kinetics measurements on polypeptides with alanine-glycine-glutamine repeating unit and tryptophan and cysteine termini showed a stronger dependence of scaling behavior on the denaturant, with $\gamma = 2.0$ in denaturing condition and $\gamma = 1.72$ in aqueous solution [115].

Most kinetics measurements of polypeptide cyclization kinetics are concerned with a system initially at equilibrium. Volk et. al. [134] studied the recombination of thiyl radicals at the end of peptides with ring initial condition, that is a nonequilibrium initial state. They found that kinetic is described by a stretched exponential $\phi(t) \sim exp(-(kt)^{\kappa})$ with $\kappa = 0.1 \pm 0.01$ and $\tau = (\kappa k)^{-1}\Gamma(-\kappa)$ different form the single exponential dependence observed for the kinetics of systems initially at equilibrium.

2. Kinetics of Loop Formation in Worm-like Chain Polymers

A common theoretical approach to calculating reaction kinetics is to approximate a high-dimensional conformational search with a one-dimensional diffusion along an effective reaction coordinate. We employed Brownian dynamics simulations to test the validity of this approximation for loop formation kinetics in the worm-like chain polymer model. This model is often used to describe polymers that exhibit backbone stiffness beyond the monomer length scale. We find that one-dimensional diffusion models overestimate the looping time and do not predict the quantitatively correct dependence of looping time on chain length or capture radius. Our findings highlight the difficulty of describing high-dimensional polymers with simple kinetic theories.

2.1 Introduction

Kramers' approach to reaction kinetics reduces the complex motion of a molecule to the diffusion of a single degree of freedom along a one-dimensional "reaction coordinate". [53] The reaction rate is then equivalent to the rate at which a diffusing particle crosses a barrier imposed by the potential energy landscape. Using this approximation, one obtains an Arrhenius equation for the special case of a high potential barrier; the general case can be solved by numerical quadrature. [48, 135]

Because of its pervasiveness, it is important to identify the limitations of Kramers' approach. When is it impossible to model reaction kinetics by 1D diffusion along an effective reaction coordinate? A well-studied example concerns the kinetics of reactants attached to flexible polymers, first described by Wilemski and Fixman. [7] In its simplest form, this problem involves reactive groups attached to each end of a polymer. A reaction occurs when the ends come close together, giving the polymer the form of a "loop". The difficulty in predicting this looping rate, from the perspective of

Kramers' rate theory, is that the polymer exhibits a spectrum of diffusional timescales, all of which matter in the overall rate of loop formation. [8] And, after many attempts, [6, 9, 64, 114] it still seems impossible to coarse-grain the flexible polymer looping problem down to a 1D diffusion model *à la* Kramers' approach. [36, 63, 66, 75, 77]

In this paper, we consider polymer looping kinetics, not for flexible polymers, but for a polymer model that includes bending stiffness called the worm-like chain (WLC). The WLC polymer model is often used to describe biopolymers, such as DNA [136] and polypeptides. [114] Applications of looping occur in the regulation of gene expression [137] and in the kinetics of protein folding. [114, 138] WLC looping kinetics were considered previously [54, 56, 57, 84, 139, 140] and it was concluded that WLC looping kinetics can be described by 1D diffusion models. [54, 56, 57, 84, 140] The rationale for this distinction from flexible polymers, as given by Jun et al. [54] and Hyeon et al. [56], is that stiffness in the WLC reduces the probability of looping, allowing the polymer time to completely establish "local equilibrium" along the reaction coordinate.

We reconsidered this problem, using Brownian dynamics simulations to confront the predictions of Kramers' rate theory for a high barrier and a more general treatment given by Szabo, Schulten, and Schulten (SSS theory). [9] We will collectively refer to these theories as "1D diffusion models" because the salient feature of this class of models is that they reduce molecular motion to a single-degree of freedom that is explored on a single time scale. We find that 1D diffusion models, while predicting reasonable qualitative trends, cannot quantitatively describe the dependence of looping time on chain length or capture radius. It seems that, similar to the case for flexible polymers, [8] the spectrum of WLC diffusional timescales matter in the rate of loop formation.

The paper is arranged as follows. In Section II we state the problem. In Section III we briefly introduce the WLC model and describe the basic length and time scales that are employed throughout the paper. In Section IV the details of the Brownian dynamic simulation are discussed. Section V reviews 1D diffusion models. Section V

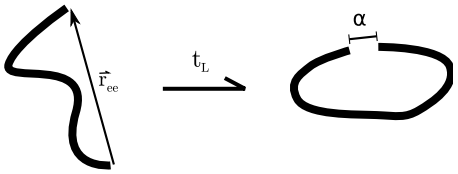

Figure 2.1. We consider the time required for a thermally average WLC polymer to diffuse into a configuration where the end-to-end vector, $\vec{r}_{ee}$ has a small length α, called the capture radius. In this configuration, the polymer has the form of a loop, so, the average time is referred to as the "looping time", t_L.

also describes the details of computing an effective diffusion coefficient for 1D diffusion models. The looping times from the Brownian dynamics simulations and 1D diffusion models are compared in Section VI.

2.2 Problem Statement

In this paper, we characterize the average time required for the two ends of a WLC polymer to diffuse to within a small separation, α, referred to as the capture radius (Fig. 2.1). In this configuration, the polymer has the form of a "loop", so, we refer to this average time as the "looping time", t_L. In experiments or polymer processes where a polymer contains reactive ends, t_L corresponds to the average time required for the formation of looped molecules.

2.3 WLC Polymer Model

The WLC is a polymer model that describes a continuous inextensible rod with potential energy due to bending. The WLC model is useful for describing real polymers that exhibit stiffness over length scales much larger than the monomer length. Prominent examples include: double-stranded DNA, [136] RNA, [141] actin, [142] collagen, [142] clatherin [143], carbon nanotubes [144] and polyanaline. [145] The

bending elasticity of WLC is parametrized by the persistence length, l_p. Many excellent textbooks [59] and reviews [58, 146] describe the WLC in detail and so, we do not repeat those descriptions here.

We non-dimensionalize the WLC model using the following length and time scales. All lengths are relative to the worm-like chain persistence length, l_p. All diffusion coefficients presented are relative to D_{l_p}, defined as the translational diffusion coefficient for a WLC with contour length equal to one persistence length. l_p and D_{l_p} together define a time-scale, $t_{l_p} \equiv l_p^2/D_{lp}$. All times presented in the paper are relative to t_{l_p}.

In order to obtain predictions for a particular WLC polymer our results need only be scaled by these quantities. For instance, in Fig. 2.5, we find that for a WLC contour length of $L = 2.2$ and a reaction radius $\alpha = 0.1$ the average looping time is $t_L \approx 10$. For double-stranded DNA, $l_p \approx 50$ nm, and $D_{lp} \approx 30$ μm^2/s, [147] so, this predicts for a 110 nm length DNA and a 5 nm reaction radius the looping time for DNA would be 800 μs.

2.4 Brownian Dynamics Simulations

We employed numerical Brownian dynamics simulations to estimate the WLC looping time. We consider the looping time calculated using this procedure to be accurate. Precision is limited only by the available computational resources. Our simulations were run on 72 cores from the Rossmann computer cluster operated by Rosen Center for Advanced Computing at Purdue University over a period of several months.

Our WLC Brownian dynamics simulation is identical to the simulation described by Wang and Gao. [70] Wang et al.'s algorithm was, in turn, derived from that of Jian and Vologodski [89] but augmented to include an inextensibility constraint. [148] We omit hydrodynamic interactions from our simulation in order to limit the number of model parameters. We verified our implementation of Wang et al.'s simulation by reproducing Ref. [70] Figures 3(a) and 7(a) and Ref. [89] Figure 6 and Table II.

Each simulation begins with a thermally averaged WLC configuration that is discretized along the polymer contour length at distances of Δl. The polymer configuration is propagated forward in time using Brownian dynamics until the distance between the two ends of the polymer is below the capture radius, α. This produces one realization of the looping time. An average looping time, t_L is obtained by repeating this procedure starting from approximately 300 different WLC configurations drawn from the equilibrium distribution.

The average looping time, t_L calculated by Brownian dynamics has a pronounced dependence on the discretization step-size, Δl (data shown in Appendix 2.9.1). This should be expected as polymer looping kinetics are sensitive to the *smallest* time scales exhibited by the polymer. [8] The discrete approximation to the WLC used in Brownian dynamics simulations truncates the infinite relaxation spectrum of the continuous WLC model and imposes an arbitrary smallest time scale. We recover the continuum limit by simulating with increasingly smaller Δl and then extrapolating to $\Delta l = 0$. This extrapolation procedure is described in detail in Appendix 2.9.1. Looping times for discrete approximations to the WLC were obtained previously. [56, 57, 140] We are the first to obtain the looping time for the continuous WLC.

2.5 1D Diffusion Models

A persistent theme in polymer looping theory is the extent to which the polymer looping time can be approximated by a single-degree of freedom diffusing along a 1D reaction coordinate given by the polymer end-to-end distance(Ref. [6] and references therein). This 1D diffusion approximation is akin to Kramers' approach to chemical reaction kinetics where multidimensional molecular motions are projected onto a single reaction coordinate explored on a single time scale. Many applications of Kramers' rate theory make an additional simplification that the rate limiting step involves a potential barrier much larger than the thermal energy. However, this simplification is not strictly necessary within the 1D diffusion approximation. Below we first describe

general solutions for the 1D diffusion approximation to the polymer looping problem and then introduce the high barrier approximation in order to obtain a Kramers' rate equation.

2.5.1 SSS Theory

Polymer looping can be phrased as a first passage time problem; we seek the time required for the polymer end-to-end distance to first passage to a value smaller than the capture radius. The formal solution to the first passage time problem for a continuous-time Markov process governed by a Fokker-Planck equation with one degree-of-freedom was obtained by Pontryagin et al. [48, 135] The solution yields a quadrature for the average time required for a particle initially at x, such that $a < x < l$ with a reflecting boundary at l and an absorbing boundary at a to leave the domain by being absorbed at a, [48]

$$t(x) = \int_a^l \frac{1}{DP_{eq}(x)}\, dx \int_x^l P_{eq}(y)\, dy. \tag{2.1}$$

P_{eq} is the equilibrium probability density and D is the particle diffusion coefficient.

This solution was first applied to polymer looping by Szabo et al. [9] They assumed that the location of the absorbing boundary is the capture radius $a = \alpha$. All subsequent treatments of this problem incorporated this assumption. [6, 56, 57, 63, 84] For the WLC, the location of the reflecting boundary is given by the maximum extension of the polymer (the inextensible contour length) $l = L$. This yields an equation,

$$t(x) = \int_\alpha^L \frac{1}{DP_{eq}(x)}\, dx \int_x^L P_{eq}(y)\, dy. \tag{2.2}$$

In order to obtain the average looping time, Eq. 2.2 is then averaged over the equilibrium distribution of end-to-end distances, $t_L = \int_\alpha^L t(x) P_{ex}(x) dx$, to obtain,

$$t_L = \int_\alpha^L \frac{1}{DP_{eq}(x)}\, dx \left(\int_x^L P_{eq}(y)\, dy \right)^2. \tag{2.3}$$

Because this solution was first applied to polymer looping by Szabo, Schulten, and Schulten, Eq. 2.3 has come to be known as "SSS theory" in the polymer literature.

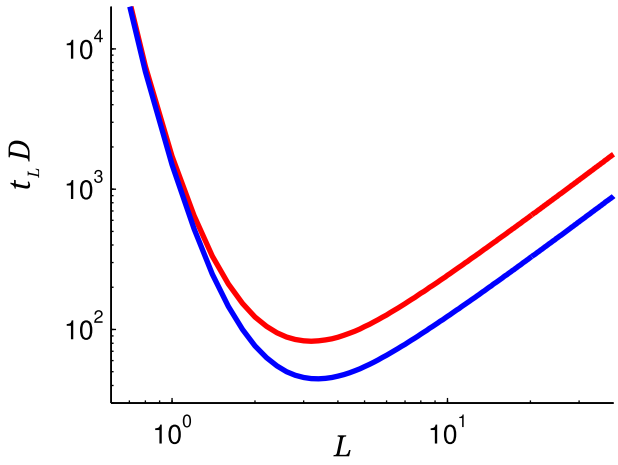

Figure 2.2. WLC looping times from single-particle reaction-diffusion models. The looping time vs. chain length for SSS theory (red line, Eq. 2.3) and Kramers approximation (blue line, Eq. 2.4). Kramers approximation approaches SSS theory in the limit of small L. For large L, Kramers approximation underestimates SSS theory by a factor of 2.

We evaluate Eq. 2.3 numerically as a function of WLC length using $\alpha = 0.1$ (red line, Fig. 2.2).The equilibrium probability density, P_{eq} was obtained from values tabulated by Mehraeen et al. [149]

2.5.2 Kramers Rate Theory

Equation 2.3 can be simplified *à la* Kramers' rate theory when the probability density around α is small (equivalently the potential barrier at α is high). This approximation, derived in Appendix 2.9.2, simplifies Eq. 2.3 to give,

$$t_L \approx \frac{1}{DP'_{eq}(\alpha)}. \tag{2.4}$$

where P'_{eq} is the derivative of the equilibrium probability density with respect to the polymer end-to-end distance. We evaluated Eq. 2.4 as a function of WLC length with $\alpha = 0.1$ (blue line, Fig. 2.2). This Kramers approximation approaches SSS theory in the limit of small WLC contour length, $L \to 0$. As L becomes large, Eq. 2.4 systematically underestimates the looping time predicted by Eq. 2.3 by a factor of 2.

Because we are interested in the extent to which the 1D diffusion models can describe the polymer looping rates and not the high barrier approximation *per se*, we do not consider Eq. 2.4 further. All subsequent comparisons between the Brownian dynamics simulations and the 1D diffusion models will be made using the more accurate SSS theory, Eq. 2.3.

2.5.3 Effective Single Particle Diffusion Constant

In order to compare predictions from the 1D diffusion models with Brownian dynamics simulations, the diffusion coefficient, D, in Eq. 2.3 and Eq. 2.4 must be specified. This problem has been discussed previously [6] and D is often assumed constant [9] and fitted to simulation data across some range of polymer lengths. [54, 56, 84] More recently, Toan et al. [6] pointed out that D should not be assumed constant but should correspond to the value that characterizes the diffusive relaxation of the polymer end-to-end vector, for a particular length. Using this procedure they are able to extend the validity of the 1D diffusion models in the calculation of a looping time for flexible polymers.

We follow Toan et. al.'s approach to this problem and extract a single diffusion constant, D_{ee} that approximates the relaxation of the WLC end-to-end fluctuation,

$$\langle \delta \vec{r}_{ee}^{\,2}(\Delta t) \rangle = \langle [\vec{r}_{ee}(t + \Delta t) - \vec{r}_{ee}(t)]^2 \rangle. \tag{2.5}$$

by a single exponential relaxation,

$$\langle \delta \vec{r}_{ee}^{\,2}(\Delta t) \rangle \sim \langle \langle \delta \vec{r}_{ee}^{\,2} \rangle \rangle (1 - e^{-\Delta t / t_{ee}}). \tag{2.6}$$

Single brackets indicate averaging over t; double brackets indicate averaging over both t and Δt. t_{ee} is characteristic relaxation time of the end-to-end vector. Jun et al. [54] have given a useful interpolation for t_{ee},

$$t_{ee} = \frac{2}{3\pi^2} \frac{L^4}{\left(\frac{\pi}{4}\right)^2 + L^2}. \tag{2.7}$$

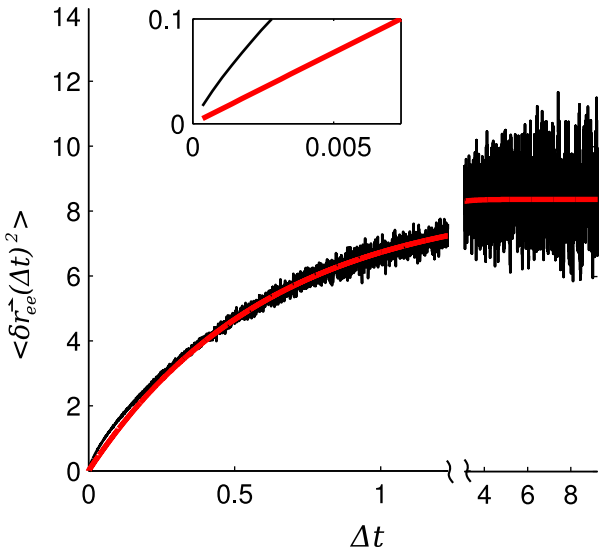

Figure 2.3. In SSS theory, relaxation of the polymer end-to-end vector is approximated by a single diffusion coefficient, D_{ee}, defined by Eq. 2.8. We extract D_{ee} from numerical simulations of the WLC conformational fluctuations. This example corresponds to $L = 3.2$. The simulated end-to-end autocorrelation (black line) is well-characterized by a single exponential relaxation (red line, Eq. 2.6) *except* in the limit $\Delta t \to 0$ (inset).

The diffusion coefficient corresponding to Eq. 2.6 (1/6 of the slope in the limit $\Delta t \to 0$) is,

$$D_{ee} = \frac{\langle\langle \delta\vec{r}_{ee}^2 \rangle\rangle}{6t_{ee}}. \tag{2.8}$$

This definition of D_{ee} differs only slightly from Toan et al.'s (see Ref. [6], Eq.9). When applied to a system that is truly characterized by a single diffusion coefficient, the definition of D_{ee} in Eq. 2.8 yields the correct diffusion coefficient. We verified this using simulations of two particles connected by a harmonic spring (not shown).

Figure 2.3 compares $\langle \delta\vec{r}_{ee}^2(\Delta t) \rangle$ obtained from a WLC Brownian dynamics simulation (black line) with a single exponential relaxation (red line, Eq. 2.6). $\langle\langle \delta\vec{r}_{ee}^2 \rangle\rangle$ in Eq. 2.6 is obtained from the limiting value of $\langle \delta\vec{r}_{ee}^2(\Delta t) \rangle$ at large Δt. t_{ee} is the time at which $\langle \delta\vec{r}_{ee}^2(\Delta t) \rangle$ draws within a factor of e^{-1} of $\langle\langle \delta\vec{r}_{ee}^2 \rangle\rangle$. While, at first glance, Eq. 2.6 provides a good description of the WLC autocorrelation function (red line is

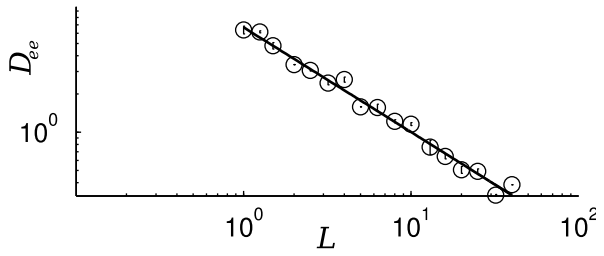

Figure 2.4. D_{ee} for different WLCs lengths. The relationship between D_{ee} obtained by simulation simulation (symbols) and WLC contour length can be described to the empirical relation, $D_{ee}(L) = 6.69/L^{0.825}$ (line).

similar to black line), it is clear that the single exponential relaxation differs from the WLC in the limit $\Delta t \to 0$ (inset in Fig. 2.3). The behavior of end-to-end fluctuations in this limit plays an important role in the scaling behavior of the looping time with capture radius. [8, 150] The fact that the WLC curve is steeper at small Δt and later converges to the single-exponential relaxation reflects the fact the WLC polymer end-to-end vector undergoes *anomalous sub-diffusion*. [81]

D_{ee} depends on the WLC length. At each length, we obtained D_{ee} for increasingly finer discretization of the WLC contour length and then extrapolated to the continuum limit, as described in Appendix 2.9.1. The end-to-end diffusion coefficients obtained in this manner for different lengths are shown in Fig. 2.4. Over the range of lengths considered, $1 \leq L \leq 40$, the relationship between D_{ee} and L could be described by (Fig. 2.4, solid line)

$$D_{ee}(L) = 6.69/L^{0.825}. \tag{2.9}$$

We use this empirical relation to obtain the single time scale predictions of the looping time from Eq. 2.3 at different lengths.

2.6 Predictions of The Looping Time

Predictions of the looping time, t_L as a function of polymer length, L at fixed capture radius, $\alpha = 0.1$ are presented in Fig. 2.5. Mean values from the Brownian

dynamics simulations are the black symbols; error bars represent the standard error of the mean (described in detail in Appendix 2.9.1). Also plotted are the predictions of SSS theory, Eq. 2.3 with D given by Eq. 2.9 (solid red line). SSS theory overestimates the looping time by factors > 3.To examine the scaling behavior of SSS theory, we divided SSS theory by an *ad hoc* factor of 3 (dashed red line). This matches the predictions of the Brownian dynamics simulations to within simulated precision over a limited range, $1.4 < L < 3.2$. Outside this range—both at smaller and larger L there are discrepancies between Brownian dynamics simulations and the predictions of SSS theory. SSS theory predicts a dependence on length that is stronger than what is observed in the simulations. On Fig. 2.5, we also indicate the polymer relaxation time, t_{ee}, obtained from simulations (blue squares) as well as those predicted by Eq. 2.7 (blue line). All of the simulated looping times exceed the polymer relaxation time.

We also investigated the dependence of the looping time, t_L on capture radius, α at fixed WLC contour length $L = 2.2$ (Fig. 2.6). Mean looping times from the Brownian dynamics simulations are the black symbols; error bars represent the standard error of the mean. Predictions based on SSS theory, Eq. 2.3 with D given by Eq. 2.9 again overestimate the looping time by a factor of 3 (solid red line). Dividing SSS theory predictions by the *ad hoc* factor of 3 we obtain agreement with the Brownian dynamics simulations for $\alpha > 0.1$ (dashed red line). For $0.025 < \alpha < 0.1$, the simulated looping times exhibit a weaker dependence on capture radius than predicted by SSS theory. As α decreases, SSS theory increasingly overestimates the looping time. For the smallest values of $\alpha < 0.025$, the dependence of the looping time on capture radius is consistent with the $t_L \propto \alpha^{-1}$ scaling expected for SSS theory (red dashed line), or, *any* 1D diffusion model in the limit $\alpha \to 0$ (green line)(cf. Appendix 2.9.2). Also, plotted is the relaxation time for the polymer, t_{ee}, from Eq. 2.7 (blue line). With the exception of the largest α value, all of the simulated looping times exceed the polymer relaxation time.

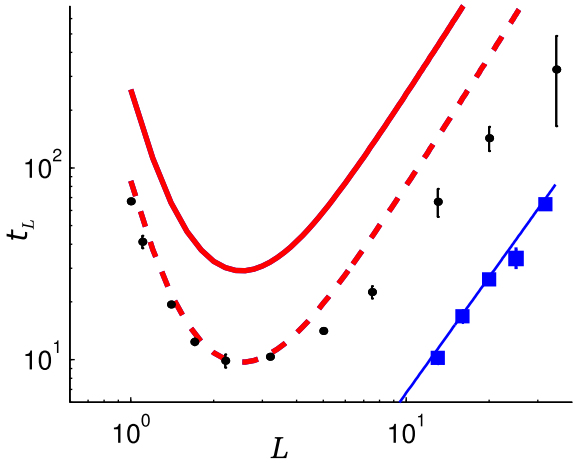

Figure 2.5. Looping time vs. WLC length at fixed capture radius, $\alpha = 0.1$. Brownian dynamics simulations (black symbols and error bars) are compared to SSS theory (solid red line). SSS theory overestimates the looping time by factors > 3. If we arbitrarily divide the predictions of SSS theory by 3 (dashed red line), we can obtain agreement with the simulation to within simulated precision in the range $1.4 < L < 3.2$. Discrepancies exist both at small L and large L. SSS theory predicts a dependence on length that is stronger than what is observed in the simulations. Also, shown are the polymer end-to-end relaxation times, t_{ee}, obtained from Brownian dynamics simulations (blue squares) and predicted by Eq. 2.7 (blue line).

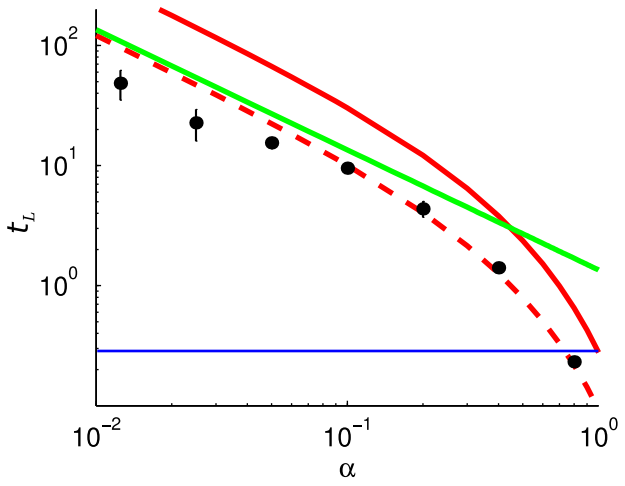

Figure 2.6. Looping time vs. reaction radius at fixed WLC length, $L = 2.2$. Brownian dynamics simulations (black symbols and error bars) are compared to SSS theory (solid red line). The SSS theory overestimates the looping time by factors > 3. If we arbitrarily divide the predictions of the SSS theory by 3 (dashed red line), we can obtain agreement with the simulation to within simulated precision for $\alpha > 0.1$. Also, plotted for comparison is the $t_L \propto \alpha^{-1}$ scaling relation (green line) that would be expected for *any* 1D diffusion model in the limit $\alpha \to 0$. The simulated WLC looping times include a region, $0.025 < \alpha < 0.1$, with weaker dependence on reaction radius than predicted by SSS theory. Also, indicated is the relaxation time, t_{ee} predicted by Eq. 2.7 (blue line).

2.7 Discussion

We used Brownian dynamics simulations to obtain looping dynamics for the WLC and explored the extent to which WLC looping dynamics could be described by SSS theory. SSS theory is an exact solution to the first passage time problem *for a single degree of freedom* and should therefore represent the ultimate accuracy that can be obtained from any 1D diffusion model; an example of a less accurate 1D diffusion model would be Kramers rate theory for a high barrier.

As previously reported, [54, 56, 84] we find that 1D diffusion models predict a dependence of looping time on WLC contour length that shares qualitative features with the Brownian dynamics simulations: there exists a minimum looping time at $L \sim 2-4$ and looping time increases sharply for short chains and increases weakly for long chains. The 1D diffusion models predict a qualitatively similar dependence of the looping time on capture radius over two orders of magnitude in capture radii. More quantitatively, we find that SSS theory everywhere overestimates the looping rate by at least a factor of 3. Dividing the predictions of SSS theory by an *ad hoc* factor of 3 reduces the discrepancy but cannot attain quantitative agreement between the predictions of SSS theory and the simulation results; SSS theory predicts a stronger dependence of the looping time on both WLC contour length and capture radius, as compared to the Brownian dynamics simulations. We conclude that the WLC looping dynamics cannot be described quantitatively over the range of parameters investigated here by a 1D diffusion model. This is reminiscent of Wilemski's and Fixman's finding for flexible polymers. [11] However, the effects are more subtle in the case of WLC polymers, as compared to flexible polymers.

This is the first work to describe the discrepancies between WLC looping dynamics and 1D diffusion models. Indeed, previous work on WLC chain looping drew the opposite conclusion; that is, that SSS theory could adequately capture WLC looping dynamics. [54, 56, 57, 84] Some of this discordance can be understood by considering the range of parameters that were investigated. Chen et al. [57, 66] and Klenin et

al. [84] for instance, both considered a narrower range of α than we considered. As seen in Fig. 2.6, scaling consistent with SSS theory can be seen within limited parameter ranges, though SSS scaling does not generally hold. Jun et al. [54] concluded that there is agreement between Kramers rate theory and Brownian dynamics simulations for short chains. However, their data are in agreement with ours, i.e. they show that Kramers rate theory predicts a stronger dependence of looping time on WLC length than what is observed in simulations; discrepancies for short chains were as large as three orders of magnitude (see Ref. [54], Fig. 2). We therefore presume that Jun et al.'s conclusion that Kramers rate theory adequately describes WLC looping is meant only in the same qualitative sense that we mentioned above. Finally, Hyeon et al. [56] employed Podtelezhnikov and Vologodskii [140] approach to calculate looping rates and used these calculations to validate Kramers rate theory. They find agreement over a range of contour lengths of $l_p < L < 10l_p$. We do not understand why these results are different from our own and from Jun et al.'s. One possibility is that Podtelezhnikov's method does not simulate the looping time directly but rather estimates it based on the simulated *unlooping* time and the equilibrium probability for the looped DNA conformations. It was recently pointed out that the distribution of configurations upon flexible loop formation is not representative of the equilibrium distribution, [26] perhaps calling into question Podtelezhnikov's approach for calculating the looping time. Since this same procedure was used by Hyeon et al. to validate Kramers rate theory, this may account for the discrepancy between their findings and our own.

Our finding that the WLC looping time includes a region that depends more weakly on reaction radius than predicted by 1D diffusion models is consistent with the known anomalous sub-diffusion of the WLC end-to-end vector. [81] It is only for simple Fickian diffusion that diffusion-limited kinetics exhibit the scaling characteristic of the 1D diffusion models, $t_L \propto \alpha^{-1}$. For anomalous sub-diffusion with mean-square displacement proportional to t^β, one expects a reaction time to scale with reaction radius as, $\alpha^{2/\beta - N}$, where N is the number of spatial dimensions. [8,150] Analysis of the

WLC end-to-end diffusion for short chains suggests that the exponent characterizing the WLC anomalous sub-diffusion is $3/4 \leq \beta \leq 7/8$. [81] In this case, the expected scaling of looping time would range from $t_L \propto \alpha^{-1/3}$ to $t_L \propto \alpha^{-5/7}$. This range is consistent with our observation of a weak dependence of looping time on capture radius for $0.025 < \alpha < 0.1$ in Fig. 2.6.

We showed that predictions of 1D diffusion models everywhere overestimate the time required for a WLC to form a loop. We suggest that this discrepancy can be partially rescued by selecting the capture radius for 1D diffusion model differently. In previous work, [6, 56, 57, 63, 84] this capture radius has been taken to be equal to the physical capture radius in the polymer looping problem. However, 1D diffusion models coarse-grain the polymer dynamics up to the slowest relaxation time of the polymer end-to-end distance. During this time, the faster modes of the polymer will move the ends of the polymer very rapidly and cause the polymer ends to explore a larger volume than is given by the physical capture radius. [8] In order for the course-grained description to be consistent with the actual polymer, the volume explored by the omitted relaxation modes should define an effective capture radius for the 1D diffusion level of description, rather than simply using the physical capture radius for the polymer looping problem. *For the parameters considered here*, the factor of 3 required to reconcile SSS theory with the WLC simulations suggests the effective reaction radius is approximately a factor of 3 times larger than the physical capture radius.

Previous work has argued that 1D diffusion models should adequately describe polymer looping dynamics provided that the looping time exceeds the relaxation time of the polymer ("local equilibrium"). [6,54,56,63] With the exception of the largest α value in Fig. 2.6, this condition is satisfied for all of the simulation conditions that we considered here. Yet, we see significant differences between WLC Brownian dynamics simulations and the predictions of 1D diffusion models. We therefore conclude that the local equilibrium condition, as it is currently understood, is not a sufficient condition

for obtaining quantitatively accurate predictions of the WLC looping time from 1D diffusion models.

One possible remedy for this would be to assert that the current criteria for local equilibrium is not stringent enough. That is, perhaps it is not sufficient for the reaction time to simply exceed the relaxation time but instead, that the reaction time must exceed the relaxation time *many fold*. In order to exclude the region of our results where WLC simulations and SSS Theory are discrepant, the local equilibrium criteria would need to exceed the reaction time by 78-fold. However, we do not favor this interpretation. Firstly, previous work has shown that a cross-over in scaling behavior occurs where the looping time is approximately equal to the polymer relaxation time. [54,57,66] Secondly, the discrepancies that we observe between WLC looping times and the 1D diffusion models in Fig. 2.6 at $0.025 < \alpha < 0.1$ occur in an intermediate region, sandwiched between two regions that exhibit the capture radius dependence predicted by SSS theory (albeit with different prefactors). For this reason, we believe that the discrepancies that we observe are related to additional necessary conditions, unrelated to "local equilibrium". One additional necessary condition may be that the effective capture radius needs to accurately reflect the volume explored by the degrees of freedom that are frozen out upon coarse-graining to the 1D diffusion model. How precisely to determine this effective reaction radius remains unclear. Brownian dynamics simulations will therefore continue to be an important tool for checking the validity of simplified kinetics models.

There are no experimental measurements of the looping kinetics of semiflexible polymers with which to compare our results. Lapidus et al. measured the looping kinetics of polypeptides. [114] Polypeptides, however, have persistence lengths that are only a few times larger than the length of a single chemical bond ($l_p \sim 0.6$ nm). Polypeptides are therefore not well-described by the WLC model which requires many degrees of freedom within a single persistence length. Since it is these underlying degrees of freedom that give rise to the discrepancies between WLC kinetics and the predictions of 1D diffusion models, we would not expect such effects to be apparent

in Lapidus et al.'s data on polypeptide looping. We are not aware of any additional experimental studies where looping kinetics of a model WLC polymer, such as DNA, have been measured.

We can make several predictions regarding the results of future experimental measurements of WLC looping kinetics. Firstly, if the looping rate of a WLC were measured over a sufficient range of capture radii, then we would expect that the looping rate would include a regime that scaled more weakly than the $t_L \propto \alpha^{-1}$ scaling predicted by 1D diffusion models. If instead, the chain length dependence of the looping rate were measured, then we predict that the experimental length dependence would be weaker than predicted by 1D diffusion models. This effect exists for both short ($L < 3l_p$) and long chains, although, the effects are more subtle and will be more difficult to resolve for short chains. A much more dramatic comparison could be made if the microscopic parameters for the reaction namely, the diffusion coefficient, capture radius, and persistence length were known independent of the looping rate. In this case, the *a priori* predictions of 1D diffusion models based on the microscopic parameters would overestimate the looping time by a substantial margin ($3\times$ for the parameters considered here). Any of these effects would indicate that the WLC contains a spectrum of degrees of freedom that contribute substantially to the kinetics of diffusion-limited reactions.

2.8 Conclusions

We evaluated the accuracy of 1D diffusion models for describing the looping dynamics of the WLC polymer model. One-dimensional diffusion models characterizes the time evolution of the chain configuration with a single time scale and leave out the fast motions of the polymer. Our results show that ignoring the short time motion leads to overestimation of the looping time and a distortion of scaling with both length and capture radius. We suggest that the introduction of an effective reaction

radius that accounts for the volume explored by the short time motions may rescue the 1D diffusion models.

2.9 Appendix

2.9.1 Extrapolating Brownian Dynamics Simulations To The Continuum Limit

Our Brownian dynamics simulations approximate the WLC with discrete contour segments and continuous time with discrete time steps. [70] In order to recover the continuum limits, we simulate with increasingly smaller contour segments, Δl and extrapolate our results for different Δl to the limit $\Delta l \to 0$. Our simulation time step, Δt is proportional to Δl so, this extrapolation also approaches the limit of continuous time.

Extrapolation to the continuum limit seems particularly important in polymer looping calculations because polymer looping times can be dominated by the *smallest* relaxation times exhibited by the polymer; [8] simulations truncate the relaxation spectrum by imposing an arbitrary smallest relaxation time and therefore might be expected to alter the predictions of the model, as compared to the usual continuous WLC. In addition, Brownian dynamic simulations are known to overestimate first passage times and converge rather slowly to the continuum limit (usually as $\sqrt{\Delta t}$). [151] Finally, inextensibility can be modeled only approximately in Brownian dynamics simulations. [148] The error in this constraint also vanishes as $\Delta l \to 0$. To our knowledge, we are the first to extrapolate simulations of WLC looping rates to determine the continuum limit.

Examples of our extrapolations are shown in Fig. 2.7 for WLCs of total lengths $L = 13$ (Fig. 2.7a) and $L = 1.4$ (Fig. 2.7b). At each Δl the dot represents the mean simulated value and the error indicates the standard error of the mean. Our extrapolation procedure is a modification of the procedure described by Öttinger. [72] In brief, we attempt least-square best-fits to the mean values simulated at M different

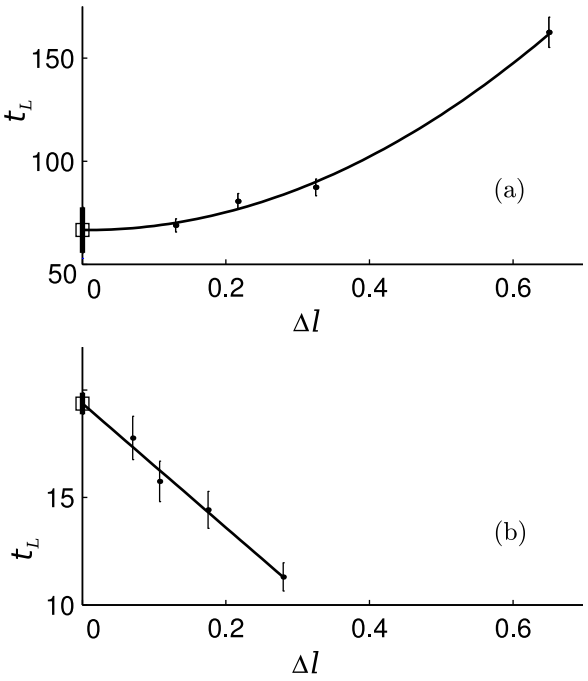

Figure 2.7. Extrapolating Brownian dynamics looping times to the continuum limit. Simulated looping times (dots and error bars) as a function of the contour length step-size, Δl used in the discrete approximation to the WLC for $L = 13$ (a) and $L = 1.4$ (b). Polynomial fits (lines) and the value extrapolated to $\Delta l = 0$ (squares). For long contour lengths,(a), the discrete approximation tends to overestimate the looping time whereas for short contour lengths,(b), the discrete approximation tends to underestimate the looping time. An identical extrapolation procedure was used to determine values of D_{ee} in the continuous limit.

Δl using polynomials of order less than $M-2$. We accept the extrapolation with the smallest chi-square probability value. [152] The extrapolated value is the intercept of the polynomial fit and the uncertainty in the extrapolated value is the square root of the zero-order term in the covariance matrix. The uncertainty in the extrapolated value is represented by the vertical lines at $\Delta l = 0$ in Figs. 2.7a and b and defines the procedure used to generate the error bars shown in Figs. 2.5 and 2.6.

The examples shown in Fig. 2.7 show that discrete approximations to the WLC model can both overestimate (in the case of $L = 13$, Fig. 2.7a) and underestimate (in the case of $L = 1.4$, Fig. 2.7b) the looping time obtained in the continuum limit. Overestimation of the looping time was typical for discrete WLCs with $L > 3$. Along the lines of Doi's [8] reasoning, this overestimation is the result of omitting degrees-of-freedom and erroneously reducing the rate at which the polymer end explores space. In the case of $L \leq 3$, the discrete simulations tend to underestimate the continuous limit. This was due to violations of the inextensibility constraint that introduce an erroneous degree of freedom (the polymer length). This error decreases as segment length decreases and the simulated discrete WLC approaches the continuum limit. [148]

An identical procedure was used to extrapolate values of the end-to-end diffusion coefficients, D_{ee} to the continuum limit. D_{ee} had a much weaker dependence on Δl, as compared to t_L.

2.9.2 Kramers Rate Theory

In this appendix we use Kramers' approximation for a high barrier to derive an analytical expression for the looping time. [47,53] This expression explicitly shows the $t_L \propto \alpha^{-1}$ in the limit $\alpha \to 0$, which is a signature of 1D diffusion models (The green line in Fig. 2.6) .Starting from Eq. 2.2, Kramers assumes that the particle begins from the minimum in an effective potential, $x_0 = x_{min}$,

$$t_L(x) = \int_{\alpha}^{x_{min}} \frac{1}{DP_{eq}(x)}\, dx \int_{x}^{L} P_{eq}(y)\, dy. \tag{2.10}$$

Additionally, Kramers assumes that $P_{eq}(x)$ around α is very small (high potential barrier approximation). Because of the $1/P_{eq}(x)$ term in Eq. 2.10, this causes t_L to be dominated by the portion of the integral around $x = \alpha$. In this region, the integral over $P_{eq}(y)$ changes little and is insensitive to the precise value of the lower bound, x. This allows the bound to be replaced by any value around α, and the two integrals to be decoupled,

$$t_L = \int_{\alpha}^{x_{min}} \frac{1}{DP_{eq}(x)}\, dx \int_{\alpha}^{L} P_{eq}(x)\, dx. \tag{2.11}$$

Substituting the dimensionless potential $f(x)$ for the probability density using the relation

$$f(x) = -\ln(P_{eq}(x)) \tag{2.12}$$

into Eq. 2.11 we obtain the familiar Kramers rate equation (compare to Ref. [47] Eq. 5.109).

$$t_L = \int_{\alpha}^{x_{min}} \frac{e^{f(x)}}{D}\, dx \int_{\alpha}^{L} e^{-f(x)}\, dx. \tag{2.13}$$

At this point, $f(x)$ is typically Taylor expanded to second order and integrated to obtain an explicit expression for t_L. In this problem, however, the right hand integral integrates over nearly the entire range of x, $\int_{\alpha}^{L} e^{-f(x)}\, dx \approx 1$. This reduces Eq. 2.13 to,

$$t_L \approx \int_{\alpha}^{x_{min}} \frac{e^{f(x)}}{D}\, dx. \tag{2.14}$$

Because this integral is dominated by the region around α, we Taylor expand $f(x)$ around $x = \alpha$. For an absorbing boundary, the first derivative of the potential is discontinuous at α; that is the potential has the form of a cusp. Hence we expand $f(x)$ to first-order only in the region just outside of α,

$$f(x) \approx f(\alpha) + f'(\alpha)(x - \alpha). \tag{2.15}$$

Inserting Eq. 2.15 into Eq. 2.14 and integrating we obtain,

$$t_L \approx \frac{e^{f(\alpha)}}{Df'(\alpha)}(e^{f'(\alpha)(x_{min}-\alpha)} - 1). \tag{2.16}$$

For a high barrier $e^{f'(\alpha)(x_{min}-\alpha)} \ll 1$. In addition from Eq. 2.12,

$$\frac{e^{f(\alpha)}}{f'(\alpha)} = \frac{-1}{P'_{eq}(\alpha)}. \tag{2.17}$$

These reduce Eq. 2.16 to a compact from

$$t_L \approx \frac{1}{DP'_{eq}(\alpha)}. \tag{2.18}$$

The explicit $\alpha-$dependence of the looping time in the limit $\alpha \to 0$ can be obtained by introducing the equilibrium Green's function $G_{eq}(x)$ defined by $P_{eq}(x) = 4\pi x^2 G_{eq}(x)$. For any non-zero $G_{eq}(0)$, $P'_{eq}(x) = 8\pi\alpha G_{eq}(0)$ in the limit $\alpha \to 0$ and Eq. 2.18 takes the form,

$$t_L \approx \frac{1}{8\pi D\alpha}\frac{1}{G_{eq}(0)}. \tag{2.19}$$

An identical expression was derived previously by Jun et al. [54] This equation shows that in the limit $\alpha \to 0$ *all 1D diffusion models* predict a looping time $t_L \propto \alpha^{-1}$ (shown as green line in Fig. 2.6). In Fig. 2.6 we showed that for WLC the looping time departs from this expected dependence. This indicates that 1D diffusion models may not be applicable to WLC in the ranges of parameter space where they are expected to be.

3. Novel Crosslinking Assays for Non-Enzymatic DNA Ligation

3.1 Introduction

Measuring the flexibility of DNA is a way of learning about the structural characteristics of this complex macromolecule. The cyclization of DNA is the established method for quantifying the flexibility of DNA. The cyclization experiments have traditionally been carried out using an enzymatic reaction in which *T4 DNA ligase* catalyzes the formation of a phosphodiester bond between juxtaposed 5′ phosphate and 3′ hydroxyl termini in duplex DNA. It is assumed in these experiments that the enzyme itself has no significant effect on the flexibility of DNA. However, it was recently found that the non-specific binding of the enzyme alters the flexibility of DNA [153]. Because of DNA breathing–the spontaneous and transient breakage of the hydrogen bonds between DNA base pairs–DNA bases get exposed to the surrounding solvent. The enzyme can then bind to these flipped out bases and stabilize these local un-pairings. These stabilized unpaired bases can enhance the flexibility of DNA.

Another limitation of the ligation assay is that ligase is inhibited by high concentration of monovalent cations (e.g. $[Na^+] > 200$ mM) and its optimal pH range is limited to pH 7.2-7.8. Moreover, the enzyme's activity quickly diminishes at room temperature. All these factors limit the range of measurements that can be done by ligation assays to a narrow range of reaction conditions where the enzyme is active.

Several groups have developed ligase-free assays over the past few years. Wiggins et. al. [146] employed atomic force microscopy to measure the bending angles of DNA on a surface as a measure of the flexibility of DNA. Vafabakhsh and Ha developed a single molecule assay in which the DNA molecules were attached to a surface and their

ends were labeled with fluorescent dyes Cy5 and Cy3 [154]. The cyclization rate was then measured by monitoring the rate of Forster energy transfer between the dyes. However, a recent simulation by Waters et. al. suggests that pinning down a polymer to a surface increases the probability of cyclization, a result that calls into question the conclusions of cyclization assays that involve DNA-surface interactions [155].

We aimed at developing a ligase-free DNA cyclization assay in which DNA is free to move in solution. To this end, we first identified the strategies for chemical ligation of DNA. There were several requirement for these strategy to be applicable to DNA cyclization experiments. First, reactive moieties must be attachable to DNA. Second, the reaction should be rapid enough so that significant amount of product is formed under the extremely low (less than 0.2 μM) concentrations compatible with DNA cyclization experiments. Third, the reaction conditions should not degrade DNA or cause damages such as strand break to DNA.

Based on these requirements we devised several strategies to label the ends of DNA and make covalent crosslinking between the ends of DNA molecules. The chemistries tested are disulfide bond formation, copper-free click chemistry, maleimide-thiol reaction and succinimide-amine reaction. The details of these methodologies are presented in the following subsections.

The starting point in our screening process was testing each reaction on oligo deoxyribonucleotides (ODN). Working with oligonucleotides instead of dsDNA allows us to initially bypass the complicated and multi-step labeling and purification needed for chemically crosslinking of dsDNA. Additionally, the crosslinking reactions for oligonucleotides can be carried out in hundreds-of-micromolar concentrations which allows us to screen for the reactive group with fastest kinetics. One strategy we conceived for crosslinking DNA is using homo-bifunctional crosslinkers. A homo-bifunctional crosslinker is a chemical structure in which two identical moieties are separated by a spacer arm such as an ethylene glycol chain. These crosslinkers are classified based on the type of chemical group they react with. Two prominent examples are maleimide–a thiol reactive moiety–and succinimide–an amine reactive moiety (see Fig. 3.1). A

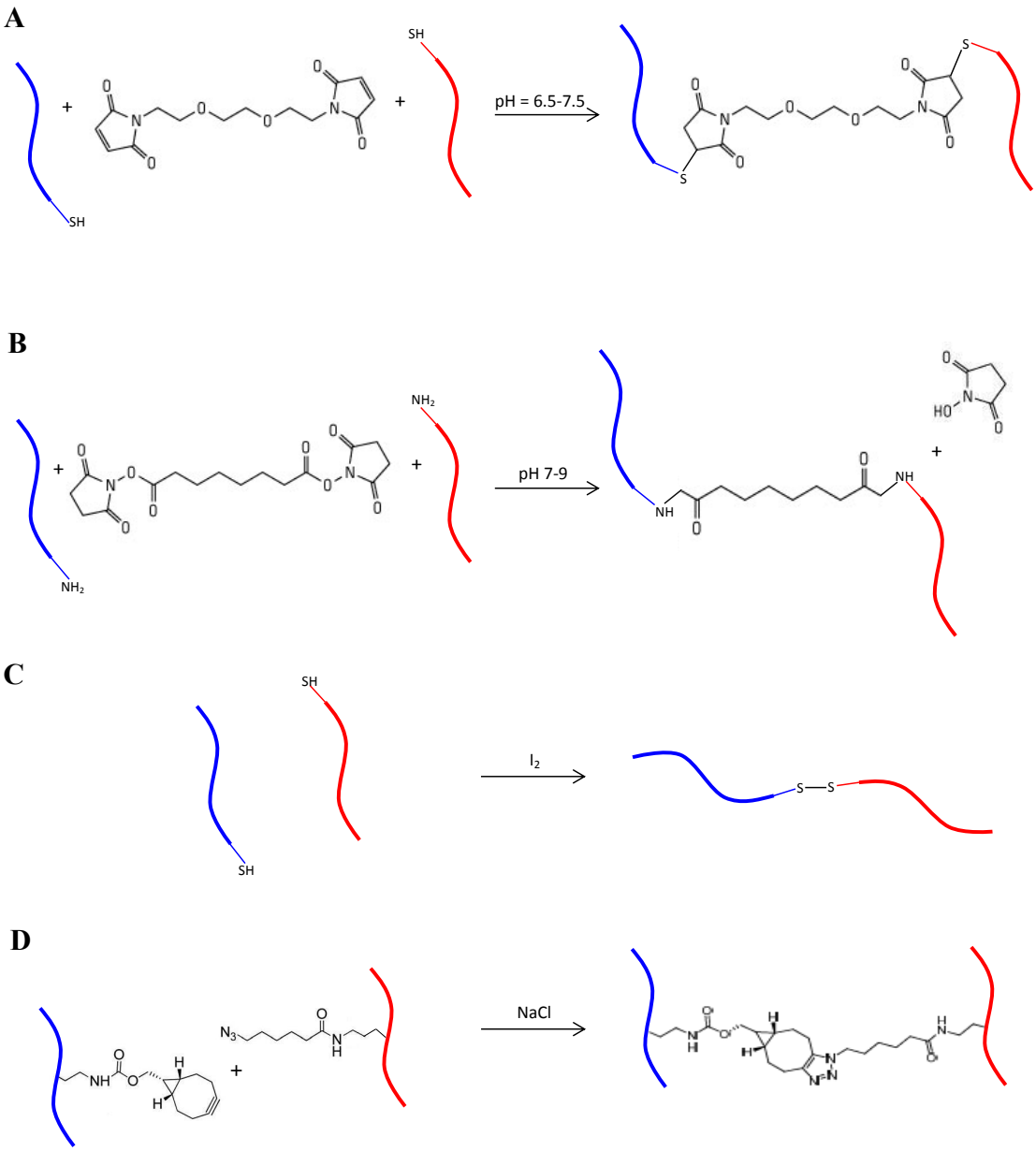

Figure 3.1. The reaction scheme for four different oligonucleotide covalent crosslinking methods. **(A)** Thiol-functionalized oligonucleotides are crosslinked by a *bis*-maleimide crosslinker. **(B)** Amine-functionalized oligonucleotides are crosslinked by a *bis*-succinimide crosslinker. **(C)** Thiol-functionalized oligonucleotides are crosslinked via Iodine-oxidation-mediated disulfide bond formation. **(D)** Azide-functionalized (red) and BCN-functionalized oligonucleotides (blue) are crosslinked through a copper-free click reaction.

third path to crosslinking two DNA fragments is through Iodine-oxidation-mediate disulfide bonding [156]. This strategy is suggested to be a fast and efficient way to couple two DNA fragments. Lastly, an approach for crosslinking that is growing in popularity due to its wide range of applicability is click chemistry.

3.2 DNA Crosslinking By Maleimide-Thiol reaction

3.2.1 Experimental Procedure

Maleimide reacts with free thiols in pH 6.5-7.5 to form a stable thioether bond [157]. We used a pegylated bis-maleimide crosslinkers, 1,8-bis(maleimido) diethylene glycol, or simply BM(PEG)2 from Pierce Biotechnology. We imagined that in the presence of thiolated oligonucleotides the maleimide groups would react with thiol groups at the ends of oligonucleotides and crosslink two oligonucleotides.

The oligonucleotide in this experiment was a 28-nt-long 5′OH-C6-SS-C6-ODN_{28} (Integrated DNA Technologies) with sequence shown in table 3.1.

Table 3.1.
The sequence of 28-mer and 21-mer oligonucleotides used in maleimide crosslinking and Iodine-mediated disulfide bonding experiments

Code	Oligonucleotide 5′ to 3′
5′SH-C6-ODN_{28}	SH-C6-TGACTGCGTGTATAACTAGCCTGCCCCG
3′SH-ODN_{21}	TTTTGTCGTATGTTAGCGTAG-p-SH

Since free thiols are prone to air oxidation, which results in disulfide bond formation, the modified oligo is synthesized and lyophilized with a protective group (OH-C6-S-) which must to be removed after reducing the disulfide bond and right before the crosslinking experiment. The disulfide bond is attached to an oxygen on the 5′ phosphate of oligonucleotide through a 6-carbon-long chain(C6). We first resuspended the crosslinker in DI H_2O. To reduce the disulfide bond we used the Bond-Breaker

TCEP Solution (tris(2-carboxyethyl)phosphine) (Pierce Biotechnology). TCEP and 5′OH-C6-SS-C6-ODN were mixed to the final concentrations [TCEP] = 2.25 mM and TCEP : 5′OH-C6-SS-C6-ODN 100:1 in PB pH 6.5, incubated at room temperature for 2 hours with several vortexing. The reduction of 5′OH-C6-SS-C6-ODN_{28} by TCEP generates two products, 5′OH-C6-SH and HS-C6-ODN_{28}. The protective group 5′OH-C6-SH then must be removed because otherwise it would compete with SH-C6-ODN_{28} for reacting with crosslinkers.

To remove the protective group (OH-C6-SH) after reduction we used OIAquick Nucleotide Removal Kit (Qiagen) and followed manufacturers' protocol. Stock solution of crosslinker BM(PEG)2 was made by dissolving in DMSO right before the crosslinking experiment. Crosslinking reactions were carried out at room temperature for 70 minutes in PB pH 6.5, 7, 7.5 with 90 μM or 9 μM of BM(PEG)2 and 9 μM of cleaned-up SH-C6-ODN_{28}. For sample 3 we did Iodine oxidation as a control to compare with Maleimide crosslinking. This sample was made by mixing equimolar amount of I_2 and cleaned-up SH-C6-ODN_{28}.

After the specified reaction time, 2× TBE-Urea sample buffer (Invitrogen) was added to the samples and samples were heated for 3 minutes at 70°C. The samples were electrophoresed on 15% TBE-Urea gels (Invitrogen) at constant 180 V using X-Cell SureLock Mini-Cell Electrophoresis system. To visualize the gels we stained the gels in a solution of 1× SYBR Gold (Invitrogen) in 1× TBE buffer for 40 minutes at room temperature while gently rocking the staining dish. The gel images were captured using GENi gel documentation system (Syngene) which emits 312 nm UV light that excites SYBR Gold.

3.2.2 Results

We observe very little dimerization for the sample that is reduced by TCEP but not yet purified. After removing the protective group by spin-column purification, we see that some of the oligonucleotides dimerize, apparently through air oxidation of

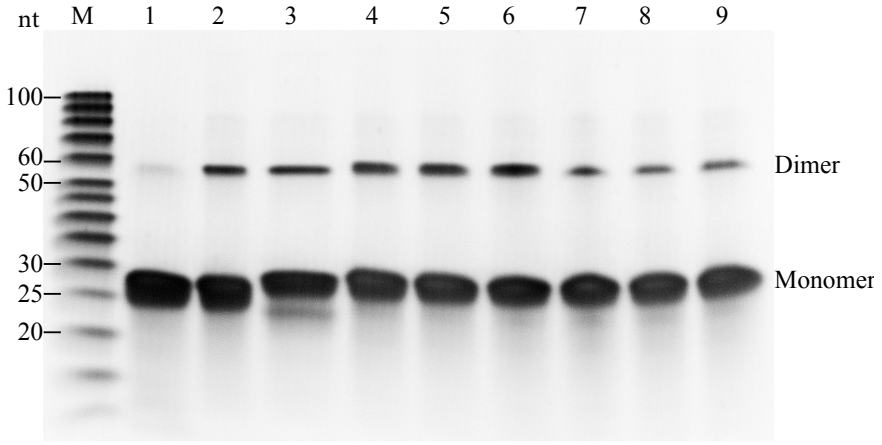

Figure 3.2. Crosslinking of thiol-functionalized oligonucleotides by a *bis*-maleimide crosslinker. Lane M: Low Molecular Weight Marker (Affymetrix). Lane 1: 5′OH-C6-SS-C6-ODN$_{28}$ reduced by TCEP before clean-up, lane 2: sample 1 after clean-up, lane 3: lane 2 oxidized by I_2, lanes 4-6: lane 2 with BM(PEG)2 : SH-C6-ODN$_{28}$ 1 : 1 in PB pH 6.5, 7 and 7.5 respectively, lanes 7-9: lane 2 with BM(PEG)2:SH-C6-ODN$_{28}$ 10 : 1 in PB pH 6.5, 7 and 7.5 respectively.

end thiols. The same results is seen when the sample is oxidized by I_2(lane 3, Fig. 3.2). Adding bis-maleimide did not result in a significant increase of dimerization. When the ratio of crosslinker to oligo was increased to 10, the yield of dimers reduced. This is because when crosslinker is in high excess, that is, for maleimides there is a shortage of thiols, most of the crosslinkers will react with only one thiolated oligo and there will not be significant dimerization. The dependence of dimerization yield on the ratio of crosslinker to oligo indicates some degree of reaction between maleimide and thiol. There could be two explanations for the fact that the majority of the oligonucleotides remain in the monomer form. First, one may ask if the crosslinker:ODN 1:1 is too high, resulting in blocking the ends of oligonucleotides by crosslinker. The objection to this hypothesis is that even when oxidation is carried out by Iodine we do not observe a high yield. This leads us to think that the reduction of the oligonucleotides with TCEP has been suboptimal. Unfortunately, there is no standard protocol for reduction of thiol-functionalized oligonucleotides by TCEP. The protocol used here

is the result of consultation with Pierce Technology scientist. A possible direction to take in the future would be to try to come up with an optimized protocol for reduction and then *complete* removal of the both protective group and TCEP.

A major problem with this approach is the hydrolysis of maleimide which competes with the reaction of maleimide with thiol groups. It is critical to keep the pH in the range 6.5-7.5. While maleimide hydrolysis occurs even at this near-neutral pH, at pH > 8 the maleimide hydrolysis would be dominant, turning maleimides to maleimic acid before they react with thiols. One does not know the hydrolysis rate and how it compares with the rate of maleimide-thiol reaction. Another challenge in working with maleimide is that extreme care should be taken to carefully desiccate the dry BM(PEG)2 as moisture can cause hydrolysis of the maleimides.

These considerations convinced us that maleimide-thiol coupling is not a good approach for crosslinking dsDNA; if the rate of hydrolysis is faster than maleimide-thiol coupling at tens-of-micromolar concentrations then at nanomolar concentrations needed for crosslinking dsDNA it would not be a suitable method.

3.3 DNA Crosslinking By Succinimide-Amine Reaction

3.3.1 Experimental Procedure

We attempted to crosslink amine-functionalized oligonucleotides by a water soluble crosslinker having amine-reactive N-hydroxysulfosuccinimide (NHS) ester at each end of an 8-carbon spacer arm named BS3 for Bis(Sulfosuccinimidyl) suberate. NHS esters are reactive toward primary amines in pH 7-9 which leads to the formation of amide bonds and the release of N-hydroxysulfosuccinimide group [157].

The advantage of this method is that unlike free thiols, amine groups do not react with each other, eliminating the need to develop protocols from reduction and purification of thiol-functionalized oligos.

The oligo used in this experiment has the same sequence as the one used in maleimide crosslinking experiment except the thiol modification was replaced by an amine moiety: $5'NH_2$-C6-ODN_{28} (Integrated DNA Technologies).

We first prepared a 1.0 mM $5'$-NH_2-C6-ODN_{28} stock solution by dissolving the oligo in 0.20 M PB pH 7. Since NHS esters can easily hydrolyze and become non-reactive, it is necessary to resuspend BS3 immediately before initiating the crosslinking reaction. We dissolved BS3 in DI H_2O, immediately before the start of crosslinking reaction. The final concentration of oligo in crosslinking reaction was 25 μM with 1, 10, 50 and 100 molar excess of BS3 and in pH 8. We tested the efficiency for four different BS3:$5'$-NH_2-C6 ODN_{28} ratios at pH 8 and two reaction conditions: 30 minutes room temperature and 2 hours on ice. Procedure for electrophoresis and visualization was the same as the procedure for maleimide reaction (see Sec. 3.2).

3.3.2 Results

A faint dimer band is seen on the gel shown in Fig. 3.3. Because this band is present even in the absence of crosslinker, we conclude that crosslinking has not occurred by BS3. We believe that the negative results is due to the hydrolysis of Sulfo-NHS ester group of BS3 which readily hydrolyzes and become non-reactive. If the rate of hydrolysis is much faster than the second order rate of amide bond formation by Sulo-NHS and amine group, no significant amount of crosslinked oligonucleotide will form.

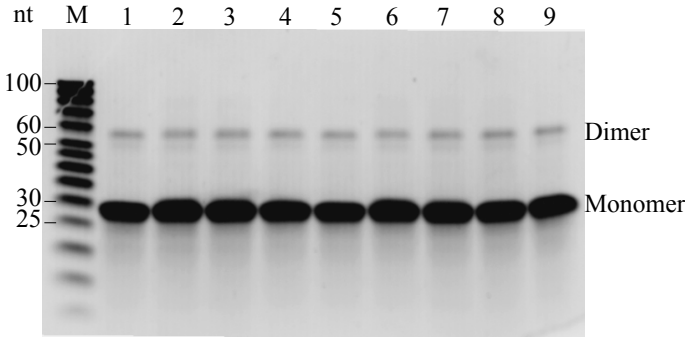

Figure 3.3. Crosslinking of amine-functionalized oligonucleotides by the *bis*-Succinimide crosslinker BS3. Lane M: Low Molecular Weight Marker, lane 1: 5′-NH_2-C6-ODN. Lanes 2-5: the samples with BS3:5′-NH_2-C6-ODN_{28} 100:1, 50:1, 10:1 and 1:1 respectively and reaction conditions 30 min at room temperature, lanes 6-9: the same as lanes 2-5 except the reaction condition was 2 hours on ice. Monomer and Dimer indicate the location of 5′-NH_2-C6-ODN_{28} monomer and its dimer.

3.4 DNA Crosslinking By Disulfide Bond Formation

3.4.1 Experimental Procedure

Disulfide bond formation is an alternative method for the crosslinking biological molecules. Upon oxidation of free thiol groups they can form disulfide bonds. Although oxygen can oxidize thiols and assist disulfide bonding it has been suggested that Iodine (I_2) can mediate disulfide bond formation much faster than oxygen [156, 158]. Oxidation with Iodine along with hydrogen peroxide (H_2O_2) and potassium ferricyanide $K_3[Fe(CN)_6]$ has been suggested as candidates for fast and efficient crosslinking strategies for nucleic acids [156, 158]. To screen the oxidants for fast, efficient and template independent crosslinking via disulfide bond formation we tested I_2, $K_3Fe(CN)_6$ and H_2O_2. We found in our experiments that Iodine is the only oxidant that oxidizes thiols and mediates disulfide bonding quickly, efficiently and without a template. In addition, the experiments show that Iodine oxidation is ratio sensitive and in the presence of excess Iodine the efficiency of reaction drops.

This has been attributed to oxidative de-sulfurization of thiophosphate whose rate increases with increasing the concentration of Iodine [158].

In the first set of experiments the efficiency of H_2O_2 and I_2 were compared for crosslinking a 3′-*thiophosphate* oligonucleotide (Fig. 3.4). This oligonucleotide was 21-nt-long and had a thiol group on a 3′ phosphate group or 3′SH-ODN_{21} (see table 3.1). 100 μM of this oligonucleotide was mixed in 10 μL of 0.03% H_2O_2 on ice for the reaction times varying from 30 minutes to 4 hours. For Iodine oxidation we tested 0.1 mM and 1 mM I_2 in saturated KI corresponding to I_2:SH 1:1 and 10:1, with both reactions kept on ice. The reason for saturating I_2 in KI is that I_2 is non-polar and hence does not dissolve in water while in the presence of KI which ionizes in water the molecular iodine reacts with I^- to form the water soluble I_3^-.

In another experiment we compared the efficiency of disulfide bonding by Iodine and potassium ferricyanide (Fig. 3.5). In this experiments 100 μM of 3′SH-ODN_{21} was in the presence of 1, 10 or 100 molar equivalent of $K_3Fe(CN)_6$ for 3 hours at RT. For $K_3Fe(CN)_6$:SH-ODN_{21} 100:1 the reaction was tested on both ice and RT. For Iodine oxidation the reaction were with 100 μM of 3′SH-ODN_{21} and 1 or 10 molar equivalent Iodine in saturated KI. For I_2:SH-ODN_{21} 100:1 the dimerization is relatively inefficient which highlights the importance of the ratio of Iodine to thiols in this reaction. The electrophoresis condition was the same as the conditions in Sec. 3.2.

3.4.2 Results

It is clear from the gel (Fig. 3.4) that in equimolar concentration of Iodine and thiophosphate the conversion of SH-ODN_{21} to its dimer is nearly complete in only 30 minutes whereas for H_2O_2 or H_2O (air oxidation) no dimerization is observed.

From the gel shown in Fig. 3.5 evident that potassium ferricyanide does not make disulfide bonds at any of the reaction conditions tested. Oppositely, I_2 generates

dimers with a very high yield. This experiments convinced us that Iodine oxidation of thiophosphate oligonucleotides is a viable path for chemically ligating dsDNA.

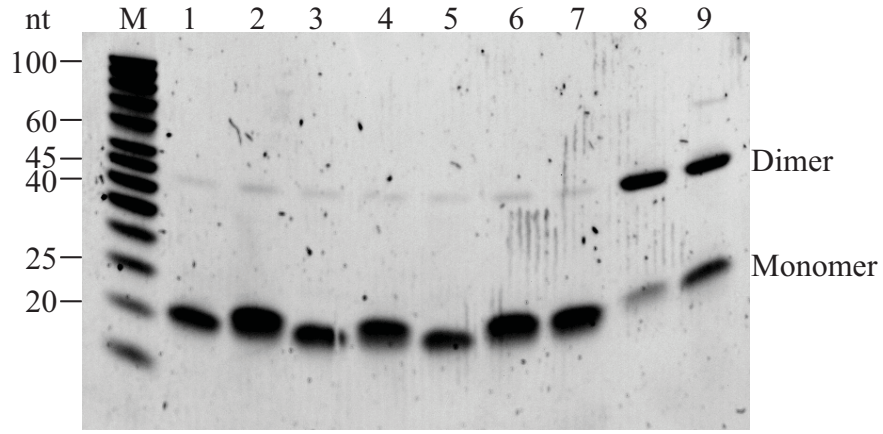

Figure 3.4. Comparison between dimerization of a 21-nt-long end thiolated oligonucleotide through disulfide bond formation in the presence of H_2O_2 and I_2. Lane M: Low Molecular Weight Marker, lanes 1 and 2: 3′SH-ODN_{21} in H_2O and H_2O_2 for 4 hours, lanes 3 and 4: 2 hours, lanes 5 and 6, 1 hour, lane 7: in H_2O_2 for 30 minutes, lane 8: in equimolar concentration of I_2 for 30 minutes, lane 9: in 10-fold excess of I_2 for 30 minutes. All reaction were on ice.

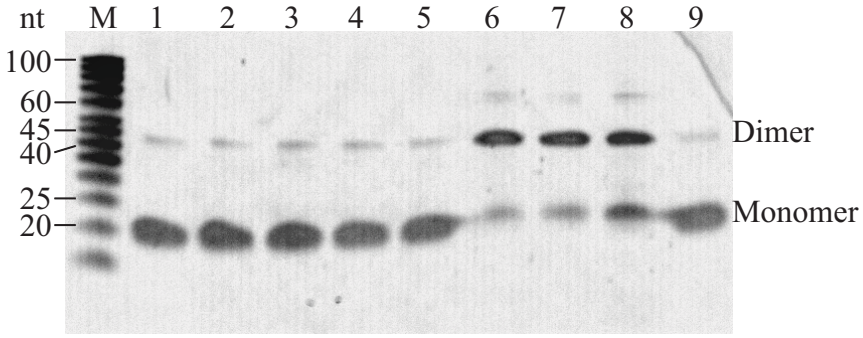

Figure 3.5. Comparison between dimerization of a 21-nt-long end thiolated oligonucleotide through disulfide bond formation in the presence of $K_3Fe(CN)_6$ and I_2. Lane M: Low Molecular Weight Marker, lane 1: 3′SH-ODN_{21}, lane 2: lane 1 plus equimolar concentration of $K_3Fe(CN)_6$, lane 3: lane 1 plus 10-fold excess of $K_3Fe(CN)_6$, lane 3: lane 1 plus 100-fold excess of $K_3Fe(CN)_6$. Lanes 2-4 reaction were at room temperature for 3 hours. Lane 5: lane 4 but on ice for 3 hours. Lanes 6 and 7: lane 1 plus equimolar concentration of I_2 reacted on ice for 3 hours and 30 minutes respectively, lane 8: lane 1 plus 10-fold excess of I_2 reacted on ice for 30 minutes, lane 9: lane 1 but kept on ice for 3 hours.

3.5 DNA Crosslinking By Click Chemistry

3.5.1 Experimental Procedure

An alternative path to crosslinking of nucleic acids is click chemistry. In click chemistry an azide moiety on a biomolecule reacts with an alkyne or its derivatives on another molecule leading to the formation of cyclic structures. In our experiment we chose a particular type of click chemistry named Strain-Promoted Azide-Alkyne Cycloaddition (SPAAC) which is an example of copper-free click reactions. The choice of a copper-free reaction was due to the fact that the copper ion commonly used in copper-based click reactions can degrade DNA. This approach has the great advantage that is *bioorthogonal*, that is, azide and alkyne moieties do not interfere with native biochemical processes inside the cell. Therefore, the approach has the potential to be applied to *in vivo* measurements.

We tested the crosslinking efficiency of ssDNA and dsDNA constructs via SPAAC reaction in aqueous solution. The chief aim of this experiment was to find a reaction that unlike Iodine-mediated disulfide bonding works over a wide range of reaction conditions.

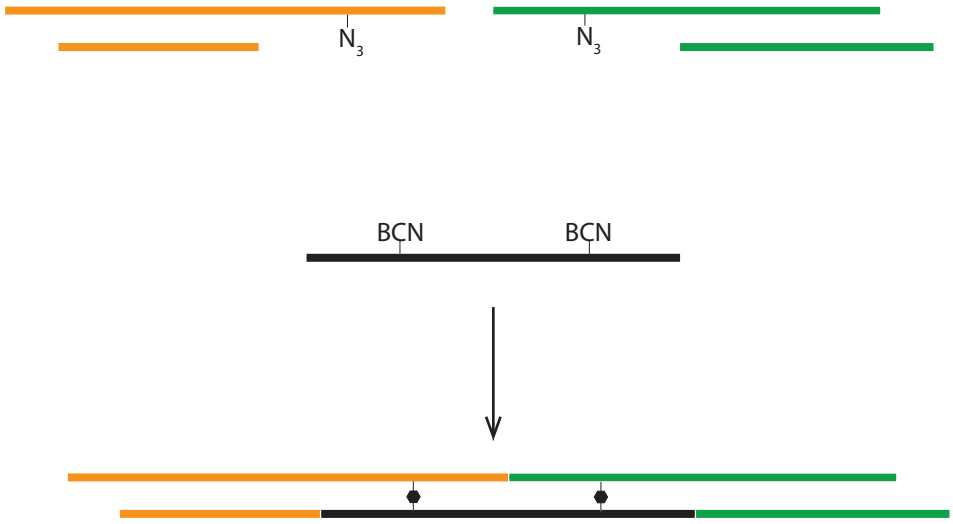

Figure 3.6. Schematic representation of crosslinking of two adapters (orange and green) via click reaction by a BCN-modified oligonucleotide(black). In the presence of NaCl hybridization of each adapter to the complementary half of the crosslinker allows azide and BCN to react quickly, leading to the formation of a triazole linkage.

These constructs have azide attached to one of their thymine bases (Table 3.2). Another oligonucleotide was designed to have two cyclooctyne derivative BCN (bicyclo[6.1.0]nonyne) attached to two of its thymine bases. This oligonucleotide acts as crosslinker. We first built partially duplex azide-modified adapters by a annealing using the same protocol described in Sec. 3.4. We mixed equimolar concentrations (0.10 μM final) of N_3-ODN_{29} + ODN_{19} and BCN_2-ODN_{14}, N_3-ODN_{33} + ODN_{15} and BCN_2-ODN_{28} and all three components in Tris-Buffered Saline (200 mM NaCl, 10 mM Tris-HCl, pH 7.5 @ RT for 1 M Tris-HCl) and let the reaction proceed for 15 minutes or 1 hour (Fig.3.7). The reactions were then terminated by adding 2× loading buffer and doing electrophoresis on a 20% TBE gel (Invitrogen). The gels were

then stained with SYBR Gold and visualized by GENi gel imaging system. The loads of each lane are 29.9 ng each adapter in lanes 2 and 3 and 18.3 ng of crosslinker in lane 1.

Table 3.2.
List of oligonucleotides used in click-chemistry-based DNA crosslinking

Code	Oligonucleotide 5′ to 3′
N_3-ODN_{29}	ACAGA$\mathbf{T}^{N_3}$ATCATATTCGTGTAATGAGAACA
ODN_{19}	CATGTGTTCTCATTACACG
N_3-ODN_{33}	CTGGTCCACACCTTAGTGAACAGA$\mathbf{T}^{N_3}$ATCATATT
ODN_{15}	TCACTAAGGTGTGGA
BCN_2-ODN_{28}	AATATGA$\mathbf{T}^{BCN}$ATCTGTATGTACA$\mathbf{T}^{BCN}$AATGTT

3.5.2 Results

We observe that in the last 2 lanes on the gel a band with mobility between $\sim$ 50-75 bp of the marker (lane M) is observed. The molecular weight of the crosslinked product formed by all 3 components is roughly equal to a 60 bp dsDNA and thus we can identify that band as the crosslinked product. The dominant product in bands 4-7 can be identified as the product of crosslinking of the crosslinker with each individual partially duplex DNA. It is clear from this gel that SPAAC reaction crosslinks the molecules in only 15 minutes, a fast reaction time considering the sub-micromlar concentration of reaction components.

The fact that this reaction is fast with a straightforward protocol and the reaction groups react selectively with each other suggest that this method is a strong candidate for cyclizing and dimerizing dsDNA.

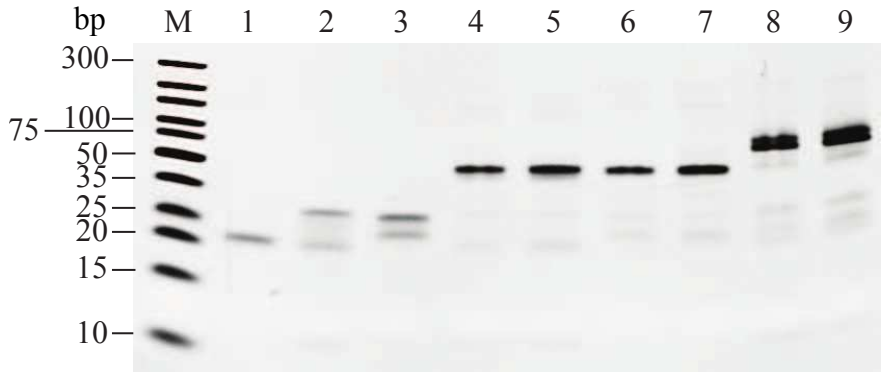

Figure 3.7. Crosslinking of adapters via copper-free click chemistry. Lane 1: GeneRuler Ultra Low Range DNA Ladder(Thermo Scientific), lane 1: BCN_2-ODN_{28}, lane 2: N_3-ODN_{29} + ODN_{19}, lane 3: N_3-ODN_{33} + ODN_{15}, lanes 4 and 5: BCN_2-ODN_{28} reacted with N_3-ODN_{29} + ODN_{19} for 15 minutes and 1 hour, lanes 6 and 7: BCN_2-ODN_{28} reacted with N_3-ODN_{33} + ODN_{15} for 15 minutes and 1 hour, lanes 8 and 9: All three components reacted for 15 minutes and 1 hour.

4. Crosslinking double-stranded DNA via Iodine oxidation

4.1 Introduction

After identifying the proper crosslinking reaction, there are three steps that need to be completed before doing the reaction for dsDNA. First is the preparation of dsDNA sample with desired length. Second, incorporation of the reactive moiety into that dsDNA and finally purification of modified dsDNA to remove any stray reactive groups that remain after modification.

There are a few DNA modifying enzyme that can incorporate either a modified nucleotide monophosphate or a modified oligonucleotide at the end of a dsDNA. A family of DNA modifying enzymes known as *polymerases* can polymerize DNA strands, that is, to put dNMP at the end of DNA. We chose DNA Polymerase I, Large (Klenow) Fragment since it is the most widely used polymerase.

To prepare DNA samples of desired length we used a group of enzymes named *Restriction Endonucleases* (REases) that digest (cut) dsDNA by recognizing a specific sequence on dsDNA and breaking the phosphodiester bonds. The product of digestion is a linear dsDNA with either blunt ends or single stranded protruding ends called sticky ends or overhangs. The number of bases in sticky ends depends on the enzyme used for cutting the DNA and is typically in low single digits.

4.2 Experimental Procedure

For our experiments we chose an REase called HindIII that generates two sticky ends with sequence 5′AGCT at the ends of DNA. We cut a plasmid (circular DNA) called pBR322 which is 4,361 bp long and has one recognition site for HindIII, hence, HindIII-pBR322 DNA is a linear 4,361 bp long DNA with 5′AGCT sticky ends.

To incorporate the thiophosphate group into the ends of HindIII-pBR322 DNA we did a polymerase reaction with modified deoxyadenosine triphosphate (2′-Deoxythymidine-5′-O-(1-Thiotriphosphate)) or simply thio-dTTP (TriLink BioTechnologies, Fig. 4.1) along with dATP, dGTP and dCTP. Klenow fills in the 5′ overhang of the dsDNA with these dNTPs and generates a dsDNA with thiophosphate moiety at its end. All our reagents were purchased from New England Biolabs unless otherwise stated. In our assay, we followed the protocol of the manufacturer: 0.1 pmol (0.3 μg) of HindIII-pBR322 was supplied with 0.66 nmol of each dNTP and 0.3 unit of Klenow in NEBuffer 2. We call the end thiolated 4361-bp-long DNA SH-DNA$_{4361}$.

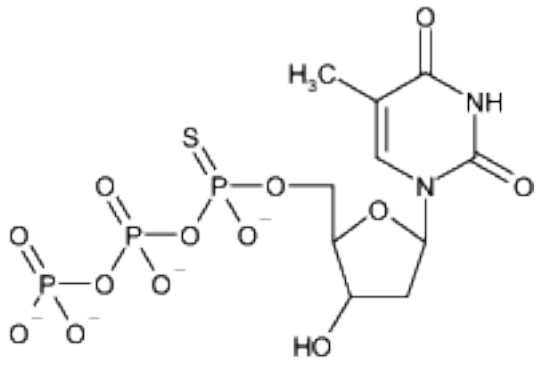

Figure 4.1. 2′-Deoxythymidine-5′-O-(1-Thiotriphosphate) or simply thio-dTTP. This modified nucleoside triphosphate is incorporated to the ends of dsDNA by Klenow. Image is taken from TriLink BioTechnologies website.

We verified the modification of dsDNA ends by a ligase assay in which the ligation pattern of modified and non-modified HindIII-pBR322 DNA are compared (Fig. 4.2). DNA with 4 nt overhang has a significantly faster ligation rate compared to a DNA ends blunted by dNTPs. In this experiment 98 μL of of either modified or non-modified DNA was added to 0.5 μL of T4 DNA Ligase (200 CEU), 1 μL T4 DNA Ligase Buffer and 1.5 μL DI H_2O. After the specified reaction time at RT, the samples were heated at 65°C for 10 minutes to heat inactivate the ligase. The sample were then mixed with 2 μL of 6× blue dye and electrophoresed on 0.8% Agarose

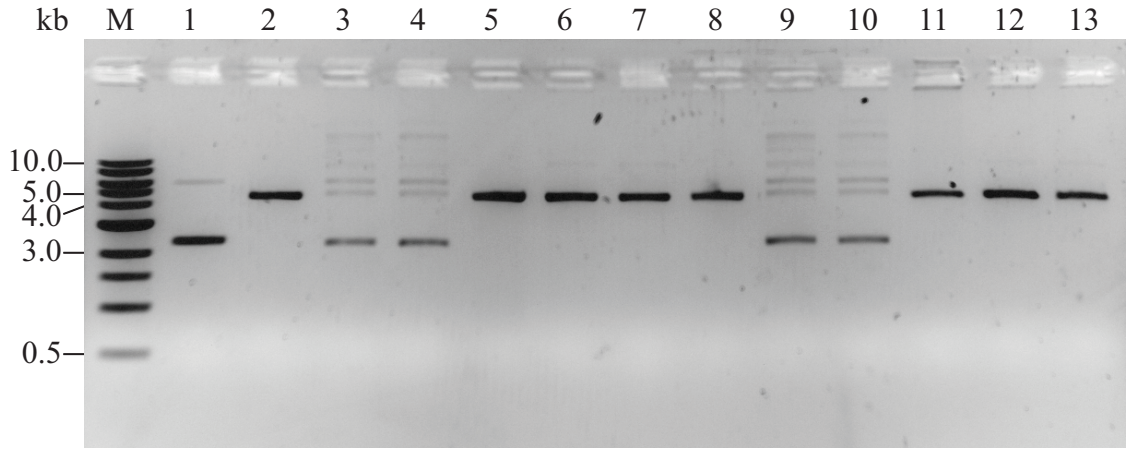

Figure 4.2. Verification of klenow end labeling assay by a ligation assay. Lane M: 1 kb DNA ladder(NEB), lane 1: pBR322. Lanes 2-7 are in *NEBuffer 2*; lane 2: HindIII-pBR322 DNA, lanes 3 and 4: HindIII-pBR322 DNA ligated for 10 minutes and 1 hour respectively, lane 5-7: HindIII-pBR322 end-filled by thio-dTTP pre-ligation, ligated 10 minutes and 1 hour respectively. Lanes 8-13 are the same as lanes 2-7 but in *CutSmart buffer*. All lanes except M contain 200 ng of DNA.

gel (Invitrogen), stained by SYBR Gold (Invitrogen) and visualized by GENi gel documentation system (Syngene). It is evident that while non-modified DNA forms circular and linear products upon ligation, no product is formed after DNA is modified with thio-dTTP.

The next step after labeling DNA is removing the stray thio-dTTP. These stray reactive species have to be removed from the solution because otherwise they will react with the thiol groups at the ends of DNA and will block the reaction between the ends of large DNA fragment(s). Unfortunately, the ratio of stray thio-dTTP to thiol at the end of DNA is 3.3×10^3 :1, meaning that a huge excess of thio-dTTP is present in the reaction. This high excess of thio-dTTP is needed for Klenow because otherwise the end modification will not be successful.

We cleaned up the reaction by using PureLink® PCR Purification Kit (Invitrogen). This kit is based on spin column nucleic acid purification where in high salt

concentration nucleic acids bind to the silica membrane while enzymes, dNTPs and ultra small DNA fragments and other contaminants are washed out.

After purifying the samples twice, we tested the reactivity of end-thiolated dsDNA by I_2 oxidation which does not yield any products (Fig. 4.3). In this particular experiment in 30 μL of 1× CutSmart buffer 1 nmol of each dNTP was mixed with 0.45 units of Klenow and 0.45 μg of HindIII-pBR322 DNA. After 15 minutes incubation at 25°C the reaction was stopped by adding EDTA to the final concentration of 10 mM and heating at 75°C for 20 minutes. The Iodine oxidation reactions were carried out in saturated KI with I_2 concentrations of 0.025 nM, 0.10 nM and 10.0 μM on ice for 10 minutes. Half of the samples were heated at 65°C for 10 minutes before loading into the gel and the other half were not heated. We did this control because we suspected that heating might lead to breaking of the disulfide bonds.

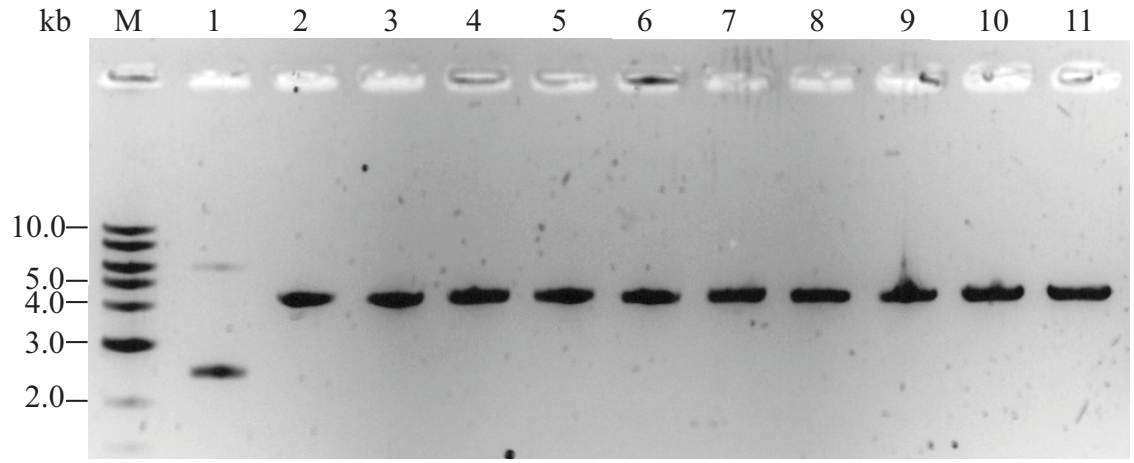

Figure 4.3. Iodine oxidation of thio-dTTP modified DNA. Lane M: 1 kb DNA Ladder, lane 1: pBR322, lane 2 and 3: SH-DNA_{4361}, lane 4 and 5: SH-DNA_{4361} in saturated KI, lanes 6 and 7: SH-DNA_{4361} reacted with 0.025 nM I_2, lanes 8 and 9: SH-DNA_{4361} reacted with 0.10 nM I_2, lanes 8 and 9: SH-DNA_{4361} reacted with 10.0 μM I_2. Lanes with odd number from 2-10 were heated at 65°C for 10 minutes before loading. Lanes 2-11 each contain 180 ng of 3′SH-DNA_{4361}.

The fact that no product is formed upon ligation of thio-dTTP strongly suggested that the modification has been successful. We suspect that the reason for the lack of any reaction would be the presence of stray thio-dTTP after purification. While our purification method will certainly remove most of the stray thio-dTTPs, we did not have any method to quantify the amount left over and given the huge excess of thio-dTTPs even 0.01% would be still a 3.3 fold excess of thio-dTTP, enough to significantly inhibit dimerization of long dsDNA.

We tested a second approach for labeling the ends of dsDNA. In this approach instead of a modified dNTP we incorporate a modified oligonucleotide into the ends of a linear DNA by using T4 DNA ligase. The advantage of this method is that the molar excess of modified oligonucleotides over DNA needed for successful modification is much less than what is needed for the incorporation of modified nucleotides by Klenow. Therefore, removing the stray modified oligonucleotides after DNA modification is easier than removing modified nucleotides.

In our experiments we used a 28-nt-long oligonucleotide (TriLink Biotechnologies) which is modified at its 5′ end to have a thiophosphate group. We made a partially duplex DNA, called *adapter*, by annealing this end-thiolated oligonucleotide to a 32-nt-long oligonucleotide (TriLink Biotechnologies) which has 28 contiguous bases complementary to the end-thiolated oligonucleotide and 4 nt overhang 5′AGCT that is complementary to the ends generated by HindIII. To anneal oligonucleotides we suspend equimolar amounts of each oligonucleotide in annealing buffer (10 mM Tris, pH $7.5 - 8.0$, 50 mM NaCl, 1 mM EDTA), heated up the solution to 86°C for 5-10 minutes and let the sample gradually cool down at room temperature for 1 hour. HindIII-pBR322 was prepared as described before and the adapter was ligated to its ends using a 350:1 adapter to HindIII-pBR322 ratio in CutSmart buffer. The final product is a 4417 bp long dsDNA with thiophosphate ends (SH-DNA_{4417}). Some of the modified DNA was then purified by PureLink PCR purification kit following the manufactures protocol for high cut-off binding buffer that removes dsDNA shorter than 300 bp in length.

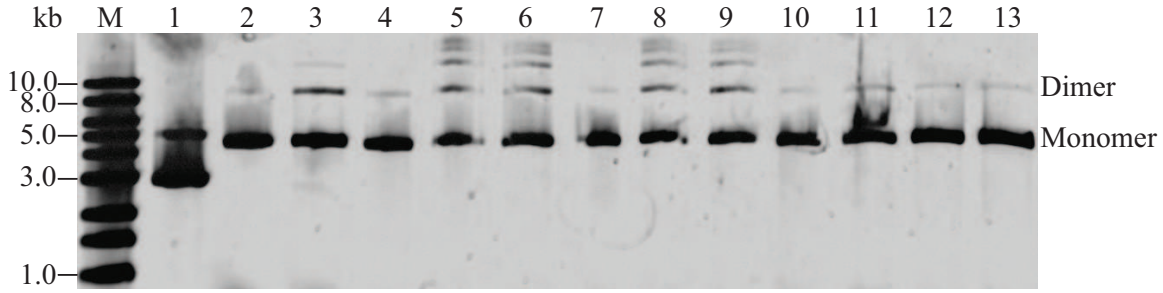

Figure 4.4. Iodine oxidation of end-thiolated dsDNA. Lane M: 1 kb DNA Ladder, lane 1: pBR322, lanes 2 and 3: SH-DNA_{4417} in H_2O and 10 μM I_2 respectively before adapter removal. Lanes 4-13 are all SH-DNA_{4417} after adapter removal. Lane 4: SH-DNA_{4417} in H_2O, Lanes 5-7: SH-DNA_{4417} in 0.100 μM I_2/saturated KI for 30 minutes, 6 hours and 27 hours respectively. Lanes 8-10: the same as 6-8 but in 10.0 μM, Lanes 11-13: the same as 5-7 but in 1.0 mM. Lanes 2−13 all contain 200 ng of SH-DNA_{4417}.

Iodine oxidation was carried out on purified and non-purified (mixed with adapters) SH-DNA_{4417} using 0.1 μM, 10.0 μM and 1.0 mM I_2 in saturated KI. These amounts of Iodine correspond to I_2:thiol 7:1, 7×10^2 and 7×10^4 and we tested 3 reaction times for each Iodine to thiol ratio: 30 minutes, 6 hours and 27 hours.

4.3 Discussion

First, it is clear from comparing the products of reaction with and without removing adapters that purification enhances the multimerization of DNA upon Iodine oxidation. Second, Comparison of the ratios suggests that while there is no difference between the reaction with 0.1 μM and 10.0 μM I_2, almost no product is formed when the concentration of I_2 is increased to 1.0 mM.

Perhaps the most counterintuitive finding here is that for all three I_2 concentrations no product is observed when the reaction time is 27 hours. This is contradictory to our intuition that with increasing the reaction time more thiolated monomer DNA would be converted to dimers and multimers.

The fact that the efficiency of Iodine-mediated dimerization is much better for oligonucleotides than dsDNA suggests that the final yield is sensitive to the concentration of thiolated DNA. We believe that this could be due to difficulty in controlling the concentration of I_2 at sub-micromolar concentrations. The Iodine is dissolved in saturated solution of KI, which has a concentration of [KI] = 8.7 M. There are two possible reactions that can alter the concentration of I_2. One is the oxidation of Iodide through the following reaction.

$$I^- \rightleftharpoons \tfrac{1}{2} I_2 + e^-$$

Or, KI can react with CO_2 and O_2 to produce potassium carbonate along with elemental Iodine.

$$4\,KI + 2\,CO_2 + O_2 \longrightarrow 2\,K_2CO_3 + 2\,I_2$$

It is possible that at concentrations in the range of $\sim 100\ \mu$M the contribution of these reactions to the total Iodine is less significant that for ultra low concentrations of ~ 200 nM.

5. Summary

In Chapter 1 I presented an extensive review of theoretical, computational and experimental aspects of polymer cyclization kinetics. The major theories of polymer cyclization kinetics are WF theory [7,11], SSS theory [9] and RG theory [34]. Among these, SSS theory is the simplest approach as it models the complex high-dimensional dynamics of polymer cyclization as diffusion along a single reaction coordinate; the end-to-end vector. While this elegant approach results in a simple analytical solution, it is not applicable to every polymer-solvent system. For instance, the model does not accurately predict the cyclization kinetics for infinitely long Rouse chain [63] or WLC [60]. More complex WF theory and RG theory have a broader range of applicability, however, their complexity does not allow simple and tractable extension to more real polymer models such as WLC.

In Chapter 2 I presented the predictions of our computer simulations for WLC cyclization kinetics. Our simulations are the first simulations that recover the continuum limit by extrapolating the results for finite discretization of chain and time steps to zero. We found that discretization commonly done in other simulations leads to overestimating the kinetics. Those simulations leave out the high-frequency fluctuations of a polymer by imposing an arbitrary time cut-off on its dynamics [54,56,84,93]. Furthermore, we examined the assumption that when local equilibrium assumption is valid, SSS theory predicts the cyclization kinetics correctly. Our simulations suggest that when high-frequency fluctuations are included in simulations, prediction of SSS theory disagree with simulations, even when local equilibrium assumption is valid.

To sum up, there is a need for developing theories that capture the underlying dynamics of polymer cyclization more adequately and are generalizable to different polymer-solvent systems. A future work would be developing theories that include non-Markovian dynamics in the dynamics of non-Gaussian polymers. An example

would be the non-Markovian dynamics of worm-like chain polymers. Since the complexity increases dramatically as one moves toward more realistic models, it is likely that those models would be highly approximative. Therefore, computer simulations will remain the best way to study the kinetics of polymer cyclization because building more realistic models of polymer dynamics in simulations is much easier than building analytical models.

In Chapters 3 and 4 I presented the results of our work on developing novel assays to crosslink DNA. Over the past few decades the ligation-based cyclization assays have been the standard technique for measuring the flexibility of DNA [159]. The underlying assumption in these experiments is that the mere function of ligase is covalently closing the DNA with juxtaposed end by catalyzing phosphodiester bond formation. However, this assumption is recently called into question [153], hence a need for developing ligase-free methods of DNA crosslinking.

We conducted extensive crosslinker screening experiments to find the viable approaches to crosslinking DNA. To this end, we tested maleimide-thiol reaction, succinimide-amine reaction, disulfide bonding and copper-free click reaction. We observed that maleimide-thiol reaction and succinimide-amine reaction do not crosslink thiol and amine modified oligonucleotides even at ~ 0.1 mM concentrations. In addition, we found that while hydrogen peroxide and potassium ferricyanide do not dimerize thiol-modified oligonucleotides, Iodine mediates dimerization in high yield and without a template. We also showed that DNA crosslinking can be achieved conveniently by SPAAC reaction. This method is an alternative that shows potential for being applicable over a wide range of reaction conditions.

In Chapter 4 I described the techniques we developed to prepare DNA samples of desired length, label them with a reactive moiety and then purify them. Our demonstration of Iodine-assisted dimerization of end-thiolated dsDNA is unprecedented and is an important step toward developing an assay for measuring the flexibility of DNA.

A future work would be fine tuning the click-chemistry-based DNA crosslinking and oxidative disulfide bonding, or coming up with other chemistries that can

crosslink DNA. This would require finding methods to obtain μg quantities of DNA of various length, verification of the sequence of those DNA molecules, developing assays that test the efficiency of purification and finally optimizing reaction condition for which the reactions occur at sub-nanomolar concentrations.

REFERENCES

REFERENCES

[1] M A Winnik. End-to-End Cyclization of Polymer Chains. (12):73–79, 1985.

[2] N Ferguson and AR Fersht. Early events in protein folding. *Current Opinions in Structural Biology*, 13(1):75–81, FEB 2003.

[3] Cox M. M. Nelson D. L. *Lehninger Principles of Biochemistry*. Freeman, New York, 5 edition, 2008.

[4] Eisuke Baba, Satoshi Honda, Takuya Yamamoto, and Yasuyuki Tezuka. Atrp–rcm polymer cyclization: synthesis of amphiphilic cyclic polystyrene-b-poly (ethylene oxide) copolymers. *Polymer Chemistry*, 3(7):1903–1909, 2012.

[5] Zhongfan Jia and Michael J. Monteiro. Cyclic Polymers: Methods and Strategies. *Journal Of Polymer Science Part A-polymer Chemistry*, 50(11):2085–2097, JUN 1 2012.

[6] Ngo Minh Toan, Greg Morrison, Changbong Hyeon, and D Thirumalai. Kinetics of loop formation in polymer chains. *J. Phys. Chem. B*, 112(19):6094–106, May 2008.

[7] Gerald Wilemski. Diffusion-controlled intrachain reactions of polymers. I Theory. *J. Chem. Phys.*, 60(3):866, 1974.

[8] M Doi. Diffusion-controlled reactions of polymers. *Chem. Phys.*, 9:455–466, 1975.

[9] A Szabo, K Schulten, and Z Schulten. First passage time approach to diffusion controlled reactions. *J. Chem. Phys.*, 72(8):4350, 1980.

[10] Gerald Wilemski. General theory of diffusion-controlled reactions. *J. Chem. Phys.*, 58(9):4009, 1973.

[11] Gerald Wilemski. Diffusion-controlled intrachain reactions of polymers. II Results for a pair of terminal reactive groups. *J. Chem. Phys.*, 60(3):878, 1974.

[12] Shilong Yang and Jianshu Cao. Theoretical analysis and computer simulation of fluorescence lifetime measurements. ii. contour length dependence of single polymers. *The Journal of chemical physics*, 121(1):572–581, 2004.

[13] Rajarshi Chakrabarti. Dynamics of end-to-end loop formation for an isolated chain in viscoelastic fluid. *Phys. A Stat. Mech. its Appl.*, 391(22):5326–5331, November 2012.

[14] Andrea Soranno, Brigitte Buchli, Daniel Nettels, Ryan R Cheng, Sonja Müller-Späth, Shawn H Pfeil, Armin Hoffmann, Everett a Lipman, Dmitrii E Makarov, and Benjamin Schuler. Quantifying internal friction in unfolded and intrinsically disordered proteins with single-molecule spectroscopy. *Proc. Natl. Acad. Sci.*, 109(44):17800–6, October 2012.

[15] Nairhita Samanta and Rajarshi Chakrabarti. End to end loop formation in a single polymer chain with internal friction. *Chem. Phys. Lett.*, 582:71–77, September 2013.

[16] Masao Doi. Theory of diffusion-controlled reactios between non-simple molecules. I. pages 107–113, 1975.

[17] Masao Doi. Theory of diffusion-controlled reaction between non-simple molecules. ii. *Chemical Physics*, 11(1):115–121, 1975.

[18] S Sunagawa and M Doi. Theory of diffusion-controlled intrachain reactions of polymers. *Polym. J.*, 1975.

[19] George H. Weiss. A perturbation analysis of the WilemskiFixman approximation for diffusion-controlled reactions. *J. Chem. Phys.*, 80(6):2880, 1984.

[20] A. V. Barzykin, K. Seki, and M. Tachiya. Diffusion-assisted long-range reaction between the ends of a polymer: Effective sink approximation. *J. Chem. Phys.*, 117(3):1377, 2002.

[21] John J Portman and Peter G Wolynes. Complementary variational approximations for intermittency and reaction dynamics in fluctuating environments. *The Journal of Physical Chemistry A*, 103(49):10602–10610, 1999.

[22] M Battezzati. An exact model calculation of the diffusion controlled intramolecular rate constant. *J. Chem. Phys.*, 74(8):4527, 1981.

[23] Goundla Srinivas. Time-dependent survival probability in diffusion-controlled reactions in a polymer chain: Beyond the Wilemski-Fixman theory. *J. Chem. Phys.*, 2002.

[24] Dmitrii E Makarov. Interplay of non-Markov and internal friction effects in the barrier crossing kinetics of biopolymers: insights from an analytically solvable model. *J. Chem. Phys.*, 138(1):014102, January 2013.

[25] I. Sokolov. Cyclization of a Polymer: First-Passage Problem for a Non-Markovian Process. *Phys. Rev. Lett.*, 90(8):1–4, February 2003.

[26] T Guérin, O Bénichou, and R Voituriez. Non-Markovian polymer reaction kinetics. *Nat. Chem.*, 4(7):568–573, January 2012.

[27] Y Oono and T Oyama. A Renormalization Group Approach and the Phenomenological Theory of a Polymer Chain. *J. Phys. Soc. Japan*, 1978.

[28] Y. Oono. Conformation space renormalization of polymers. II. Single chain dynamics based on chain diffusion equation model. *J. Chem. Phys.*, 75(2):1009, 1981.

[29] Y. Oono. Conformation space renormalization of polymers. I. Single chain equilibrium properties using Wilson-type renormalization. *J. Chem. Phys.*, 75(2):993, 1981.

[30] Ben OShaughnessy. Diffusion-controlled reactions in entangled polymer systems. *J. Chem. Phys.*, 94(5):4042, 1991.

[31] Barry Friedman and Ben O'Shaughnessy. Universal Behavior in Reacting Polymer Systems. 60(1):64–67, 1988.

[32] Barry Friedman and Ben O'Shaughnessy. Theory of intramolecular reactions in polymeric liquids. *Macromolecules*, 26(18):4888–4898, August 1993.

[33] Barry Friedman and Ben O'Shaughnessy. Kinetics of intermolecular reactions in dilute polymer solutions and unentangled melts. *Macromolecules*, 26(21):5726–5739, October 1993.

[34] Barry Friedman and B O'Shaughnessy. Theory of polymer cyclization. *Phys. Rev. A*, 40(10):5950–5959, 1989.

[35] B Friedman and C Yeung. Renormalization group analysis of polymer cyclization with non-equilibrium initial conditions. *Eur. Phys. J. E. Soft Matter*, 21(1):25–31, September 2006.

[36] Chuck Yeung and Barry Friedman. Cyclization of Rouse chains at long- and short-time scales. *J. Chem. Phys.*, 122(21):214909, June 2005.

[37] Alexander Yu Grosberg and Alexei R Khokhlov. *Statistical physics of macromolecules*. American Institute of Physics New York, 1994.

[38] Pierre-Gilles De Gennes. *Scaling concepts in polymer physics*. Cornell university press, 1979.

[39] Leo P Kadanoff. Scaling laws for Ising models near T_c. *Physics*, 2(6):263–272, 1966.

[40] Pierre-Gilles De Gennes. *Scaling concepts in polymer physics*. Cornell university press, 1979.

[41] Yoshitsugu Oono. *Statistical Physics of Polymer Solutions: Conformation-Space Renormalization-Group Approach*, pages 301–437. John Wiley & Sons, Inc., 2007.

[42] Karl F. Freed and A. L. Kholodenko. Renormalization group description of polymer excluded volume. *J. Stat. Phys.*, 30(2):437–447, February 1983.

[43] Karl F. Freed. Polymer excluded volume and the renormalization group. *Acc. Chem. Res.*, 18(2):38–45, February 1985.

[44] C Yeung and B. A. Friedman. Relation between cyclization of polymers with different initial conditions. *Europhys. Lett.*, 73(4):621–627, February 2006.

[45] P. G. de Gennes. Kinetics of diffusion-controlled processes in dense polymer systems. I. Nonentangled regimes. *J. Chem. Phys.*, 76(6):3316, 1982.

[46] Peter Hanggi, Peter Talkner, and Michal Borkovec. Reaction-rate theory : fifty years after Kramers. 62(2), 1990.

[47] H Risken. *The Fokker-Planck equation: methods of solution and applications*, volume v. 18. Springer-Verlag, 1989.

[48] GH Weiss. First passage time problems in chemical physics. *Adv. Chem. Phys.*, 1967.

[49] D J Bicout and Attila Szabo. First passage times, correlation functions, and reaction rates. 106(February):10292–10298, 1997.

[50] NG Van Kampen. *Stochastic processes in physics and chemistry*, volume 1. Elsevier, 1992.

[51] Paul C. Bressloff and Jay M. Newby. Stochastic models of intracellular transport. *Rev. Mod. Phys.*, 85(1):135–196, January 2013.

[52] J. M. Deutch. A simple method for determining the mean passage time for diffusion controlled processes. *J. Chem. Phys.*, 73(9):4700, 1980.

[53] H A Kramers. Brownian motion in a field of force and the diffusion model. (4):284–304, 1940.

[54] S Jun and J Bechhoefer. Diffusion-limited loop formation of semiflexible polymers: Kramers theory and the intertwined time scales of chain relaxation and closing. *Europhys. Lett.*, 420, 2003.

[55] Suckjoon Jun and John Bechhoefer. Role Of Polymer Loops In DNA Replication. *Physics in Canada*, 59(2):85–92, 2003.

[56] Changbong Hyeon and D Thirumalai. Kinetics of interior loop formation in semiflexible chains. *J. Chem. Phys.*, 124(10):104905, March 2006.

[57] J. Z. Y Chen, H.-K Tsao, and Y.-J Sheng. First-passage time of cyclization dynamics of a wormlike polymer. *Europhys. Lett.*, 65(3):407–413, February 2004.

[58] Hirmi Yamakawa. Statistical-mechanics of wormlike chains. *Pure Appl. Chem*, 46(2):135–141, 1976.

[59] H Yamakawa. *Modern theory of polymer solutions*. Harper & Row, NY, 1971.

[60] Reza Afra and Brian A Todd. Kinetics of loop formation in worm-like chain polymers. *J. Chem. Phys.*, 138(17):174908, May 2013.

[61] P Reimann, G J Schmid, and P Hänggi. Universal equivalence of mean first-passage time and Kramers rate. *Phys. Rev. E*, 60(1):1–4, 1999.

[62] Klaus Schulten. Dynamics of reaction involving diffusive barrier crossing.

[63] Richard W. Pastor, Robert Zwanzig, and Attila Szabo. Diffusion limited first contact of the ends of a polymer: Comparison of theory with simulation. *J. Chem. Phys.*, 105(9):3878, 1996.

[64] A.. Amitai, I. Kupka, and D. Holcman. Computation of the Mean First-Encounter Time Between the Ends of a Polymer Chain. *Phys. Rev. Lett.*, 109(10):1–5, September 2012.

[65] A. Amitai and D. Holcman. Diffusing Polymers in Confined Microdomains and Estimation of Chromosomal Territory Sizes from Chromosome Capture Data. *Phys. Rev. Lett.*, 110(24):248105, June 2013.

[66] Jeff Chen, Heng-Kwong Tsao, and Yu-Jane Sheng. Diffusion-controlled first contact of the ends of a polymer: Crossover between two scaling regimes. *Phys. Rev. E*, 72(3):1–7, September 2005.

[67] Patrick T Underhill and Patrick S Doyle. On the coarse-graining of polymers into bead-spring chains. *J. Non-Newtonian Fluid Mech.*, 122(1):3–31, 2004.

[68] Madan Somasi, Bamin Khomami, Nathanael J Woo, Joe S Hur, and Eric SG Shaqfeh. Brownian dynamics simulations of bead-rod and bead-spring chains: numerical algorithms and coarse-graining issues. *J. Non-Newtonian Fluid Mech.*, 108(1):227–255, 2002.

[69] C. Cruz, F. Chinesta, and G. Régnier. Review on the Brownian Dynamics Simulation of Bead-Rod-Spring Models Encountered in Computational Rheology. *Arch. Comput. Methods Eng.*, 19(2):227–259, May 2012.

[70] Jizeng Wang and Huajian Gao. A generalized bead-rod model for Brownian dynamics simulations of wormlike chains under strong confinement. *J. Chem. Phys.*, 123(8):084906, August 2005.

[71] Bin Liu, Jizeng Wang, Xiaojun Fan, Yong Kong, and Huajian Gao. An effective beadspring model for polymer simulation. *J. Comput. Phys.*, 227(5):2794–2807, February 2008.

[72] Hans Christian Öttinger. *Stochastic processes in polymeric fluids: tools and examples for developing simulation algorithms*, volume 1. Springer Berlin, 1996.

[73] M Doi and SF Edwards. *The theory of polymer dynamics*. Claredon, Oxford, 1986.

[74] D L Ermak and J A McCammon. Brownian Dynamics With Hydrodynamic Interactions. *J. Chem. Phys.*, 69(4):1352–1360, 1978.

[75] M Sakata and M Doi. Computer simulation of the intramolecular reaction of polymers. *Polym. J.*, 1976.

[76] Marta Ortiz-Repiso and Antonio Rey. Intramolecular Reaction Rates of Flexible Polymers. 2. Comparison with the Renormalization Group Theory. *Macromolecules*, 31(23):8363–8369, November 1998.

[77] Alexei Podtelezhnikov and Alexander Vologodskii. Simulations of polymer cyclization by Brownian dynamics. *Macromolecules*, 9297(97):6668–6673, 1997.

[78] Ting Cui, Jiandong Ding, and Jeff Z. Y. Chen. Mean First-Passage Times of Looping of Polymers with Intrachain Reactive Monomers: Lattice Monte Carlo Simulations. *Macromolecules*, 39(16):5540–5545, August 2006.

[79] Ryan R Cheng, Takanori Uzawa, Kevin W Plaxco, and Dmitrii E Makarov. Universality in the timescales of internal loop formation in unfolded proteins and single-stranded oligonucleotides. *Biophys. J.*, 99(12):3959–68, December 2010.

[80] Daniel Seaton, Stefan Schnabel, David Landau, and Michael Bachmann. From Flexible to Stiff: Systematic Analysis of Structural Phases for Single Semiflexible Polymers. *Phys. Rev. Lett.*, 110(2):028103, January 2013.

[81] Tanniemola Liverpool. Dynamics of inextensible semiflexible filaments. *Phys. Rev. E*, 72(2):1–15, August 2005.

[82] Andrew James Spakowitz. Semiflexible Polymers : Fundamental Theory and Applications in DNA Packaging Thesis by. 2004, 2004.

[83] Takashi Norisuye. Semiflexible polymers in dilute solution. *Progress in polymer science*, 18(3):543–584, 1993.

[84] Konstantin V Klenin and Jorg Langowski. Modeling of intramolecular reactions of polymers: an efficient method based on Brownian dynamics simulations. *J. Chem. Phys.*, 121(10):4951–4960, September 2004.

[85] A Balaeff, C R Koudella, L Mahadevan, and K Schulten. Modelling DNA loops using continuum and statistical mechanics. *Philos. Trans. A. Math. Phys. Eng. Sci.*, 362(1820):1355–71, July 2004.

[86] Arti Dua and Binny J. Cherayil. The dynamics of chain closure in semiflexible polymers. *J. Chem. Phys.*, 116(1):399, 2002.

[87] J Shimada and H Yamakawa. Ring-closure probabilities for twisted wormlike chains. Application to DNA. *Macromolecules*, 698(14):689–698, 1984.

[88] L Ringrose, S Chabanis, P O Angrand, C Woodroofe, and A F Stewart. Quantitative comparison of DNA looping in vitro and in vivo: chromatin increases effective DNA flexibility at short distances. *EMBO J.*, 18(23):6630–6641, December 1999.

[89] Hongmei Jian, Alexander V Vologodskii, and Tamar Schlick. A Combined Wormlike-Chain and Bead Model for Dynamic Simulations of Long Linear DNA. *J. Comput. Phys.*, 136(1):168–179, September 1997.

[90] Yanwei Wang, Douglas R Tree, and Kevin D Dorfman. Simulation of dna extension in nanochannels. *Macromolecules*, 44(16):6594–6604, 2011.

[91] Elena F. Koslover and Andrew J. Spakowitz. Discretizing elastic chains for coarse-grained polymer models. *Soft Matter*, 9(29):7016–7027, 2013.

[92] H Merlitz, K Rippe, K V Klenin, and J Langowski. Looping dynamics of linear DNA molecules and the effect of DNA curvature: a study by Brownian dynamics simulation. *Biophys. J.*, 74(2 Pt 1):773–9, February 1998.

[93] Alexei A. Podtelezhnikov and Alexander V Vologodskii. Dynamics of Small Loops in DNA Molecules. *Macromolecules*, 33(7):2767–2771, April 2000.

[94] Mitchell A. Winnik, T. Redpath, and D. H. Richards. The Dynamics of End-to-End Cyclization in Polystyrene Probed by Pyrene Excimer Formation. *Macromolecules*, 13(2):328–335, March 1980.

[95] Mitchell A. Winnik. Cyclization Dynamics of Polymers. 17. Probe Effects on Detection of Polymer End-to-End Cyclization. pages 1517–1518, 1985.

[96] Schnabel W Mita I Horie, K and H Ushiki. Alpha-omega-dianthrylpolystyrene in benzene and cyclohexane solutions as Studied by triplet-triplet absorption-measurements. *Macromolecules*, 14(5):1422–1428, 1981.

[97] Seung-Tong Cheung, Mitchell A Winnik, and Anthony E C Redpath. Cyclization Dynamics of Polymers , 5 a) The Effects of Solvent on End-to-End Cyclization of Poly (ethy1ene oxide) Probed by Intramolecular Pyrene Excimer Formation. 1824:1815–1824, 1982.

[98] K P Ghiggino, M J Snare, and P J Thistlethwaite. Cyclization dynamics in poly(ethylene oxide) - chain-length and Temperature-dependence. *European Polymer Journal*, 21(3):265–272, 1985.

[99] T Kanaya, K goshiki, M Yamamoto, and Y Nishijima. Intramolecular end-to-end excimer formation of Bis(1-pyrenylmethoxy)carbonyl)alkanes - a study of end-to-end Collisional frequency on a chain molecule. *Journal Of The American Chemical Society*, 104(13):3580–3587, 1982.

[100] AT Reis e Sousa, EMS Castanheira, A Fedorov, and JMG Martinho. Polystyrene cyclization using pyrene excimer formation. Effect of geminate pairs in good solvents. *Journal Of Physical Chemistry A*, 102(32):6406–6411, 1998.

[101] JPS Farinha, S Picarra, K Miesel, and JMG Martinho. Fluorescence study of the coil-globule transition of a PEO chain in toluene. *Journal Of Physical Chemistry B*, 105(43):10536–10545, 2001.

[102] J. M. G. Martinho, A. T. Reis e Sousa, and Mitchell A. Winnik. Effect of temperature and solvent on the cyclization of a polystyrene chain. *Macromolecules*, 26(17):4484–4488, August 1993.

[103] Mitchell A. Winnik, a.E.C. Redpath, Katherine Paton, and Jarda Danhelka. Cyclization dynamics of polymers: 10 Synthesis, fractionation, and fluorescent spectroscopy of pyrene end-capped polystyrenes. *Polymer (Guildf).*, 25(1):91–99, January 1984.

[104] Andrew M Sinclair, Mitchell A Winnik, and Gerard Beinert. Cyclization Dynamics of Polymers. 18. Capture Radius Effects in the End-to-End Cyclization Rate of Polymers, Excimers vs. Exciplexes. (c):5798–5800, 1985.

[105] Jose M G Martinhob, Maria Helena Martinhob, Mitchell A Winnik, and Gerard Beinert. Effect of chain length. 25, 1989.

[106] Sylvie Boileau, Franqoise Mdchin, M Jose, and Mitchell A Winnik. End-to-End Cyclization of a Pyrene End-Capped Poly(bispheno1 A-diethylene glycol carbonate). pages 215–220, 1989.

[107] Hirayanagi K Sindo Y Horie K Ushiki, H and I Mita. Molecular-weight dependence of intramacromolecular end-to-end Photodimerization rate of alpha,omega-dianthryl-polystyrene in Dilute-solution. *Polymer Journal*, 15(11):811–819, 1983.

[108] T Costa, J Seixas de Melo, and H D Burrows. Fluorescence behavior of a pyrene-end-capped poly(ethylene oxide) in organic solvents and in dioxane-water mixtures. *J. Phys. Chem. B*, 113(3):618–26, January 2009.

[109] Hl Xu, Jmg Martinho, M A Winnik, and G Beinert. Cyclization dynamics of polymers .24. Transient effects in diffusion Controlled reactions .7. Transient effects in diffusion-controlled Polymer cyclization. *Makromolekulare Chemie-macromolecular Chemistry And Physics*, 190(6):1333–1343, 1989.

[110] P Svirskaya, J Danhelka, AEC Redpath, and M A Winnik. Cyclization dynamics of polymers .7. Applications of the pyrene excimer technique to the internal dynamics of poly(dimethylsiloxane) chains. *Polymer*, 24(3):319–322, 1983.

[111] AEC Redpath and MA Winnik. Cyclization dynamics of polymers .9. The effect of polymer concentration On the slowest internal relaxation mode of a labeled polystyrene chain. *Polymer*, 24(10):1286–1290, 1983.

[112] S Lee and MA Winnik. Cyclization rates for two points in the interior of a polymer chain. *Macromolecules*, 30(9):2633–2641, May 1997.

[113] O Bieri, J Wirz, B Hellrung, M Schutkowski, M Drewello, and T Kiefhaber. The speed limit for protein folding measured by triplet-triplet energy transfer. *Proc. Natl. Acad. Sci. U. S. A.*, 96(17):9597–9601, August 1999.

[114] Lisa J. Lapidus, Peter J. Steinbach, William A. Eaton, Attila Szabo, and James Hofrichter. Effects of Chain Stiffness on the Dynamics of Loop Formation in Polypeptides. Appendix: Testing a 1-Dimensional Diffusion Model for Peptide Dynamics. *J. Phys. Chem. B*, 106(44):11628–11640, November 2002.

[115] Marco Buscaglia, Lisa J Lapidus, William a Eaton, and James Hofrichter. Effects of denaturants on the dynamics of loop formation in polypeptides. *Biophys. J.*, 91(1):276–88, July 2006.

[116] Fang Huang and Werner M Nau. Photochemical techniques for studying the flexibility of polypeptides. *Res. Chem. Intermed.*, 31(7-8):717–726, September 2005.

[117] Florian Krieger, Beat Fierz, Oliver Bieri, Mario Drewello, and Thomas Kiefhaber. Dynamics of Unfolded Polypeptide Chains as Model for the Earliest Steps in Protein Folding. *J. Mol. Biol.*, 332(1):265–274, September 2003.

[118] Stephen J Hagen, Linlin Qiu, and Suzette a Pabit. Diffusional limits to the speed of protein folding: fact or friction? *J. Phys. Condens. Matter*, 17(18):S1503–S1514, May 2005.

[119] M Buscaglia, B Schuler, LJ Lapidus, WA Eaton, and J Hofrichter. Kinetics of intramolecular contact formation in a denatured protein. *Journal of Molecular Biology*, 332(1):9–12, Sep 2003.

[120] Kiyohiko Kawai, Hiroko Yoshida, Akira Sugimoto, Mamoru Fujitsuka, and Tetsuro Majima. Kinetics of transient end-to-end contact of single-stranded DNAs. *J. Am. Chem. Soc.*, 127(38):13232–13237, September 2005.

[121] Takanori Uzawa, Ryan R Cheng, Kevin J Cash, Dmitrii E Makarov, and Kevin W Plaxco. The length and viscosity dependence of end-to-end collision rates in single-stranded DNA. *Biophys. J.*, 97(1):205–210, July 2009.

[122] Takanori Uzawa, Takashi Isoshima, Yoshihiro Ito, Koichiro Ishimori, Dmitrii E. Makarov, and Kevin W. Plaxco. Sequence and Temperature Dependence of the End-to-End Collision Dynamics of Single-Stranded DNA. *Biophysical Journal*, 104(11):2485–2492, Jun 2013.

[123] G Bonnet, O Krichevsky, and A Libchaber. Kinetics of conformational fluctuations in DNA hairpin-loops. *Proceedings Of The National Academy Of Sciences Of The United States Of Americ*, 95(15):8602–8606, 1998.

[124] Xiaojuan Wang and Werner M Nau. Kinetics of end-to-end collision in short single-stranded nucleic acids. *J. Am. Chem. Soc.*, 126(3):808–13, January 2004.

[125] AEC Redpath and MA Winnik. Cyclization dynamics of polymers .2. Dynamics and thermodynamics of end-to-end cyclization of polystyrene in a theta-solvent. *Journal Of The American Chemical Society*, 102(22):6869–6871, 1980.

[126] Jean Duhamel. Global analysis of fluorescence decays to probe the internal dynamics of fluorescently labeled macromolecules. *Langmuir*, 30(9):2307–24, March 2014.

[127] AEC Redpath and M A Winnik. The dynamics of polymer cyclization 3. excluded volume effects in the end-to-end cyclization of polystyrene probed by intramolecular pyrene excimer formation. *Annals of the New York Academy of Sciences*, 366(1):75–92, 1981.

[128] Alan Van Orden and Jaemyeong Jung. Fluorescence Correlation Spectroscopy for Probing the Kinetics and Mechanisms of DNA Hairpin Formation. 89(1):1–16, 2007.

[129] Kiyohiko Kawai, Kei Miyamoto, Sachiko Tojo, and Tetsuro Majima. Formation of pyrene dimer radical cation in DNA reflecting DNA dynamics in the time range of 1 micros to 1 ms. *J. Am. Chem. Soc.*, 125(4):912–5, January 2003.

[130] Kiyohiko Kawai, Hiroko Yoshida, Tadao Takada, Sachiko Tojo, and Tetsuro Majima. Formation of Pyrene Dimer Radical Cation at the Internal Site of Oligodeoxynucleotides. *J. Phys. Chem. B*, 108(35):13547–13550, September 2004.

[131] Peng Qu, Xinxing Yang, Xun Li, Xiaoxue Zhou, and Xin Sheng Zhao. Direct measurement of the rates and barriers on forward and reverse diffusions of intramolecular collision in overhang oligonucleotides. *J. Phys. Chem. B*, 114(24):8235–8243, June 2010.

[132] J Kubelka, J Hofrichter, and WA Eaton. The protein folding 'speed limit'. *Current Opinion In Structural Biology*, 14(1):76–88, FEB 2004.

[133] Isabella Daidone, Hannes Neuweiler, Soeren Doose, Markus Sauer, and Jeremy C. Smith. Hydrogen-Bond Driven Loop-Closure Kinetics in Unfolded Polypeptide Chains. *Plos Computational Biology*, 6(1), Jan 2010.

[134] Martin Volk, Yuriy Kholodenko, Helen S M Lu, Edward A Gooding, William F Degrado, and Robin M Hochstrasser. Peptide Conformational Dynamics and Vibrational Stark Effects Following Photoinitiated Disulfide Cleavage. *J. Phys. Chem. B*, 5647(97):8607–8616, 1997.

[135] L Pontryagin. On statistical investigation of dynamic systems. (March 1962), 1962.

[136] C Bustamante, SB Smith, J Liphardt, and D Smith. Single-molecule studies of DNA mechanics. *CURRENT OPINION IN STRUCTURAL BIOLOGY*, 10(3):279–285, JUN 2000.

[137] J-F Allemand, S Cocco, N Douarche, and G Lia. Loops in DNA: an overview of experimental and theoretical approaches. *Eur. Phys. J. E. Soft Matter*, 19(3):293–302, March 2006.

[138] Stephen J Hagen, James Hofrichter, and William A Eaton. Rate of Intrachain Diffusion of Unfolded Cytochrome c. 5647(96):2352–2365, 1997.

[139] K. P. Santo and K. L. Sebastian. Dynamics of loop formation in a semiflexible polymer. *Phys. Rev. E*, 80(6):1–16, December 2009.

[140] A A PoPodtelezhnikov, C Mao, N C Seeman, and A. Vologodskii. Multimerization-cyclization of DNA fragments as a method of conformational analysis. *Biophys. J.*, 79(5):2692–704, November 2000.

[141] G. Caliskan, C. Hyeon, U. Perez-Salas, R. Briber, S. Woodson, and D. Thirumalai. Persistence Length Changes Dramatically as RNA Folds. *Phys. Rev. Lett.*, 95(26):268303, December 2005.

[142] Erich Sackmann. Intra- and extracellular macromolecular networks: physics and biological function. *Macromol. Chem. Phys.*, 195(1):7–28, January 1994.

[143] a J Jin and R Nossal. Rigidity of triskelion arms and clathrin nets. *Biophys. J.*, 78(3):1183–94, March 2000.

[144] M Sano, A Kamino, J Okamura, and S Shinkai. Ring closure of carbon nanotubes. *Science*, 293(5533):1299–301, August 2001.

[145] Chetna Dhand, Maumita Das, Monika Datta, and B D Malhotra. Recent advances in polyaniline based biosensors. *Biosens. Bioelectron.*, 26(6):2811–21, February 2011.

[146] Paul A. Wiggins, Thijn Van der Heijden, Fernando Moreno-Herrero, Andrew Spakowitz, Rob Phillips, Jonathan Widom, Cees Dekker, and Philip C. Nelson. High flexibility of DNA on short length scales probed by atomic force microscopy. *Nature Nanotechnology*, 1(2):137–141, NOV 2006.

[147] E. Petrov, T. Ohrt, R. Winkler, and P. Schwille. Diffusion and Segmental Dynamics of Double-Stranded DNA. *Phys. Rev. Lett.*, 97(25):1–4, December 2006.

[148] Berk Hess, Henk Bekker, Herman J. C. Berendsen, and Johannes G. E. M. Fraaije. LINCS: A linear constraint solver for molecular simulations. *J. Comput. Chem.*, 18(12):1463–1472, September 1997.

[149] Shafigh Mehraeen, Bariz Sudhanshu, Elena Koslover, and Andrew Spakowitz. End-to-end distribution for a wormlike chain in arbitrary dimensions. *Phys. Rev. E*, 77(6):24–27, June 2008.

[150] Ralf Everaers and Angelo Rosa. Multi-scale modeling of diffusion-controlled reactions in polymers: renormalisation of reactivity parameters. *J. Chem. Phys.*, 136(1):014902, January 2012.

[151] Theo M. a. O. M. Barenbrug, E. a. J. F. (Frank) Peters, and Jay D. Schieber. Accurate method for the Brownian dynamics simulation of spherical particles with hard-body interactions. *J. Chem. Phys.*, 117(20):9202, 2002.

[152] William H Press, Saul A Teukolsky, William T Vetterling, and Brian P Flannery. *Numerical recipes in C*, volume 2. Citeseer, 1996.

[153] Chongli Yuan, Xiong Wen Lou, Elizabeth Rhoades, Huimin Chen, and Lynden A Archer. T4 dna ligase is more than an effective trap of cyclized dsdna. *Nucleic acids research*, 35(16):5294–5302, 2007.

[154] Reza Vafabakhsh and Taekjip Ha. Extreme bendability of DNA less than 100 base pairs long revealed by single-molecule cyclization. *Science*, 337(6098):1097–1101, AUG 31 2012.

[155] James T Waters and Harold D Kim. Equilibrium statistics of a surface-pinned semiflexible polymer. *Macromolecules*, 46(16):6659–6666, 2013.

[156] Valeri G Metelev, Oxana A Borisova, Eugene M Volkov, Tatiana S Oretskaya, and Nina G Dolinnaya. New chemically reactive dsdnas containing single internucleotide monophosphoryldithio links: reactivity of 5?-mercapto-oligodeoxyribonucleotides. *Nucleic acids research*, 29(19):4062–4069, 2001.

[157] Greg T Hermanson. *Bioconjugate techniques*. Academic press, 2013.

[158] Sergei M Gryaznov and Robert L Letsinger. Template controlled coupling and recombination of oligonucleotide blocks containing thiophosphoryl groups. *Nucleic acids research*, 21(6):1403–1408, 1993.

[159] Alexander Vologodskii, Quan Du, and Maxim D Frank-Kamenetskii. Bending of short DNA helices. *Artif. DNA. PNA XNA*, 4(1):1–3, January 2013.

VITA

VITA

Reza Afra earned his B.S. in 2003 in physics from University of Kashan in Iran. He then decided to pursue a Master's degree in physics and studied the phase transition in solids at the University of Isfahan. He completed his Master's degree in 2007. Fascinated by the beauty of physics, he pursued a PhD at Purdue University where he studied kinetics of loop formation in polymers and obtained PhD in 2015.